Quaternary Science Reviews 294 (2022) 107721

Contents lists available at ScienceDirect

Quaternary Science Reviews

journal homepage: www.elsevier.com/locate/quascirev

An integrative geochronological framework for the Pleistocene So'a basin (Flores, Indonesia), and its implications for faunal turnover and hominin arrival

Gerrit D. van den Bergh [a, *, 2], Brent V. Alloway [a, b, 2], Michael Storey [c], Ruly Setiawan [a, d], Dida Yurnaldi [a, d], Iwan Kurniawan [d], Mark W. Moore [e], Jatmiko [f], Adam Brumm [a, g], Stephanie Flude [c, h], Thomas Sutikna [a, i], Erick Setiyabudi [j], Unggul W. Prasetyo [j], Mika R. Puspaningrum [a, k], Ifan Yoga [j], Halmi Insani [j], Hanneke J.M. Meijer [l, m], Barry Kohn [n], Brad Pillans [o], Indra Sutisna [j], Anthony Dosseto [p], Susan Hayes [a], John A. Westgate [q], Nick J.G. Pearce [r, s], Fachroel Aziz [j], Rokus Awe Due [t, 1], Michael J. Morwood [a, 1]

[a] Centre for Archaeological Science, School of Earth, Atmospheric and Life Sciences, University of Wollongong, Wollongong, NSW, 2522, Australia
[b] Instituto de Geografía, Pontificia Universidad Católica de Chile, Santiago, Chile
[c] Quadlab, Natural History Museum of Denmark, University of Copenhagen, Copenhagen, 12 DK, 1350, Denmark
[d] Centre for Geological Survey, Geological Agency of Indonesia, Jl. Diponegoro No. 57, Bandung, 40122, Indonesia
[e] Archaeology and Palaeoanthropology, University of New England, Armidale, NSW, 2351, Australia
[f] Badan Riset dan Inovasi Nasional, Organisasi Riset Arkeologi, Bahasa dan Sastra, Jl. Condet Pejaten No.4, (formerly: Pusat Penelitian Arkeologi Nasional), Jakarta, 12510, Indonesia
[g] Australian Research Centre for Human Evolution, Environmental Futures Research Institute, Griffith University, Nathan, QLD, 4111, Australia
[h] S.Flude Consulting, Cruden Bay, Scotland, UK
[i] Australian Research Council Centre of Excellence for Australian Biodiversity and Heritage, University of Wollongong, Wollongong, NSW, 2522, Australia
[j] Museum Geologi, Geological Agency of Indonesia, Jl. Diponegoro No. 57, Bandung, 40122, Indonesia
[k] Palaeontology and Quaternary Geology Research Group, Faculty of Earth Science and Technology, Bandung Institute of Technology, Jl Ganesha 10, Bandung, Indonesia
[l] University Museum, Department of Natural History University of Bergen, Bergen, Norway
[m] Human Origins Program, National Museum of Natural History, Smithsonian Institution, Washington DC 20013, USA
[n] School of Earth Sciences, University of Melbourne, Melbourne, VIC, 3010, Australia
[o] Research School of Earth Sciences, The Australian National University, Canberra, ACT, 0200, Australia
[p] Wollongong Isotope Geochronology Laboratory, School of Earth, Atmospheric and Life Sciences, University of Wollongong, Wollongong, NSW, 2522, Australia
[q] Department of Earth Sciences, University of Toronto, Toronto, Ontario, M5S 3B1, Canada
[r] Department of Geography & Earth Sciences, Aberystwyth University, Wales, SY23 3DB, United Kingdom
[s] Dipartimento di Scienze Biologiche, Geologiche e Ambientali, Università di Bologna, 40126, Bologna, Italy
[t] Pusat Penelitian Arkeologi Nasional, Jl. Condet Pejaten No. 4, Jakarta, 12510, Indonesia

ARTICLE INFO

Article history:
Received 17 June 2022
Received in revised form
14 August 2022
Accepted 17 August 2022
Available online 14 September 2022

Handling Editor: Donatella Magri

ABSTRACT

Flores represents a unique insular environment with an extensive record of Pleistocene fossil remains and stone artefacts. In the So'a Basin of central Flores these include endemic *Stegodon*, Komodo dragons, giant tortoises, rats, birds and hominins, and lithic artefacts that can be traced back to at least one million years ago (1 Ma). This comprehensive review presents important new data regarding the dating and faunal sequence of the So'a Basin, including the site of Mata Menge where *Homo floresiensis*-like fossils dating to approximately 0.7 Ma were discovered in 2014. By chemical fingerprinting key silicic tephra originating from local and distal eruptive sources we have now established basin-wide tephrostratigraphic correlations, and, together with new numerical ages, present an update of the chronostratigraphy of the So'a Basin, with major implications for the faunal sequence. These results show that a giant

* Corresponding author.
E-mail address: gert@uow.edu.au (G.D. van den Bergh).
[1] Deceased.
[2] These authors contributed equally to this work.

https://doi.org/10.1016/j.quascirev.2022.107721

Keywords:
Island evolution
Megafauna
Tephrochronology
$^{40}Ar/^{39}Ar$ dating
Archaeology
Homo floresiensis
Stegodon

tortoise and the diminutive proboscidean *Stegodon sondaari* last occurred at the site of Tangi Talo ~1.3 Ma, and not 0.9 Ma as previously thought. We also present new data suggesting that the disappearance of giant tortoise and *S. sondaari* from the sedimentary record occurred before, and/or was coincident with, the earliest hominin arrival, as evidenced by the first records of lithic artefacts occurring directly below the 1 Ma Wolo Sege Tephra. Artefacts become common in the younger layers, associated with a distinct fauna characterized by the medium-sized *Stegodon florensis* and giant rat *Hooijeromys nusatenggara*. Furthermore, we describe a newly discovered terrace fill, which extends the faunal record of *Stegodon* in the So'a Basin to the Late Pleistocene. Our evidence also suggests that the paleoenvironment of the So'a Basin became drier around the time of the observed faunal transition and arrival of hominins on the island, which could be related to an astronomically-forced climate response at the onset of the Mid-Pleistocene Transition (MPT; ~1.25 Ma) leading to increased aridity and monsoonal intensity.

1. Introduction

Following nearly two decades of research since the initial discovery of *Homo floresiensis* in Liang Bua, the evolutionary history and immediate ancestry of this now-extinct hominin species continues to be debated (e.g., Argue et al., 2017; Argue et al., 2009; Baab et al., 2016; Brown et al., 2004; Jungers et al., 2009; Kaifu et al., 2011; Morwood et al., 2005; Young, 2020). The age and stratigraphic contexts of the *H. floresiensis* fossils from Liang Bua have recently been revised to 100–50 ka ago (Sutikna et al., 2016), which, while considerably older than the first published estimate of ~12 ka, is still substantially younger than the assemblage of fossils of a small-toothed and small-jawed hominin excavated from the open site of Mata Menge in the So'a Basin. The Mata Menge hominins, dated to ~700 ka (Brumm et al., 2016), are interpreted on the basis of morphological characters to be the most likely ancestors of the Liang Bua hominins (van den Bergh et al., 2016). To date, comparative analyses of the Liang Bua *H. floresiensis* cranial, dental and skeletal morphological features have been inconclusive regarding ancestry, and two competing hypotheses continue to dominate the debate. One hypothesis proposes that *H. floresiensis* represents a dwarfed insular descendant of *H. erectus* (Brown et al., 2004; Kaifu et al., 2011; Lyras et al., 2009; van den Bergh et al., 2016; Zanolli et al., 2022), while the other proposes a more archaic, small-bodied ancestor, such as *Homo habilis* or an Australopithecine (Argue et al., 2017; Brown and Maeda, 2009; Jungers et al., 2009; Tocheri et al., 2007). Given the absence of additional, and more substantive, *H. floresiensis* fossil assemblages, and the lack of any recoverable aDNA, establishing the timing of the initial hominin colonization of Flores is important for resolving ancestral identity. This paper presents a detailed stratigraphy of the artefact- and fossil-bearing sequences within the So'a Basin, as well as descriptions of key associated tephra marker beds with inferences regarding their eruptive provenance. Together, this evidence provides the geological and paleontological context bracketing the period of hominin first arrival on Flores, and the role that Pleistocene volcanic activity, climatic fluctuations, and/or the introduction of hominins to this isolated ecosystem may have played on the observed faunal changes during this time.

2. Setting and stratigraphic subdivision

The So'a Basin is a ~400 km^2 intra-arc basin located in central Flores (Fig. 1). This geological depression comprises a dissected grassland savannah plain with numerous small rounded hillocks and occasional deep valleys cut by the Ae Sesa River and its tributaries, which drain to the northeast through a deeply incised gorge cutting through basement rocks (Brumm et al., 2016; Maringer and Verhoeven, 1970a; Suminto et al., 2009). The basin is almost entirely surrounded by active and inactive stratovolcanoes, remnant caldera structures and associated flanking volcaniclastic fans. The northwestern portion of the So'a Basin encroaches into a large (~15 km (E-W) by 8 km (N–S)) remnant caldera (the Welas Caldera), which has a deeply dissected crater wall breached to the southeast. Little is known about the eruptive age of this caldera structure, but two K–Ar dates from a 'caldera-forming' pumiceous tuff provide disparate ages of 1.66 ± 0.11 Ma (980723–06) and 2.52 ± 0.30 Ma (980723–06), with the older age considered the more reliable (Muraoka et al., 2002). Within the Welas Caldera are two mound-shaped topographic high points encircled, and onlapped by, lacustrine sediments: a ~1 km diameter lava dome located to the west (Wolo Mowa), and a ~2 km diameter basaltic cinder cone complex situated in the east (Wolo Muo). Other possible remnant caldera structures are located to the east of the So'a Basin: the Keli Lambo Volcanic Complex and a caldera structure near Raja, which lies in between the active Ebu Lobo Volcano to the southwest and the inactive Keli Lambo Volcanic Complex to the northeast (Fig. 1). The southwestern margin of the So'a Basin is occupied by the Bajawa Cinder Cone Complex (BCCC), a clustered field of 60+ craters of basaltic andesite to andesite composition (54–61 wt % SiO_2) that have been active since 0.73 Ma (Sucipta et al., 2006), and which includes the active Inelika Volcano (Fig. 1).

Palaeontological and archaeological research began in the So'a Basin during the late 1950s, when Theodorus 'Theo' Verhoeven (1907–1990) commenced excavations at Ola Bula and recovered an assemblage of *Stegodon* remains (Verhoeven, 1958). In 1960, the Geological Survey of Indonesia embarked on a regional survey of the basin to clarify its fossil-bearing stratigraphy (Hartono, 1961), while Verhoeven continued to perform test excavations at other sites, establishing that *Stegodon* fossils were associated with stone artefacts at Mata Menge and the nearby site of Boa Leza (Maringer and Verhoeven, 1970a). Follow-up research in the basin identified three main stratigraphic units. From oldest to youngest these are the Ola Kile Formation, the Ola Bula Formation, and younger volcanic rocks that lap onto the basin sequence along the western and southern basin margins, and are associated with still-active volcanoes (O'Sullivan et al., 2001; Sondaar et al., 1994; Suminto et al., 2009; van den Bergh, 1999). Overall, this stratigraphic subdivision has continued to provide a reliable basis for the palaeontological and archaeological research undertaken within the So'a Basin – including this current study. A more detailed basin stratigraphy is required, however, to place all the key fossil and archaeological sites and excavations in a chronological and environmental context.

3. Methodology

This section constitutes a brief summary of the methods applied. Further details regarding the analytical procedures, standards,

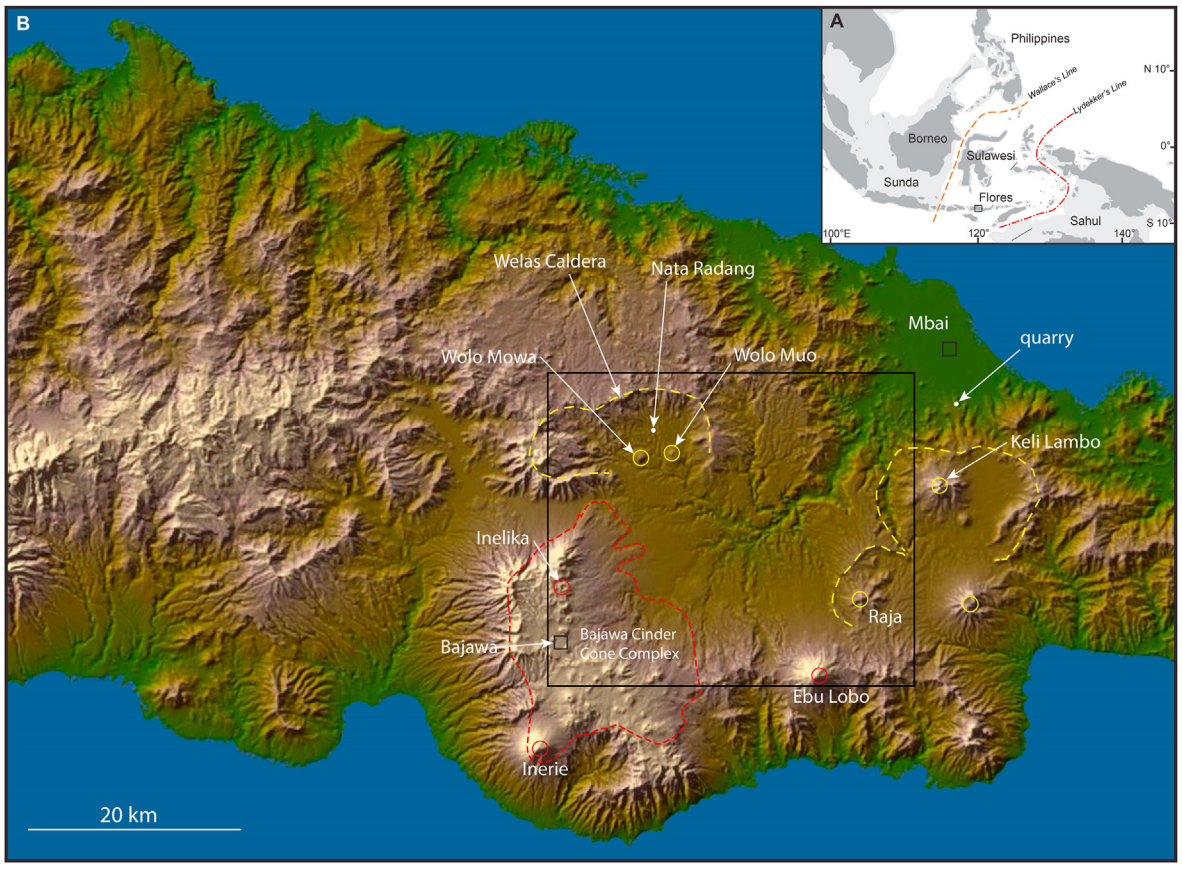

Fig. 1. Location of Flores within Wallacea (**A**) and DEM of Central Flores and the So'a Basin (**B**)
Rectangle is the area enlarged in Fig. 2A. Yellow dotted lines indicate caldera structures; red circles: active volcanoes; yellow circles: major inactive volcanic centres. The Bajawa Cinder Cone Complex on the southwestern margin of the So'a Basin (red dashed line) consists of at least 60+ cones of basaltic andesite to andesite composition that are considered to have been active since 0.73 Ma (Sucipta et al., 2006). (For interpretation of the references to color in this figure legend, the reader is referred to the Web version of this article.)

constants, and so forth, are provided in the Appendices. Excavation methods are detailed in Brumm et al. (2016).

3.1. Geodesy

From 2010 until 2019 we have undertaken multiple field campaigns in the So'a Basin. Initially, stratigraphic sections were exposed at a number of key sites by excavating 1-m wide slot trenches covering the entire basin-fill sequence. Simultaneously, we conducted archaeological and palaeontological excavations at key sites. Stratigraphic sections were recorded and systematically sampled for geochemical analyses, and for palaeomagnetic and numerical dating purposes. The spatial coordinates of concrete pillars erected as reference points for further surveying at key sites and sections were determined using a Trimble Differential GPS. The reference points were calibrated against the Triangulation point at Rakalaba east of Bajawa (Bakosurtanal). All coordinates were recorded in the WGS 84 UTM system (Zone 51S), with all elevations in this paper given as ellipsoidal heights. Total stations (Topcon OS100 and Leica TS11) were used to measure dense grids of surface coordinates and construct detailed topographic maps with 1-m contour intervals of the areas surrounding key excavation sites (see Appendix-A), as well as to record the 3D-coordinates of all excavated finds.

3.2. Chemical fingerprinting of tephra

Glass shard major and trace element determinations were conducted on primary rhyolitic airfall and mass-flow tephra layers to allow the identification and correlation of key stratigraphic markers throughout the basin. In addition, potential correlatives from adjacent field sites were included in the geochemical analyses. Major element data were acquired using a JEOL Superprobe housed at Victoria University of Wellington. Trace elements analyses on glass shards were performed by laser ablation (LA) ICP-MS at the Research School of Earth Sciences, Australian National University (Canberra). Selected trace elements of mafic agglutinated scoria and diabase samples were analysed using nebulation inductively coupled plasma mass spectrometry (SN-ICP-MS) at the Department of Geography and Earth Sciences, Aberystwyth University. See Appendix B for details.

3.3. Dating techniques

Age determinations of key tephra marker beds and fossil occurrences were conducted using various methods. The single crystal $^{40}Ar/^{39}Ar$ technique was applied on potassium-rich minerals (hornblende and feldspar) from three samples of rhyolitic tephra at the Quaternary Dating Laboratory of Roskilde University (see Appendix C for details). Another method applied on apatite grains from one rhyolitic tephra sample was the (U–Th-Sm)/He dating technique, carried out at the School of Earth Sciences, University of Melbourne (**see** Appendix D **for details**).

In addition, two late Pleistocene *Stegodon* tooth samples were subjected to U-series dating at the Wollongong Isotope Geochronology Laboratory, University of Wollongong, using laser ablation

multicollector ICP-MS (**see** Appendix E **for details**). Two charcoal samples (Wk-48668 and Wk-48669) from the same Late Pleistocene lahar terrace deposit from which two *Stegodon* tooth samples originated, were sent to the University of Waikato Radiocarbon Dating Laboratory for Accelerator Mass Spectroscopy (AMS) radiocarbon (^{14}C) dating. Samples were pre-treated with hot HCl, rinsed and treated with multiple hot NaOH washes, filtered, rinsed and dried. Both conventional AMS ^{14}C ages are provided in the text, as well as the calibrated ^{14}C ages, using OxCal v4.3.2.

Other age estimates obtained by additional techniques and reported in previous published sources are fission-track dating on zircon crystals from tephra pumice clasts and tuffaceous layers; isothermal plateau fission-track (ITPFT) dating of glass shards; combined U-series and electron spin resonance (ESR) dating on *Stegodon* molar fragments. In three stratigraphic sections the obtained numerical ages were combined with magnetic polarity measurements.

3.4. Stable isotope analysis on fossil tooth enamel

In order to reconstruct the feeding ecology of vertebrates and changes in this ecology over time, stable isotope analysis (δ^{13}C and δ^{18}O) was performed on fossil tooth enamel of adult individuals of *Stegodon* and *Hooijeromys* from various localities, covering the entire temporal range of the vertebrate-bearing sequence. Stable isotope values are reported in ‰ and relative to VPDB (δ^{13}C) and VSMOW (δ^{18}O). The carbon isotope ratio (δ^{13}C) in body tissues of herbivores, including the relatively stable tooth enamel, reflects the types of vegetation consumed. This allows for the detection of trends in relative proportions in diets of plants with different photosynthetic pathways for CO_2 assimilation, namely C_3 plants (most trees shrubs and high-altitude or high-latitude grasses) and C_4 plants (tropical grasses and sedges). As feeding behavior in opportunistic herbivores such as elephants is heavily influenced by available resources, changes in the proportion of C_3 versus C_4 plants in paleo-diets over time is thought to be strongly correlated with changes in vegetation cover and climate (Cerling et al., 1999; DeNiro and Epstein, 1978; Puspaningrum et al., 2020). The δ^{18}O incorporated in animal tissues depends on the δ^{18}O fractionation in drinking water and food, which is in turn the result of a complex function of geographical, climatic, and ecological conditions, and hence more difficult to interpret. However, on a tropical island such as Flores it can be expected that the δ^{18}O values become more positive when the contribution of precipitation to surface drinking water decreases and/or evapo-transpiration increases (see Puspaningrum et al., 2020, and references therein).

4. Stratigraphy

Field research and dating between 2010 and 2019 on a number of stratigraphic sections has produced a working model of the stratigraphy across the So'a Basin (Fig. 2). Here we describe the major stratigraphic divisions from earliest to latest.

4.1. Ola Kile Formation

The Ola Kile Formation (hereafter OKF) is a southward tilted (~5°) basement of indurated fluvio-volcaniclastic deposits of at least 100 m thick, that comprise pyroclastic flows, andesitic breccias, lava flows, laharic diamicts and subordinate tuffaceous sandstones and siltstones with intervening lithified palaeosols. One of the most prominent units so far recognised within this formation is a 26-m + thick weathered ignimbrite with basal coarse-grained surge (~1.3-m thick) and fall (~2.8-m thick) subunits in the eastern part of the basin (Setiawan, 2018); see Fig. 2: Lowo Mali Ignimbrite). The source of this ignimbrite deposit is unknown, but based on its flow-surge-fall facies architecture and very coarse-grained pumice (P) and lithic (L) clast componentry (i.e., P_{max} 8 × 7 cm; L_{max} 5 × 4 cm), it is likely that this deposit is source-proximal and relates to a voluminous late stage eruptive event sourced from either the Keli Lambo or Raja Caldera (Fig. 1). A single Zircon Fission Track (ZFT) age for the ‘upper part’ of the OKF in the eastern part of the basin has provided an age of 1.86 ± 0.12 Ma (O'Sullivan et al., 2001). The dating sample is reported to have been taken below the angular unconformity with the overlying Ola Bula Formation (see below), but it is not clear whether this sample originates from the uppermost part of the OKF sequence (Lowo Mali Ignimbrite) or from an older interval, though it does provide a maximum age for the onset of deposition of the overlying Ola Bula Formation.

4.2. Ola Bula formation

The Ola Bula Formation (hereafter OBF) overlies the OKF with an angular unconformity and comprises as much as 70 m of largely undeformed and flat-lying volcano-sedimentary deposits. The OBF has been subdivided into three lithological members named (from base to top): Tuff, Sandstone and Limestone Members (Suminto et al., 2009; van den Bergh, 1999). The basal Tuff Member consists of dominantly metre-to decimetrre-thick pyroclastic (primary) and fluvio-volcaniclastic (secondary) deposits interbedded with subordinate well-developed palaeosols and pedogenically-altered fluviatile silts, sands and conglomerate lenses. Locally a 3 m thick sequence of thin-bedded lacustrine silts and clays is incorporated in the Tuff Member (Fig. 2: Dena Biko Section 272.8 - 276 m). The Tuff Member is only 8 m thick along the NE margin of the basin (at Kobatuwa I) but increases to 33 m thickness in the central basin area (near Tangi Talo) and decreases in thickness again further east.

The basal tuffaceous deposits grade upwards into a middle 20–30 m thick Sandstone Member dominated by well-developed palaeosols overprinted on variably textured conglomerate lenses, sandstones and siltstones, which were deposited by braided rivers. Along the northwestern basin margin, the Sandstone Member encompasses fluvial gravels and sands alternating with clay-textured mudflow deposits (cohesive mass flows; see Appendix F for field criteria) containing diatoms with intervening palaeosols and infrequent basaltic-andesite tephra inter-beds. The latter perceptibly coarsen and thicken northwards towards the Welas Caldera. This mudflow-sandstone-gravel facies association is of limited lateral extent and is deposited in a north-south oriented paleovalley eroded into the basal deposits of the Tuff Member. Further east and along the southern basin margin the Sandstone Member is characterized by an alternation of conglomerates and siltstones, both heavily overprinted by sub-aerial weathering and palaeosol formation.

The middle Sandstone Member is overlain by an 8.5 m thick sequence of thin-bedded lacustrine sediments (Gero Limestone Member, GLM) that caps the basin infill and registers the presence of a basin-wide lake, which formerly extended into the Welas Caldera (Fig. 2). This interval consists predominantly of laminated micritic freshwater limestones, clays and silts, and is interbedded by abundant coarse-grained basaltic and sporadic fine-textured silicic tephra. Palaeosols and infilled polygonal shrinkage cracks

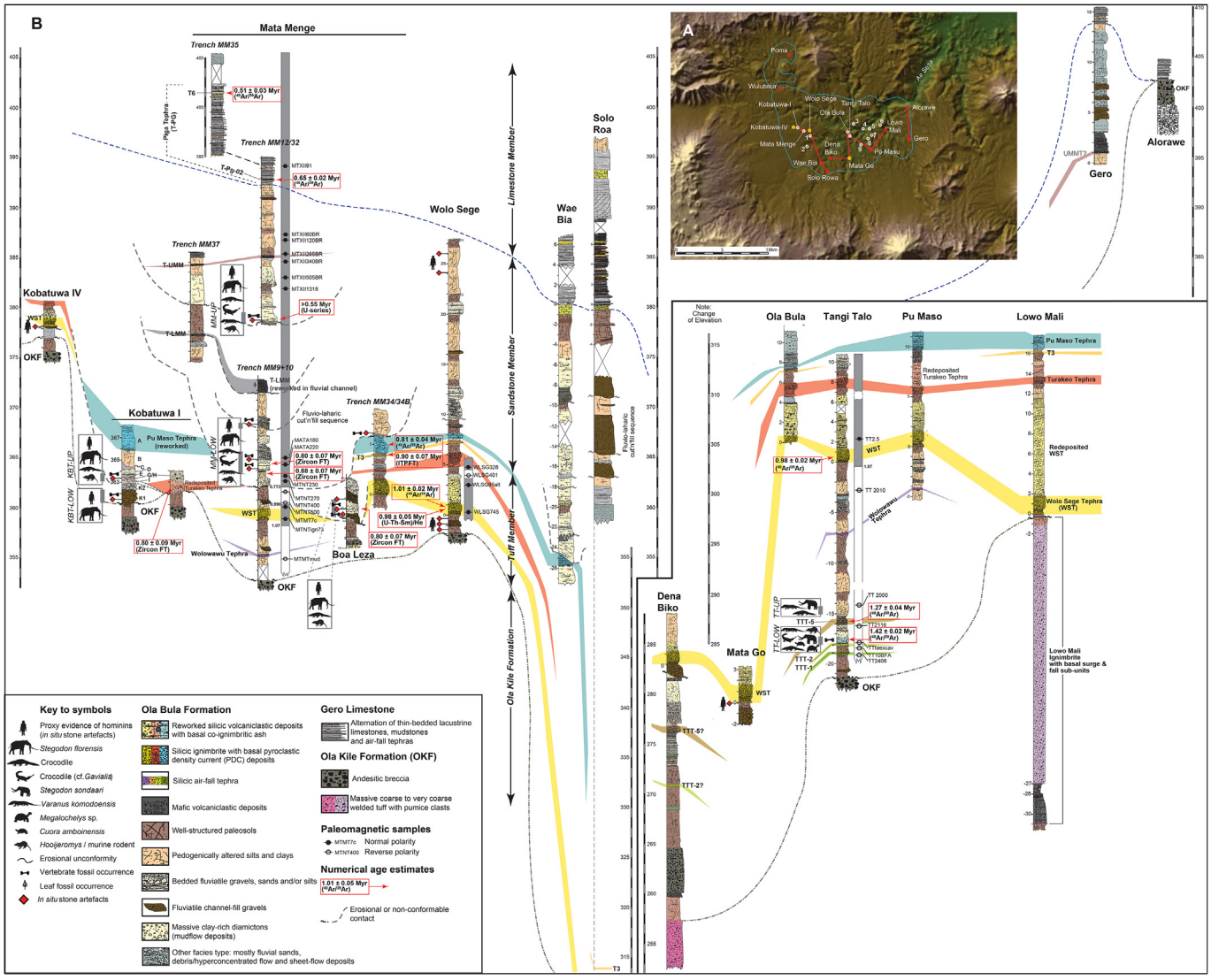

Fig. 2. Stratigraphy, chronology, fossil content and palaeomagnetic polarity of the Ola Bula Formation (OBF) deposits at key So'a Basin sections (arranged west to east) **A,** Connected dots show the locations of the stratigraphic sections shown in B; white dots indicate fossil vertebrate localities; yellow dots indicate archaeological sites lacking faunal evidence; red dots indicate other localities mentioned in the text. Numbers of localities are: 1 = Boa Leza; 2 = Ruda Olo; 3 = Mala Huma; 4 = Ulu Mala Kata; 5 = Ngamapa; 6 = Pauphadhi; 7 = Kopo Watu; 8 = Dozu Dhalu; 9 = Wolo Keo. Blue line corresponds with the minimum lake extension during deposition of the Gero Limstone Member based on outcrops of lacustrine deposits. **B**, Colored bands indicate the key tephra marker beds recognizable throughout the basin, which serve as the main correlative tie points between sections. Available numerical ages are indicated in red outlined boxes. Scales to the left and right show ellipsoid elevations; each section is shown according to its relative elevation as measured by DGPS. Palaeomagnetic samples were analysed for the Mata Menge, Wolo Sege, and Tangi Talo sections, with open circles indicating reversed polarities of sampled levels and black dots normal polarities. (For interpretation of the references to color in this figure legend, the reader is referred to the Web version of this article.)

are not uncommon within the lacustrine sequence, indicating fluctuating lake levels and occasional sub-aerial exposure along the lake margins. Along the northeastern basin margin the GLM directly overlies the OKF unconformably (Fig. 2 Alorawe Section). In the southern Solo Roa section the thin-bedded lacustrine GLM sequence is conformably overlain by a 7 m thick clastic sequence that includes 2.5 m high northward dipping clinoforms interpreted as a Gilbert-type delta prograding into the lake.

Stone artefacts and abundant vertebrate fossils are found at numerous localities within the Sandstone Member, commonly in direct association within the same layers. Vertebrate fossils are much less common in the Tuff Member and have so far only been encountered in the central part of the basin near Tangi Talo, where the Tuff Member reaches its maximum thickness. Stone artefacts in the Tuff Member appear to be restricted to the uppermost part, and have not been found associated with vertebrate fossils in this sub-unit. Freshwater algae (oogonia), plant, diatom, fish, ostracod and gastropod fossils have been identified within the GLM, as well as pollen assemblages. Previously the age of the OBF has been reported as ranging from over 1.01 Ma to 0.51 ± 0.03 Ma (Brumm et al., 2010a; Brumm et al., 2016; Morwood et al., 1998; O'Sullivan et al., 2001). Here we show that the basal age of the OBF and the oldest fossil assemblage dates to at least 1.4 Ma.

4.3. Younger volcanics

Along the western, southern and eastern basin margins, younger volcaniclastic sequences mantle the OBF. These include

basaltic to basaltic-andesite lava flow deposits, interbedded with coarse-grained fluvio-volcanic detritus, originating from the surrounding upland volcanoes such as the Bajawa Cinder Cone Complex (BCCC) and the Ebu Lobo Volcano. At a site called Ulu Mala Kata, near the confluence of two major rivers, the Ae Sesa and the Lowo Lele (Fig. 2), a massive laharic sequence of at least 6 m thick forms a remnant fill terrace.

5. Key stratigraphic units

5.1. Silicic tephra deposits

Silicic tephra (>63 wt % SiO_2) deposits have played a pivotal role in refining the fossil- and artefact-bearing stratigraphy within the So'a Basin, enabling improved basin-wide correlations as well as more specific targeting of prospective sites for excavation at relevant time-intervals (Brumm et al., 2010a, 2016). Silicic tephra are prevalent within two stratigraphic intervals that correspond with the upper GLM (Figs. 2, 3A-D) and the lower Tuff Member (Figs. 2 and 3E, F). To date, no silicic tephra have been identified within the middle Sandstone Member.

Silicic tephra are typically represented as fine-grained vitric-rich tephra-falls, pumice-rich ignimbrites (gas-supported mass-flow deposits) and ashy-pumiceous debris-hyperconcentrated-flood flow (water-supported mass flow deposits), with each category of deposit able to be distinguished in the field by their sedimentary characteristics (**see** Appendix-F; Fig. 2). Because silicic tephra deposits are minimally affected by intense tropical surficial weathering (cf. basaltic to basaltic andesite deposits), it is a relatively straightforward exercise to geochemically characterise glass shard and mineral constituents utilising the techniques of electron microprobe (EMP) and laser ablation inductively coupled plasma mass spectrometry (LA-ICP-MS) (Figs. 4 and 5; Table 1; Table B1). Similarly, a number of different radiometric dating methods (i.e., $^{40}Ar/^{39}Ar$, and fission track) have been applied to tephra mineral and glass constituents (Table 2). Radiometric ages have also been corroborated with palaeomagnetic polarity data retrieved from tephra-bearing sequences (i.e., Fig. 2).

5.1.1. Silicic mass-flow deposits

Three prominent silicic mass-flow deposits (Wolo Sege, Turakeo and Pu Maso) are widely recognised throughout the So'a Basin as occurring in close stratigraphic succession, but are separated by well-developed palaeosols (Fig. 6A–C). Of the three mass-flow deposits, Wolo Sege Tephra is the most extensive and stratigraphically significant. Turakeo and Pu Maso mass-flow deposits have a similar field expression, but can be distinguished by a fine-grained silicic ash bed (T3) of distinct mineralogy and glass geochemistry occurring within an intervening palaeosol, as well as by the ubiquity of exceptionally large accretionary lapilli within the texturally finer Pu Maso deposits (see Fig. 6D). It is important to emphasize that field correlation of individual mass-flow deposits can be problematic, particularly in medial to distal areas from an eruptive source area, because they sometimes display transitional sedimentary characteristics indicative of rapid lateral transformation from hot, gas-supported pyroclastic flow/surge into water-supported debris-hyperconcentrated-flood flow deposits (Alloway et al., 2004; Pillans et al., 2005; Smith and Lowe, 1991). Similarly, many outcropping mass-flow deposits may initially display features indicative of primary emplacement but can upwardly transition to reworked deposits. Since the depositional character of silicic mass-flow deposits can vary both laterally and vertically across the So'a Basin, the identity of key tephra units is here verified and correlated on the combined basis of unique depositional architecture and stratigraphic association, which is further verified by glass-shard major- and trace-element chemistry and numerical dating chronology.

5.1.2. Wolo Sege tephra

The Wolo Sege Tephra (WST; previously referred to as Wolo Sege Ignimbrite: Brumm et al., 2010a; Brumm et al., 2016) is the most extensive and stratigraphically significant metre-thick silicic mass-flow deposit within the So'a Basin fossil-bearing sequences. It was first recognised in the west-central part of the basin at the Wolo Sege archaeological site (Brumm et al., 2010a). Within the Wolo Sege type section (Figs. 2, 7A-B), the WST immediately overlies a well-structured palaeosol containing *in situ* stone artefacts developed into artefact-bearing fluviatile conglomerate and siltstone sediments ~2 m above the unconformable contact with the underlying breccias of the OKF. Hornblende crystals extracted from WST at this site yielded a $^{40}Ar/^{39}Ar$ age of 1.02 ± 0.02 Ma (Brumm et al., 2010a, 2016), which also provides a minimum age for the stone artefacts directly underlying WST.

Throughout the So'a Basin, WST has a unique depositional architecture that can be subdivided into three distinctive sub-units enabling an unambiguous field correlation (i.e., Fig. 7A–B): a lower planar-to cross-stratified unit containing accretionary lapilli (dominantly pyroclastic surge with fall component), a middle massive to weakly stratified pumiceous unit (pyroclastic flow) and an upper redeposited unit comprising regular, massive to planar bedded (dcm-to mm-laminae), well sorted, light grey to pale yellow, coarse to fine sandy vitric ash and conspicuous accretionary lapilli. The middle pumice unit is further characterized by the presence of both white and grey pumice (<10%) and the occurrence of large hornblende crystals. WST is now widely recognised at numerous sites, including Mata Go (Figs. 2, 7D-E), where an *in situ* stone artefact (Fig. 7E–F) protrudes into basal WST from the surface of an underlying palaeosol, and at Kobatuwa IV (Figs. 2 and 7C), where stone artefacts also occur *in situ* in a conglomerate lens directly underlying WST.

Based on sedimentary architecture and glass shard major element composition, WST is correlated to the upper part of the Tangi Talo fossil site located in the central part of the So'a Basin (Fig. 7G–H). At Tangi Talo WST was directly dated using the same radiometric technique applied to WST at Wolo Sege. An indistinguishable hornblende $^{40}Ar/^{39}Ar$ isochron age of 0.98 ± 0.02 Ma (SF-FLO12-TT1) was determined (**see** Appendix-C, Figs. C2, C4). These results are further supported by a hornblende $^{40}Ar/^{39}Ar$ isochron age of 1.01 ± 0.05 Ma for WST in the Mata Menge section (Brumm et al., 2016), and an apatite (U–Th-Sm)/He age of 0.98 ± 0.05 Ma (±2 se) for WST at its type section (see Appendix D). In addition, these WST ages are further supported by palaeomagnetic polarity data from both the Tangi Talo and Mata Menge sections, which indicate a clear polarity change from normal to reverse just below WST, consistent with the base of the Jaramillo normal subchron, dated at 1.07 Ma (see Fig. 2; Yurnaldi et al., 2018).

5.1.3. Other silicic tephra with unique correlation potential

While many airfall tephra beds of silicic composition have been identified throughout the OBF sedimentary succession, there are two white fine-grained vitric-rich ash beds of distinct glass chemistry that standout with unique, regional correlation potential (Figs. 4 and 5; Table 1; Table B1). One is a silicic ash bed (T6) that is exposed at Mata Menge (Trench MM-35: see Fig. 2) within the uppermost part of the lacustrine GLM (Fig. 8 Set A). Here T6 tephra occurs as a discrete cm-thick normal bedded, fine sandy-silt

Fig. 3. Silicic tephra within Ola Bula Formation (OBF)
A–D: Silicic tephra from the Gero Limestone Member (GLM) and E–F: some prominent silicic tephra from the lower Tuff Member (TM). **A, B.** Coarse-grained pyroclastic surge deposits occurring at Nata Radang (08° 36′ 20.9″ S; 121° 03′14.0″ E) located in the northwest inner sector of Welas Caldera; **C**, Subaqueous 0.6 m thick silicic hyperconcentrated flow deposit (Poma tephra; 08° 36′ 52.6″ S; 121° 04′31.4″ E; see Fig. 2a for location) enveloped by planar-bedded lacustrine silts of GLM with basaltic tephra inter-beds; **D**, Subaqueous 1.2 m thick silicic hyperconcentrated flow deposit (Wulubara tephra; 08° 39′ 04.4″ S; 121° 03′37.5″ E; see Fig. 2a for location) enveloped by lacustrine silts of GLM; **E,** Pyroclastic flow deposit of Wolo Sege Tephra with closely underlying Wolo Wawu Tephra interbedded with fluviatile gravels, sands and silts with intervening well-developed palaeosols (08° 42′ 28.8″ S; 121° 09′41.5″ E); **F,** Stratified coarse pumiceous lapilli bed of Lowo Lele Tephra (TTT-5) at Tangi Talo (08° 41′ 52.8″ S; 121° 08′10.1″ E) Excavation TT-G (see also Fig. 14). TTT-5 is underlain by a complex cut-and-fill sequence of multiple pedogenically-altered mudflow deposits with intervening deformed lenses of fluvial-bedded sands and silts. The basal mudflow shown is rich in pumice fragments and contains abundant vertebrate fossils at its base. The stratigraphic positions of samples (10/TT/001 and SF-FLO12-TT7) retrieved for $^{40}Ar/^{39}Ar$ dating are indicated with yellow squares (Fig. 2; see Appendix C). (For interpretation of the references to color in this figure legend, the reader is referred to the Web version of this article.)

textured vitric ash and is stratigraphically associated with numerous dark grey ash and lapilli inter-beds of mafic composition (collectively referred to as Piga Tephra). A single feldspar crystal $^{40}Ar/^{39}Ar$ age of 0.51 ± 0.03 Ma was determined for T6 (Brumm et al., 2016).

Another distinctive silicic ash bed (T3) occurs at several So'a Basin localities (i.e. Mata Menge, Kopowatu, Lowo Mali; see Fig. 2) within a prominent palaeosol intervening between Turakeo (lower) and Pu Maso (upper) tephras. In this context the T3 tephra occurs as a cm-thick, massive to normal bedded, biotite bearing, silt-textured vitric ash (i.e., Fig. 8 Set B). The very fine texture of T3 remains the same irrespective of its depositional context, which, together with T3's location throughout So'a Basin, indicates a likely distal source. A glass shard isothermal plateau fission-track (ITPFT) mean age of 0.90 ± 0.07 Ma (based on two independent age determinations) was resolved for T3 at Mata Menge (slot Trench MM-34) (Brumm et al., 2016). This age is also consistent with a hornblende $^{40}Ar/^{39}Ar$ age of 0.81 ± 0.04 Ma derived from Pu Maso Tephra closely overlying T3, and within the same slot trench section (Brumm et al., 2016).

5.2. Mafic airfall tephra

Tephra inter-beds of mafic (i.e. basaltic andesite to andesite; 54–61 wt% SiO_2) composition are concentrated in the middle to upper portions of the OBF sedimentary succession (Figs. 2 and 9), but are of limited correlative value as they are numerous and difficult to differentiate and geochemically analyse. The oldest occur as two dark grey, cm-thick normal bedded scoriaceous coarse ash inter-beds (named upper Mata Menge Tephra [T-UMM] and Lower Mata Menge Tephra [T-LMM]) within the uppermost Sandstone Member in the vicinity of Mata Menge. No direct radiometric

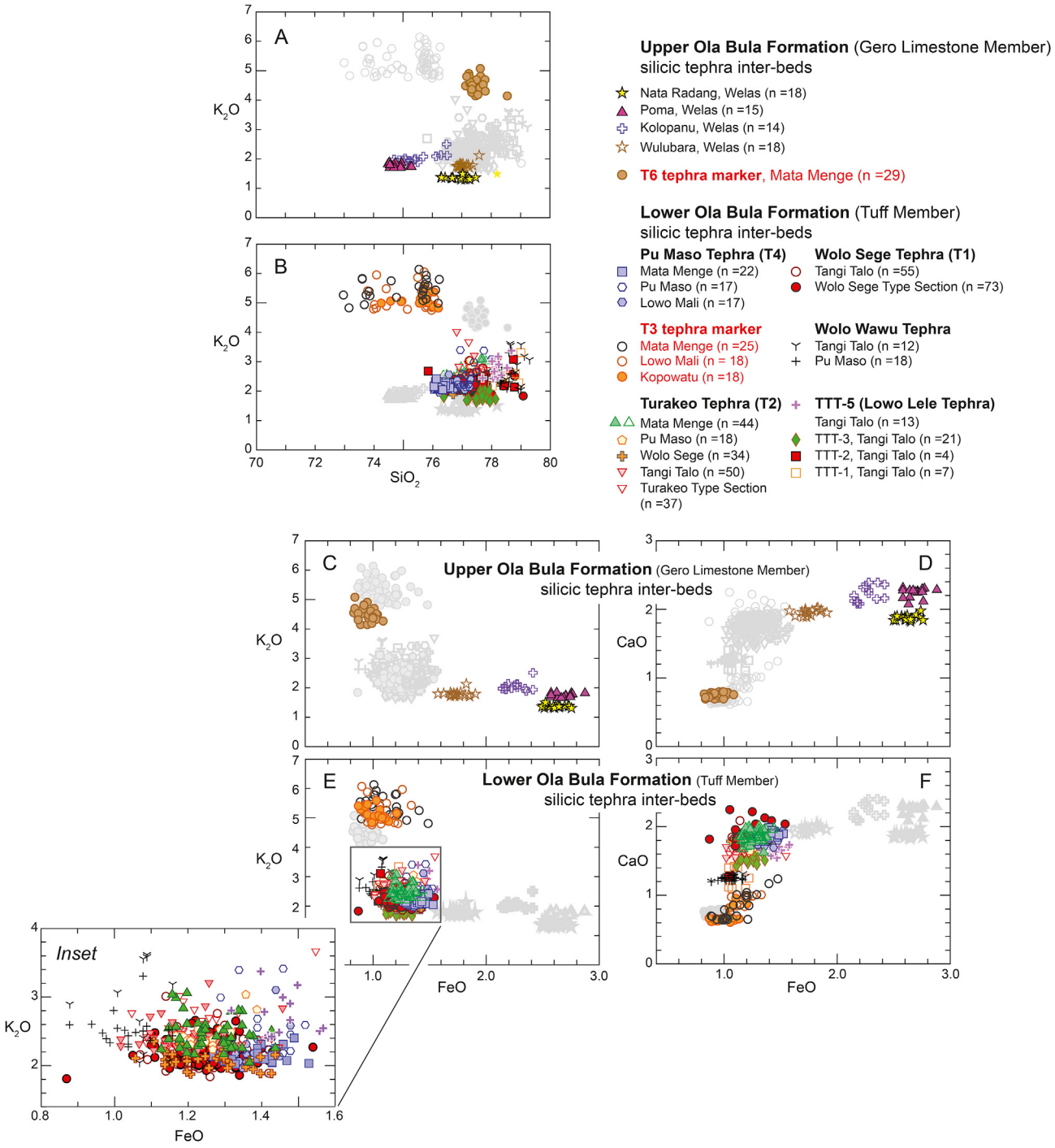

Fig. 4. Selected major element compositions (weight percent SiO_2 vs. K_2O and FeO vs. CaO and K_2O) of glass shards from key silicic tephra within the upper Ola Bula Formation (Gero Limestone Member; **A, C, D**) and lower Ola Bula Formation (Tuff Member; **B, E, F**)
While major element glass compositions of most tephra within TM are geochemically indistinguishable (except T3 tephra marker), a number of key tephra within this compositional grouping can be distinguished since they consistently occupy subtly different overlapping fields. The overall compositional grouping likely indicates derivation from the same eruptive centre and over a sustained period of time. Discrete compositional groupings of tephra are more discernible within GLM and appear to suggest intermittent eruptions from different centres. The identity of tephra with indistinct glass chemistry can often be readily distinguished in the field by a combination of stratigraphic position and association, as well as by morphological expression.

ages have been determined for tephra from this lower stratigraphic interval.

In closely overlying lacustrine sediments of the GLM, the occurrence of mafic tephra becomes significantly more numerous (n > 58 (Setiawan, 2018);), typically comprising mm-to cm-thick, massive to graded inter-beds of moderate-to well-sorted dark grey scoriaceous ash and lapilli, as well as grey to brown poorly-sorted muddy ash. These tephra exhibit depositional features indicative of explosive magma-water interactions that resulted in magmatic-phreatomagmatic eruptive products. Informally named Piga tephra (PGt), these tephra inter-beds are sequentially numbered upward from the basal contact of the Limestone Member. At Mata Menge

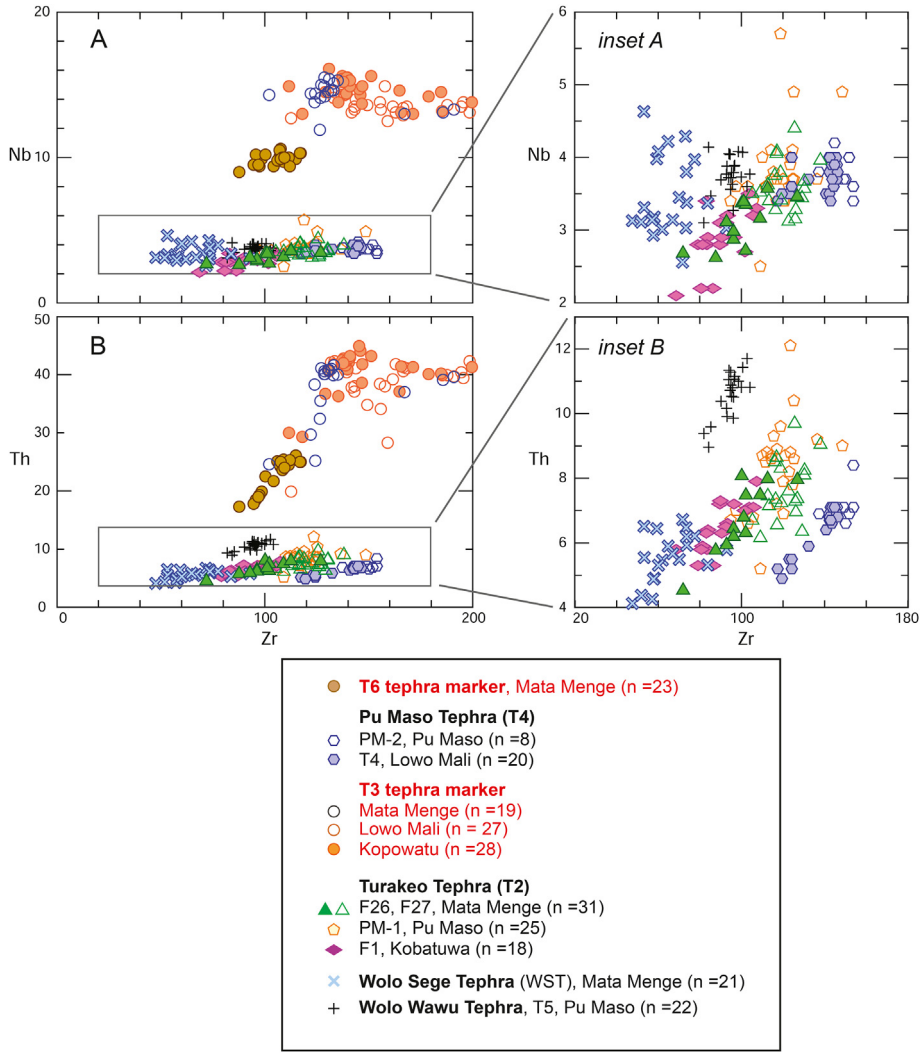

Fig. 5. A, B, Selected trace-element compositions (Zr *vs.* Nb and Th) of glass shards from key So'a tephra obtained by LA-ICP-MS analysis at ANU, Canberra (seeTable B2) Compositional groupings have strong semblance to those indicated from major-element EMP analysis (see Fig. 4) with T3 and T6 having distinctively different trace-element composition. Insets A and B indicate key tephra of similar composition (Wolo Sege-Turakeo-Pu Maso), which occupy subtly different overlapping fields and can be distinguished. Trace element concentrations are in ppm.

(slot Trench MM-12 and Excavation MM-32), T-Pg-02 positioned just above the base of the Limestone Member has a single crystal (hornblende) $^{40}Ar/^{39}Ar$ age of 0.65 ± 0.02 Ma (Brumm et al., 2016).

Piga tephra can be traced within the Welas Caldera to roadside sections (i.e., Wulubara, Poma; see Fig. 2A) where fine-grained tuffaceous lacustrine sediments are interbedded by abundant mafic lapilli and ash beds that are perceptibly thicker and coarser grained than the mafic inter-beds of the Limestone Member at Mata Menge. Within the Welas Caldera these tephra beds are frequently associated with scoria-bearing debris flow deposits and metre-thick sequences of coarse fragmented scoria and bombs. Bulk solution nebulization ICP-MS (SN-ICP-MS) analyses (see Table B) conducted on selected magmatic-phreatomagmatic tephra from Mata Menge are geochemically indistinguishable from analyses of agglutinated scoria and diabase samples retrieved from a basaltic cinder cone (Wolo Muo; east, Fig. 1) and lava dome (Wolo Mowa, west, Fig. 1) within the Welas Caldera (Fig. 9G and H). At present, it is not known if the two intra-caldera mafic domes are temporally related, but the emergence of the eastern cone complex certainly occurred during an interval when the Welas Caldera contained an extensive lake, and explosive water-magma interactions generated a succession of phreatomagmatic-magmatic fall units and sub-aqueous scoria-bearing debris flow deposits, as well as clay-rich, cohesive mass-flow (mudflow) deposits that extended down ancestral tributaries directly adjacent to the Welas intra-caldera lake.

6. Key fossil- and artefact-bearing sections

In the following section key sites within the So'a Basin are described according to their arrangement from west to east as indicated in Fig. 2, and not in chronological order.

6.1. Kobatuwa

6.1.1. Kobatuwa site stratigraphy

In 2005–2006 three excavations were undertaken at the site Kobatuwa-I in western part of the So'a Basin (Fig. 2). The

Table 1
Summary of major-element glass shard compositions of silicic volcaniclastic beds within sedimentary sequences of So'a Basin. Beds are arranged in stratigraphic order from top (youngest) to bottom (oldest).

Tephra	Section	Sample	*Probe Run*	SiO_2	Al_2O_3	TiO_2	FeO	MgO	MnO	CaO	Na_2O	K_2O	Cl	H_2O	*n*
Nata Radang (surge)	**Welas**	*12_19_08*	*Nov 13, 2012*	76.97 (0.45)	12.61 (0.18)	0.28 (0.04)<	2.60 (0.13)	0.33 (0.06)	0.13 (0.03)	1.85 (0.11)	3.92 (0.31)	1.37 (0.05)	*n.d.*	4.56 (1.30)	*18*
	Wolo Meze	**F3** *15_04_01*	*May 8, 2015*	76.51 (0.45)	12.59 (0.17)	0.31 (0.04)	2.68 (0.13)	0.28 (0.06)<	0.14 (0.02)	1.92 (0.14)	3.91 (0.34)	1.47 (0.17)	0.18 (0.01)	4.29 (1.14)	*24*
Poma (hyperconcentrated flow)	**Welas**	**4-T1** *12_11_22*	*Aug 24, 2012*	74.76 (0.26)	14.15 (0.13)	0.49 (0.02)	2.69 (0.09)	0.51 (0.02)	0.12 (0.03)	2.23 (0.07)	3.19 (0.40)	1.76 (0.07)	0.11 (0.01)	4.49 (1.25)	*15*
Kolopanu (pyroclastic flow/ Ignimbrite)	**Welas**	*12_19_09*	*Nov 13, 2012*	75.43 (0.54)	13.80 (0.17)	0.41 (0.02)	2.25 (0.08)	0.62 (0.04)	0.08 (0.02)	2.23 (0.12)	3.31 (0.71)	2.00 (0.07)	*n.d.*	5.11 (1.14)	*14*
Wulubara (hyperconcentrated-debris flow)	**Welas**	*12_19_07*	*Nov 13, 2012*	77.06 (0.20)	12.82 (0.12)	0.34 (0.02)	1.75 (0.08)	0.47 (0.03)	0.07 (0.02)	1.96 (0.04)	3.84 (0.27)	1.79 (0.09)	*n.d.*	4.73 (1.52	*18*
T6 (tephra marker; fine vitric ash)	**Mata Menge**	**F6** *15_04_03*	*May 8, 2015*	77.48 (0.27)	12.40 (0.12)	0.18 (0.02)	0.95 (0.07)	0.14 (0.02)	0.10 (0.02)	0.74 (0.03)	3.15 (0.23)	4.52 (0.23)	0.35 (0.02)	4.42 (0.64)	*29*
Pu Maso (pyroclastic-hyperconcentrated-flood flow)	**Mata Menge**	**F29** *15_03_06*	*May 8, 2015*	76.25 (0.17)	13.80 (0.09)	0.24 (0.02)	1.38 (0.07)	0.41 (0.02)	0.10 (0.02)	1.89 (0.04)	3.56 (0.17)	2.15 (0.11)	0.21 (0.11)	6.03 (0.87)	*22*
	Pu Maso	**Po-2** *12_21_20*	*Nov 15, 2012*	77.01 (0.36)	13.68 (0.15)	0.22 (0.01)	1.40 (0.07)<	0.39 (0.03)<	0.09 (0.02)	1.85 (0.06)	2.90 (0.62)	2.46 (0.43)<	*n.d.*	6.17 (1.88)	*17*
	Lowo Mali	**LM-T4** *12_21_23*		76.78 (0.43)	13.62 (0.19)	0.22 (0.02)	1.37 (0.06)<	0.39 (0.03)<	0.10 (0.02)	1.80 (0.06)	3.48 (0.52)	2.24 (0.27)	*n.d.*	5.20 (1.39)	*17*
(airfall)	**Mbai**	**F14** *15_01_06*	*May 8, 2015*	76.90 (0.55)	13.64 (0.30)	0.21 (0.03)	1.27 (0.10)	0.35 (0.04)	0.11 (0.02)	1.65 (0.13)	3.47 (0.55)	2.19 (0.35)	0.20 (0.08)	5.90 (2.05)	*25*
T3 (tephra marker; fine vitric ash)	**Mata Menge**	**F28** *15_03_05*	*May 8, 2015*	74.97 (1.08)	13.77 (0.62)	0.17 (0.02)	1.11 (0.15)	0.12 (0.03)	0.13 (0.04)	0.81 (0.18)	3.17 (0.42)	5.40 (0.34)	0.33 (0.08)	5.30 (0.90)	*25*
	Lowo Mali	**LM-T3** *12_21_22*	*Nov 15, 2012*	75.05 (0.83)	13.83 (0.53)	0.15 (0.01)	1.06 (0.13)	0.14 (0.02)	0.11 (0.02)	0.78 (0.15)	3.70 (0.34)	5.17 (0.43)	*n.d.*	2.92 (0.62)	*18*
	Kopowatu	*12_21_24*		75.60 (0.51)	13.54 (0.39)	0.14 (0.01)	1.03 (0.09)	0.13 (0.02)	0.11 (0.05)	0.69 (0.10)	3.63 (0.34)	5.13 (0.21)	*n.d.*	3.13 (0.86)	*18*
Turakeo Tephra (pyroclastic-hyperconcentrated-flood flow)	**Wolo Sege**	**WS-J (up)** *12_12_25*	*Aug 24, 2012*	77.13 (0.17)	13.60 (0.12)	0.19 (0.02)	1.24 (0.08)	0.33 (0.02)	0.08 (0.02)	1.79 (0.04)	3.39 (0.12)	2.08 (0.09)	0.17 (0.01)	3.96 (0.53)	*17*
		WS-I (lwr) *12_12_26*		77.66 (0.33)	13.54 (0.21)	0.18 (0.01)	1.26 (0.12)	0.33 (0.03)	0.08 (0.02)	1.80 (0.05)	2.90 (0.24)	2.08 (0.14)	0.18 (0.01)	5.96 (1.32)<	*17*
	Pu Maso	**Po-1** *12_21_19*	*Nov 15, 2012*	77.16 (0.19)	13.45 (0.12)	0.19 (0.01)	1.25 (0.06)	0.35 (0.05	0.08 (0.02)	1.77 (0.07)	3.29 (0.47)	2.44 (0.20)	*n.d.*	5.20 (1.99)	*18*
	Turakeo	*12_22_26*	*Nov 15, 2012*	77.20 (0.33)	13.37 (0.25)	0.19 (0.02)	1.25 (0.10)	0.33 (0.02)	0.08 (0.02)	1.75 (0.07)	3.32 (0.41)	2.50 (0.28)	*n.d.*	4.61 (1.17)	*38*
	Tangi Talo	*12_22_29*	*Nov 15, 2012*	77.22 (0.25)	13.38 (0.14)	0.18 (0.02)	1.20 (0.08)	0.33 (0.03)	0.07 (0.02)	1.74 (0.08)	3.47 (0.29)	2.42 (0.17)	*n.d.*	4.36 (0.89)	*50*
	Mata Menge	**F27** *15_03_04*	*May 8, 2015*	76.96 (0.34)	13.51 (0.13)	0.21 (0.02)	1.27 (0.09)<	0.35 (0.02)	0.07 (0.02)	1.84 (0.07)	3.16 (0.38)	2.45 (0.25)	0.17 (0.01)	6.40 (0.84)	*25*
		F26 *15_03_03*		77.00 (0.34)	13.53 (0.18)	0.22 (0.02)	1.26 (0.07)	0.37 (0.03)	0.07 (0.02)	1.86 (0.11)	2.49 (0.23)	2.60 (0.32)	0.17 (0.01)	6.26 (0.84)	*19*
	Kobatuwa	**F1** *15_03_01*		76.66 (0.49)	13.73 (0.27)	0.20 (0.02)	1.31 (0.09)<	0.35 (0.02)	0.09 (0.03)	1.92 (0.16)	2.92 (0.63)	2.62 (0.31)	0.20 (0.04)	6.43 (1.40)	*19*
	Mbai	**F15** *15_04_06*		77.69 (0.46)	13.19 (0.22)	0.16 (0.02)	1.05 (0.11)	0.26 (0.04)	0.10 (0.03)	1.45 (0.10)	3.53 (0.45)	2.40 (0.26)	0.16 (0.02)	5.22 (1.05)	*24*
Wolo Sege (pyroclastic-hyperconcentrated-flood flow)	**Wolo Sege**	**WSI—H (redeposited** *12_12_27*	*Aug 24, 2012*	77.17 (0.30)	13.70 (0.14)	0.17 (0.02)	1.28 (0.07)	0.31 (0.02)	0.07 (0.03)	1.84 (0.04)	3.15 (0.30)	2.10 (0.12)	0.20 (0.01)	4.75 (1.29)	*14*
		WSI-G1 (ignimbrite) *12_12_28*		77.30 (0.23)	13.70 (0.10	0.18 (0.02)	1.28 (0.07)	0.32 (0.02)	0.07 (0.02)	1.85 (0.04)	3.03 (0.16)	2.07 (0.09)	0.20 (0.01)	5.74 (1.44)	*16*
		WSI—F2 *12_08_01*	*Sept 14, 2012*	76.80 (0.12)	13.64 (0.09)	0.17 (0.01)	1.23 (0.06)<	0.35 (0.02)	0.08 (0.02)	1.89 (0.03)	3.55 (0.17)	2.28 (0.07)	*n.d.*	6.03 (1.04)	*13*
		WSI—F1 *12_12_29*	*Aug 24, 2012*	77.23 (0.33)	13.68 (0.10)	0.17 (0.02)	1.25 (0.09)	0.32 (0.01)	0.09 (0.02)	1.86 (0.03)	3.08 (0.32)	2.12 (0.14)	0.20	5.86 (1.49)	*15*
		WSI-D (surge/ fall) *12_12_30*		77.33 (0.33)	13.61 (0.08)	0.16 (0.00)	1.25 (0.04)	0.30 (0.02)	0.09 (0.02)	1.86 (0.06)	3.09 (0.32)	2.13 (0.07)	0.18 (0.03)	5.05 (1.15)	*6*
		WSI—C (surge/fall) *12_11_19*		77.53 (0.74)	13.57 (0.70)	0.18 (0.02)	1.23 (0.15)	0.32 (0.04)	0.08 (0.03)	1.90 (0.16)	2.79 (0.36)	2.22 (0.17)	0.19 (0.02)	6.51 (3.17)	*17*
		WSI—B (surge) *12_11_20*		77.54 (0.67)	13.75 (0.34)	0.18 (0.02)	1.27 (0.12)	0.32 (0.03)	0.08 (0.02)	1.91 (0.13)	2.46 (0.68)	2.31 (0.22)	0.18 (0.02)	5.82 (2.39)	*15*
	Tangi Talo	**TT-T8** *12_11_23*		77.27 (0.19)	13.75 (0.08)	0.18 (0.02)	1.28 (0.08)	0.32 (0.01)	0.08 (0.02)	1.86 (0.03)	2.95 (0.37)	2.11 (0.25)<	0.20 (0.01)	5.48 (1.11)	*17*
		TT-T7 *12_11_24*		77.30 (0.23)	13.69 (0.31)	0.19 (0.03)	1.25 (0.08)	0.33 (0.02)	0.09 (0.02)	1.85 (0.06)	2.94 (0.32)	2.16 (0.26)	0.20 (0.01)	5.35 (1.47)	*19*
															19

Table 1 (*continued*)

Tephra	Section	Sample	*Probe Run*	SiO_2	Al_2O_3	TiO_2	FeO	MgO	MnO	CaO	Na_2O	K_2O	Cl	H_2O	*n*
		TT-T6		76.73	13.66	0.17	1.26	0.33	0.09	1.85	3.59	2.11	0.21	3.82	
		12_10_13		(0.13)	(0.08)	(0.01)	(0.07)	(0.02)	(0.02)	(0.03)	(0.12)	(0.08)	(0.01)	(0.86)	
	Mata	**F13**	*May 8,*	76.80	13.69	0.20	1.23	0.35	0.09	1.87	3.11	2.46	0.21	5.73	*25*
	Menge	*15_03_02*	*2015*	(0.34)	(0.21)	(0.02)	(0.06)	(0.03)	(0.02)	(0.05)	(0.54)<	(0.16)<	(0.04)	(1.36)	
Wolowawu	**Tangi Talo**	**TT-T5**	*Aug 24,*	78.86	12.74	0.16	1.08	0.24	0.08	1.25	2.62	2.77	0.19	6.30	*12*
Tephra		*12_10_14*	*2012*	(0.24)	(0.18)	(0.01)	(0.08)	(0.02)	(0.02)	(0.04)	(0.56)	(0.62)	(0.01)	(3.20)<	
(airfall ash)	**Pu Maso**	**Po-5**	*Nov 15,*	78.22	12.76	0.15	1.04	0.24	0.07	1.23	3.77	2.52	n.d.	3.60	*18*
		12_21_21	*2012*	(0.28)	(0.15)	(0.01)	(0.07)	(0.01)	(0.02)<	(0.03)	(0.34)	(0.23)<		(0.88)	
Lowo Lele	**Tangi Talo**	**TTT-5**	*Nov 15,*	78.20	12.12	0.23	1.45	0.27	0.06	1.66	3.28	2.73	*n.d.*	3.98	*13*
Tephra (pum. lapilli airfall)		*12_22_30*	*2012*	(0.24)	(0.14)	(0.02)	(0.07)	(0.02)	(0.03)	(0.06)	(0.37)	(0.31)		(1.80)	
Unnamed tephra (redeposited pum. vitric sands)		**TTT-3**	*Aug 24,*	77.64	13.57	0.17	1.24	0.30	0.12	1.54	3.41	1.80	0.22	5.37	*20*
		12_10_16	*2012*	(0.15)	(0.44)	(0.02)	(0.07)	(0.03)	(0.02)	(0.07)	(0.22)	(0.13)	(0.02)	(1.27)	
Unnamed tephra (airfall ash)		**TTT-2**		78.67	12.85	0.14	1.05	0.21	0.10	1.27	3.08	2.46	0.17	4.94	*3*
		12_10_17		(0.19)	(0.13)	(0.01)	(0.01)	(0.01)	(0.03)	(0.01)	(0.54)	(0.53)	(0.01)	(0.26)	
Unnamed tephra (airfall ash)		**TTT-1**		78.56	12.95	0.17	1.11	0.23	0.09	1.25	2.89	2.55	0.18	5.61	*7*
		12_10_18		(0.36)	(0.29)	(0.04)<	(0.07)	(0.02)	(0.03)	(0.15)	(0.44)		(0.02)	(1.51)	
Glass standards	**ATHO-G**		*Aug 24,*	75.59	12.20	0.24	3.27	0.11	0.09	1.70	3.75	2.64	0.04	99.62	*29*
			2012	(0.28)	(0.12)	(0.02)	(0.10)	(0.03)	(0.01)	(0.03)	(0.16)	(0.04)	(0.01)	(0.47)	
			Sept 14,	75.60	12.20	0.23	3.27	0.10	0.10	1.72	3.75	2.61	*n.d.*	99.57	*31*
			2012	(0.55)	(0.12)	(0.02)	(0.09)	(0.01)	(0.02)	(0.03)	(0.10)	(0.03)		(0.65)	
			Nov 13,	75.60	12.20	0.23	3.27	0.11	0.09	1.70	3.75	2.64	*n.d.*	99.59	*49*
			2012	(0.37)	(0.11)	(0.02)	(0.09)	(0.02)	(0.01)	(0.03)	(0.30)	(0.04)		(0.60)	
			Nov 15,	75.59	12.20	0.23	3.27	0.11	0.09	1.70	3.75	2.64	0.04	99.63	*54*
			2012	(0.28)	(0.11)	(0.02)	(0.09)	(0.02)	(0.01)	(0.02)	(0.45)	(0.04)	(0.01)	(0.67)	
			May 8,	75.57	12.21	0.26	3.29	0.10	0.11	1.72	3.73	2.64	0.04	99.66	*119*
			2015	(0.34)	(0.09)	(0.02)	(0.12)	(0.01)	(0.02)	(0.03)	(0.31)	(0.06)	(0.01)	(0.52)	
			Oct 28,	75.60	12.20	0.26	3.27	0.10	0.10	1.70	3.73	2.64	0.04	97.73	*88*
			2015	(0.33)	(0.08)	(0.03)	(0.18)	(0.01)	(0.03)	(0.03)	(0.30)	(0.06)	(0.01)	(0.53)	

All major element determinations were made on a JEOL Superprobe (JXA-8230) housed at Victoria University of Wellington, using the ZAF correction method. Analyses were performed using an accelerating voltage of 15 kV under a static electron beam operating at 8 nA. The electron beam was defocused between 10 and 20 μm. Oxide values are recalculated to 100% on a volatile-free basis. Total Fe expressed as FeO_t. Mean and ±1 standard deviation (in parentheses), based on *n* analyses. All samples normalised against glass standard ATHO-G. *n.d.* – not determined. Individual analyses available upon request. Analyst: B.V. Alloway.

excavations are numbered KBT-I-T1 to KBT-I-T3 (see Appendix A). At KBT-I-T2 an assemblage of comparatively large *in situ* stone artefacts (cores and flakes) was recovered from a fluvial boulder conglomerate with an erosive base (Jatmiko et al., 2009), which cuts down unconformably into an indurated mudflow of the OKF. KBT-I-T1 also yielded a small number of *Stegodon* fossils and stone artefacts, but KBT-I-T3, excavated in the upper part of the OKF proved to be sterile (Jatmiko et al., 2009). In 2010, new excavations were initiated at three sites west of KBT-I, numbered KBT-II to KBT-IV. KBT-IV (Fig. 2; Appendix A) is located at 460 m west of KBT-I and is the westernmost section within the So'a Basin where the WST has been observed. Here a 5 × 1 m test excavation (Fig. 7C) revealed the WST directly overlying a 25 cm thick pedogenically-altered boulder conglomerate lens, from which nine redeposited (water-rolled) stone artefacts were retrieved but no fossils. This channel fill cuts down in an indurated palaeosol pertaining to the top of the OKF. At KBT–II–T1 a trench was excavated in an indurated palaeosol of the OKF, which also appeared to be sterile.

The focus of the investigation, however, remained on KBT-I, where large-scale excavations are ongoing at KBT-I-T2 (Figs. 2 and 10A-E). Excavation KBT-I-T2 is situated along the west slope of a south-north oriented dry river valley. Excavations at this site have revealed a complex cut-and-fill sequence of multiple, stacked dominantly fluvio-laharic sediments that unconformably overly lithified volcaniclastic deposits and a prominent palaeosol of the OKF (Fig. 10D and E). A 2m thick fluvial boulder conglomerate lens that has cut down into the OKF (Layer K in Fig. 10D and E; this is the same layer that was excavated in 2005 and indicated as T2 in (Jatmiko et al., 2009)), is overlain by a series of strongly lithified mass-flow deposits (Layers E-J) and redeposited silicic ash deposits (Layers C-D). The basal part of the conglomerate (sub-Layer K_1) contains both stone artefacts and rare redeposited (water-rolled) *S. florensis* molar fragments, with the latter representing the earliest record of this taxon (see below). Layer K is in turn overlain by a clay-rich mass-flow (lahar) deposit with large angular boulders and contains comparatively abundant fossil material together with stone artefacts (Layer I) (Fig. 10B, E). Towards the south Layer I is truncated by a fluvial channel fill unit containing a reworked silicic ash lens (W_1) and pumice lens (W_2; see Fig. 10D), which can be geochemically correlated with the Turakeo Tephra (Fig. 5). This channel fill is in turn overlain by a series of further mass-flow deposits, two of which (Layers G-H) are tabular sheets of coarse-grained massive lahars containing abundant fossils and stone artefacts and volcanic pebbles. The upper 10–20 cm of Layer G is fluvially reworked and shows parallel lamination (Layer F), and is in turn overlaid by a sequence of clay-rich ashy mudflows (Layers E-C) with internal erosional surfaces. These mudflows are capped by a well-structured palaeosol (Layer B). The top of the excavated sequence at KBT-I is a 2 m thick interval of redeposited silicic ash (Layer A) correlated with Pu Maso Tephra based on its facies architecture, stratigraphic association and mineral content; however, this correlation should be regarded as provisional as it needs to be confirmed by geochemical fingerprinting. The Pu Maso Tephra is elsewhere (Mata Menge Trench 34, see Appendix A) dated at 0.81 ± 0.04 Ma (Brumm et al., 2016). This is in accordance with two zircon fission-track ages of 0.8 ± 0.9 Ma and 0.7 ± 0.7 Ma for two tuff layers reportedly from below and above, respectively, the main fossil-bearing layers at Kobatuwa (Jatmiko et al., 2009; O'Sullivan et al., 2001). The lower sample was originally obtained from the reworked Turakeo Tephra lens in the channel-fill (Layer W_1) (see in Jatmiko et al., 2009), but the exact stratigraphic level of the younger sample was not documented.

Table 2
Summary of ages (±1σ) determined for volcaniclastic sediments and fossils located within So'a Basin and acquired using different dating techniques.

Stratigraphic Unit		Layer/Sample	Section	Technique	Mineral phase	Age (Ma or ka)	References
Ae Sesa Terrace	Ae Sesa Terrace fill		Ulu Mala Kata	U-series	Stegodon tooth enamel	>34.2 +3.0/ −0.5 ka	*UMK15-1a; this study*
				U-series	Stegodon tooth enamel	>31.0 +0.5/ −0.7 ka	*UMK15-1b; this study*
				AMS	charcoal	47.699 ± 1.342 BP	*Wk-48668; this study*
				AMS	charcoal	45.807 ± 1.042 BP	*Wk-48669; this study*
Ola Bula Formation	Gero Limestone Member	T6 tephra marker	Mata Menge	40Ar/39Ar	Feldspar	0.51 ± 0.03 Ma	Brumm et al. (2016)
		PGT-2 Tephra	Mata Menge	40Ar/39Ar	Hornblende	0.65 ± 0.02 Ma	Brumm et al. (2016)
		/ 14	Gero	FT	Zircon	0.65 ± 0.06 Ma	O'Sullivan et al. (2001)
		/ 13	Gero	FT	Zircon	0.68 ± 0.07 Ma	O'Sullivan et al. (2001)
	Sandstone Member	/ 4	Mata Menge	FT	Zircon	0.75 ± 0.07 Ma	O'Sullivan et al. (2001)
		/ 1	Kobatuwa	FT	Zircon	0.75 ± 0.06 Ma	O'Sullivan et al. (2001)
		MM-UP/ #3543A, # 3543B	Mata Menge	U-series	Hominin tooth	>0.55 Ma	Brumm et al. (2016)
		MM-UP/ #3541, #3542, #3544	Mata Menge	U-Series/ ESR	2 Stegodon molar fragments	0.36–0.69 Ma	Brumm et al. (2016)
		MM-LOW/A	Mata Menge	FT	Zircon	0.80 ± 0.07 Ma	Morwood et al. (1999)
		MM-LOW/B	Mata Menge	FT	Zircon	0.88 ± 0.07 Ma	Morwood et al. (1999)
	Tuff Member	(Tuff Member?)/2	Kobatuwa	FT	Zircon	0.70 ± 0.07 Ma	O'Sullivan et al. (2001)
		/ 3; Unit E (= reworked Turakeo Tephra)	Kobatuwa	FT	Zircon	0.80 ± 0.09 Ma	O'Sullivan et al. (2001); Jatmiko et al. (2009)
		Pu Maso Tephra	Mata Menge	40Ar/39Ar	Hornblende	0.81 ± 0.04 Ma	Brumm et al. (2016)
		T3 Tephra marker	Mata Menge	ITPFT	Glass	0.90 ± 0.07 Ma	Brumm et al. (2016)
		Wolo Sege Tephra	Wolo Sege	40Ar/39Ar	Hornblende	1.01 ± 0.02 Ma	Brumm et al. (2010a, 2016)
		Wolo Sege Tephra	Tangi Talo	40Ar/39Ar	Hornblende	0.98 ± 0.05 Ma	*SF-FLO-TTI; this study*
		Wolo Sege Tephra	Wolo Sege	(U-Th-Sm)/He	Apatite	0.98 ± 0.05 Ma	*WS-08; this study*
		TTT-5 Lowo Lele Tephra	Tangi Talo	40Ar/39Ar	Hornblende	1.27 ± 0.03 Ma	*SF-FLO12-TT7; this study*
		C/Pumice-rich lahar	Tangi Talo	FT	Zircon	0.90 ± 0.07 Ma	Morwood et al. (1999)
		TTT-3 pumice mudflow[a]	Tangi Talo	40Ar/39Ar	Plagioclase	1.42 ± 0.02 Ma	*10/TT/001; this study*
Ola Kile Formation		/ 10	Kopowatu	FT	Zircon	1.86 ± 0.12 Ma	O'Sullivan et al. (2001)
		'Caldera forming' tuff	Welas (loc. 12)	K-Ar	Whole rock	1.66 ± 0.11 Ma	Muraoka et al. (2002)
		'Caldera forming' tuff	Welas (loc. 11)	K-Ar	Whole rock	2.52 ± 0.30 Ma	Muraoka et al. (2002)

[a] This dating sample originates from the same layer as sample C from the Pumice rich lahar reported by Morwood et al. (1999)

WST is not recorded at KBT-I but can be observed along the opposite, eastern side of the valley bottom at KBT-I, and at KBT-IV, which is further west, and where it directly overlies a conglomeratic fluvial cut-and-fill deposit with *in situ* stone artefacts (Figs. 2 and 7C).

6.1.2. *Kobatuwa fauna and archaeology*

The fossil taxa that were excavated from Layers I, G and H are predominantly *S. florensis*, with a Minimum Number of Individuals (hereinafter MNI) of 39, based on dental remains. Only two rolled *Stegodon* molars have been recovered from the older conglomerate layer (Layer K_1; fauna assemblage KBT-LOW). These molar fragments are above the maximum size range for *Stegodon sondaari*, and allow attribution to *Stegodon* cf. *florensis* (see Jatmiko et al., 2009: p. 114). The fragments predate the emplacement of the Turakeo Tephra, which in turn underlies the T3 tephra, and which has been dated at 0.90 ± 0.07 Ma in the Mata Menge section (Brumm et al., 2016). With a minimum age of 0.9 Ma, these fossils represent the oldest documented *S. florensis* remains to date. At present it is unknown if the Kobatuwa fossils from Layer K are younger or older than the emplacement of the WST around 1 Ma, because the latter is not developed at the excavation site.

In addition to *Stegodon* remains, Layers G and H contain the remains of crocodiles, represented by a dextral mandible fragment, a left half of a skull and a dextral maxilla fragment, together with some isolated teeth and postcranial elements. The skull and mandible show similarities with *Crocodylus siamensis* from Java (Setiyabudi, 2017). Fossils of microvertebrates are very rare at Kobatuwa, which may be partly due to the fact that the fossil-bearing layers G, H and I are extremely hard and the excavated rock could not be wet-sieved. However, the recovery of a tibia fragment of an unidentified giant rat and a single molar fragment indicate that murine rodents were present at this stage.

Enamel samples of seven excavated adult *Stegodon* molar fossils from Layers F/G/H were extracted for stable isotope analysis ($\delta^{13}C$ and $\delta^{18}O$) (for the analytical methods see Appendix G and Brumm

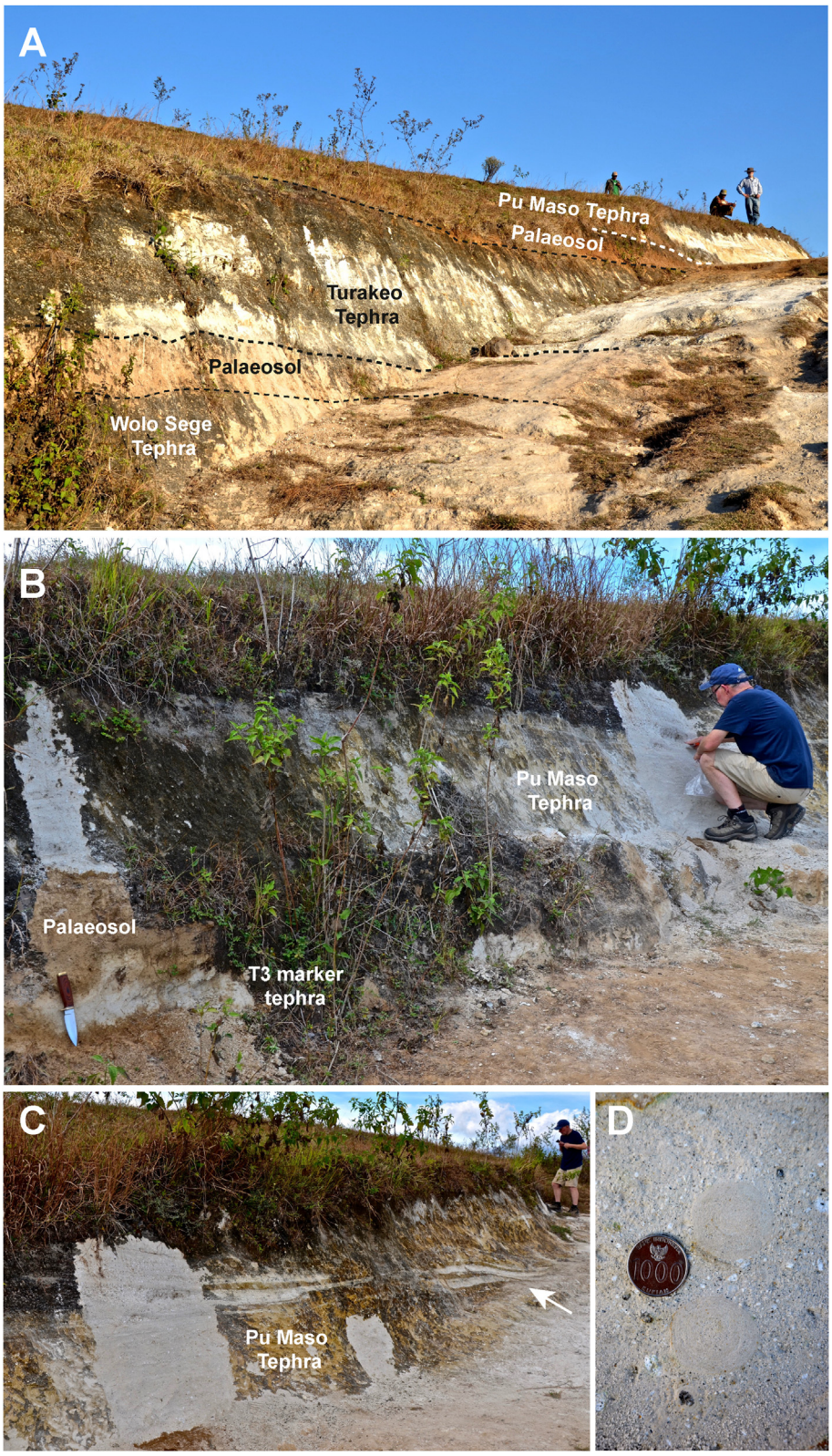

Fig. 6. **A,** Three prominent silicic mass-flow deposits (bottom to top: Wolo Sege, Turakeo and Pu Maso) occurring in close stratigraphic succession at Lowo Mali (08° 41′ 30.0″ S; 121° 10′56.9″ E); **B,** Pu Maso Tephra at Lowo Mali separated from T3 marker tephra, below by an intervening 0.3 m thick palaeosol; **C,** Low-angle cross-bedded pyroclastic (surge) beds of Pu Maso Tephra well expressed at Lowo Mali and indicate a northward-directed paleo-flow direction; **D,** Large (~35 mm diameter) accretionary lapilli within the lower pyroclastic flow sub-unit of Pu Maso Tephra at Lowo Mali. The ubiquity and large size of accretionary lapilli within Pu Maso Tephra enables this tephra to be distinguished from the underlying Turakeo Tephra.

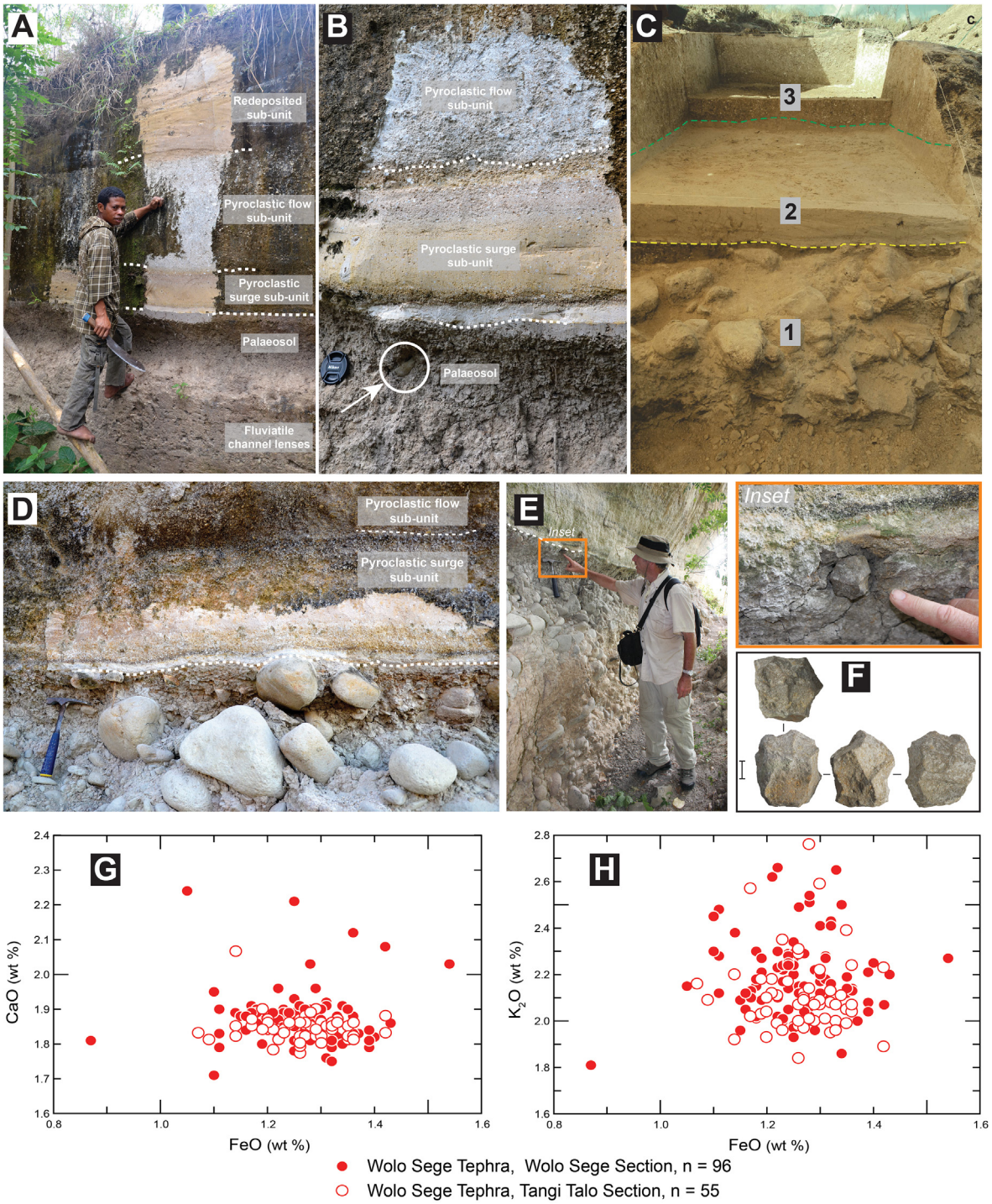

Fig. 7. A-B, Wolo Sege Tephra (WST) at its Wolo Sege Type Section (08° 41′ 26.3″ S; 121° 05′59.6″ E)
Here, the depositional architecture of WST is well expressed and can be subdivided into three distinct sub-units that reflect sequential inundation of the local landscape by pyroclastic surge, pyroclastic flow, and redeposited hyperconcentrated flood flow deposits; **C,** the 1 × 5 m trench excavated at Kobatuwa-IV west of KBT-I. Here the WST, consisting of a lower pyroclastic surge sub-unit with accretionary lapilli (Layer 2) and an upper pumiceous pyroclastic flow sub-unit (Layer 3), directly overlies a pedogenically-overprinted bouldery conglomerate lens (Layer 1) that has yielded 7 stone artefacts; **D,** WST at Mata Go (08° 43′ 06.7″ S; 121° 08′19.3″ E). Here, basal surge beds of WST perceptibly 'pinch-and-swell' over river channel boulders protruding from the underlying palaeosol; **E with inset, F,** A solitary *in situ* bifacially worked radial core was retrieved at the WST/underlying palaeosol contact (scale bar shown in F is 10 mm); **G, H,** Selected glass shard major-element compositions (weight percent FeO vs. CaO and K2O) from WST from the Wolo Sege type section compared with its Tangi Talo correlative. Field correlation of WST between both key sections is confirmed by indistinguishable elemental data.

et al. (2016)). In the tropics C_3 plants are represented by most tree species and high-altitude grasses, whereas C_4 plants comprise most tropical and subtropical grasses. The $\delta^{13}C$ values of fossil herbivore teeth have been widely used in reconstructing paleo-diets of herbivores, and indirectly the vegetation cover and changes thereof through time (e.g., Cerling et al., 2015; Lister, 2013). For the Kobatuwa sample the $\delta^{13}C$ values vary between −6.2‰ and −0.26‰ (Fig. 11; Table G.1). Three individuals have $\delta^{13}C$ values below −5‰

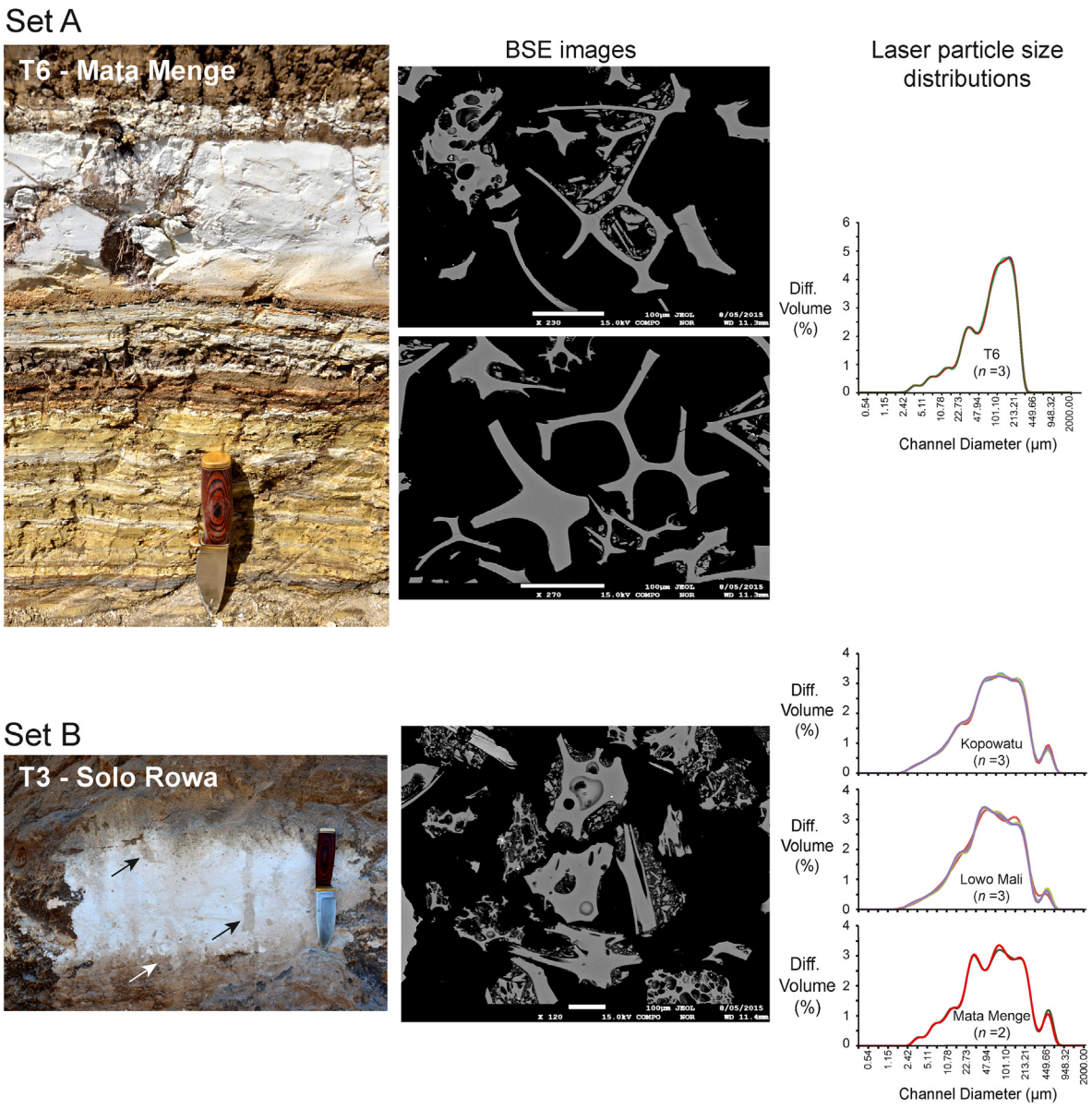

Fig. 8. Two white fine-grained vitric-rich ash beds (T6 and T3) with distinct glass shard geochemistry (see Figs. 4 and 5) have unique correlation potential within OBF sedimentary sequences

Set A, T6 marker bed (~15-cm-thick) occurs within lacustrine sediments of GLM at Mata Menge (08° 41′ 29.2″ S; 121° 05′30.3″ E). Selected backscatter (BSE) images reveal thin-bubble wall shaped shards with conspicuous aggregates of finely comminuted glassy fragments adhering to vesicle recesses and voids. Triplicate laser particle size distributions expressed as microns (µm) versus volume % indicate a pronounced fine-medium ash mode (100–250 µm) and a subordinate secondary coarse silt mode (~40 µm); **Set B,** T3 marker bed (~20-cm-thick) occurs within fluviatile fine sands below Pu Maso Tephra at Solo Rowa (08° 43′ 20.4″ S; 121° 07′11.4″ E). Here, T3 is massive with no discernible bedding but shows evidence of post-depositional insect burrowing and root penetration (indicated by arrows). BSE images indicate dominantly vesicular equant-to elongated-shaped shards with adhering comminuted glass fragments. Laser particle size analyses reveal a broad ash mode (20–250 µm). Note that the fine-grained texture of T3 Tephra remains the same irrespective of its location within the So'a Basin and likely indicates a distal eruptive source.

and four individuals have $\delta^{13}C$ values above −2‰. For large herbivore tooth enamel $\delta^{13}C$ values of between −8‰ and −2‰ are generally considered as indicative of mixed feeders that have a diet of both C_3 and C_4 plants, while values above −2‰ indicate grass feeders or grazers (Cerling et al., 1999; Puspaningrum et al., 2020). The four *Stegodon* individuals with values above −2‰ thus had a diet dominated by C_3 grasses.

The Kobatuwa stone artefact assemblage is composed of flakes and cores from reducing locally-available water-rolled cobbles, and reflects the same pattern seen across all of the So'a Basin sites (Appendix H, Table H.1). Kobatuwa, however, is unusual in the high proportion of cores reduced bifacially and centripetally, resulting in 'radial' cores (n = 27). Three 'perforators' were also recovered, consisting of small versions of the picks documented at Wolo Sege; at Kobatuwa, however, these forms were made on flakes rather than cobbles. Perforators also occur in small numbers at Mata Menge and Liang Bua.

The Kobatuwa artefacts have undergone various degrees of taphonomic rounding, with some in fresh 'as struck' condition. A conjoin set was recovered from Layer G/H, and to date is the earliest *in situ* conjoin set recovered in Southeast Asia. The set consists of a flake which conjoins onto a scar on a bifacial radial core, indicating that the reduction of the artefact occurred close to or at this location. This may also indicate that core reduction occurred where the

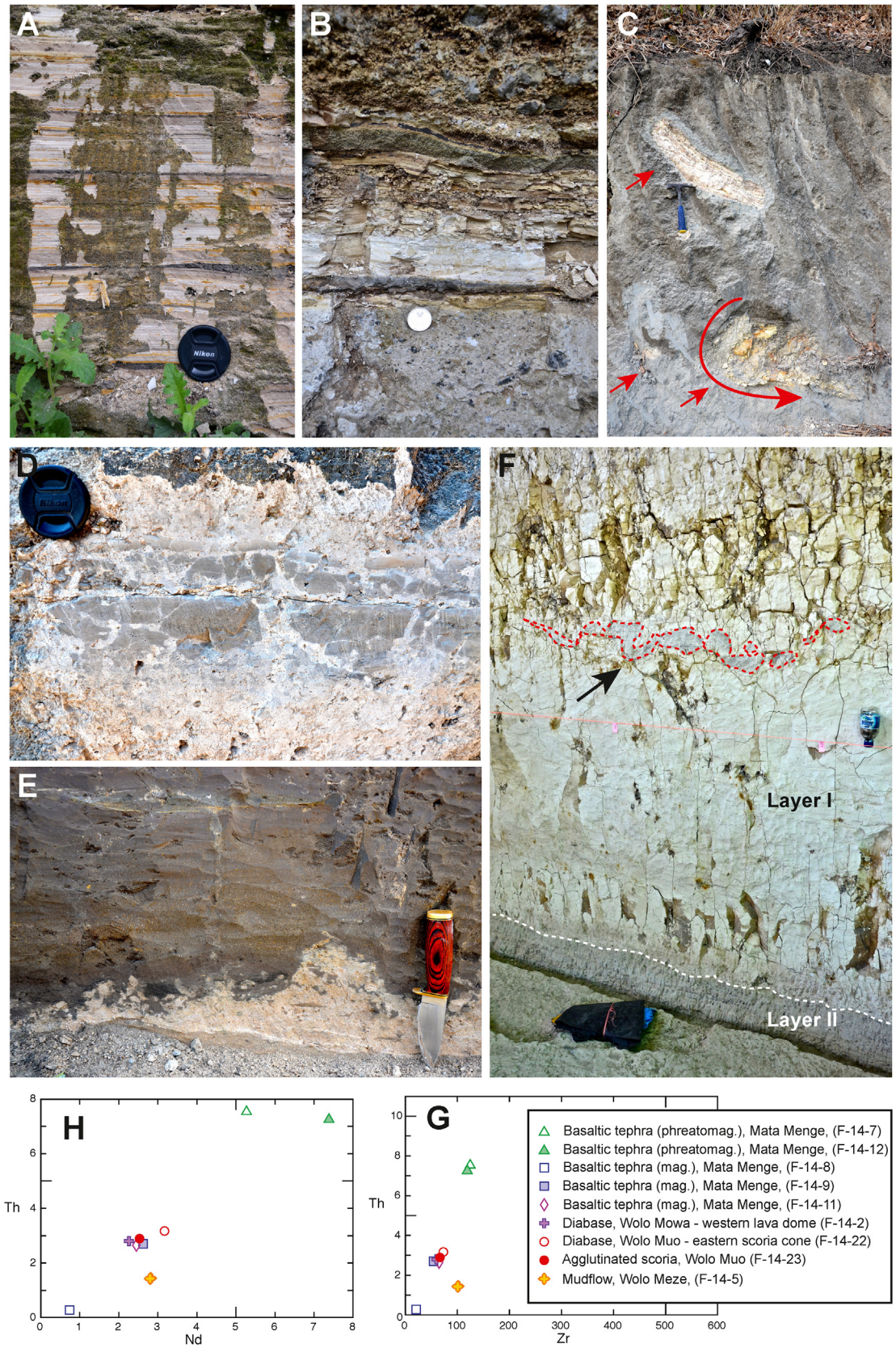

Fig. 9. Volcaniclastic inter-beds of mafic composition are concentrated in the upper portions of OBF, and are particularly conspicuous within GLM lacustrine sediments within Welas Caldera

A, At Poma Section (08° 36′ 52.6″ S; 121° 04′ 31.4″ E) multiple cm-thick phreatomagmatic and magmatic tephra beds are clearly visible within laminated lacustrine sediments of GLM; **B**, Nearby at Wulubara (08° 39′ 02.2″ S; 121° 03′ 38.8″ E) subordinate laminated lacustrine sediments are interbedded by numerous scoriaceous coarse ash and lapilli layers with intervening m-thick subaqueous scoriaceous debris-flow deposits; **C,** At Wolo Meze (08° 38′ 20.8″ S; 121° 03′ 41.0″ E), located mid-way between two intra-caldera basaltic

stones were sourced, with flakes carried back to a (presently unidentified) living or task site.

6.2. Mata Menge

6.2.1. Mata Menge site stratigraphy

At Mata Menge, the total preserved thickness of OBF unconformably overlying OKF is 52 m, including an uppermost 13-m thick interval of GLM recorded in two step trenches that stratigraphically partially overlap, one adjacent to Excavation 32 (slot Trench 12) and one on a hill 600 m further southwest (slot Trench 35, see Appendix A).

Mata Menge is a highly significant fossil-bearing site located towards the north-west margin of the So'a Basin, and has long been of archaeological interest (Fig. 2). Mata Menge, and the nearby site Boa Leza (Appendix A), were discovered and first excavated between 1963 and 1965 by Theo Verhoeven. At this same locality in 1968, Verhoeven undertook a further excavation with Johannes Maringer (Maringer and Verhoeven, 1970a), and described stone artefacts associated with *Stegodon*, crocodile and rodent fossils. In 1991–92, an Indonesian-Dutch team identified Verhoeven's former excavation site at Mata Menge and the *Stegodon* layer was re-excavated, confirming the association of fossil remains with stone artefacts (Sondaar et al., 1994). A series of zircon fission track dates provided the first numerical age for the layer, estimated to be between 8.8 ± 0.7 Ma and 8.0 ± 0.7 Ma (Morwood et al., 1997, 1998). Following the discovery of *H. floresiensis* at Liang Bua in 2003 (Brown et al., 2004), between 2004 and 2009 small-scale excavations at Mata Menge were resumed by an Australian-Indonesian-Dutch team led by the late Mike Morwood (Brumm et al., 2006; Brumm et al., 2010b; van den Bergh et al., 2009a), with these covering an area of 82 m^2 and directly adjacent to Verhoeven's original Mata Menge excavations. The principal aim of these excavations was to recover fossil remains of the Mata Menge toolmaker and putative ancestor of *H. floresiensis*. Between 2010 and 2014 the scale of the Mata Menge excavation was increased, but because working near the original Verhoeven site would imply removing increasingly large quantities of predominantly sterile overburden, the same fossil-bearing interval was excavated in a gently sloping surface area 30–80 m to the northwest of Verhoeven's original site (see Brumm et al., 2016: Fig. 1). Systematic high-volume excavations (560 m^2; see Fig. 12) resulted in the recovery of more than 11,500 fossil specimens and over 1680 stone artefacts (this figure only includes stone artefacts from trenches T1-T8, T23 and T27; Appendix H). The vast majority of the fossils originate from a ~3 m thick multi-layered interval, consisting of up to 0.8 m thick lenses of tuffaceous fluvial silts and sands showing frequent cut-and-fill sequences, with intercalations of minor gravels and clay-rich, cohesive mass-flow (mudflow) deposits (Fig. 12B, E). Fourteen separate lens-shaped layers were recognised, with variable concentrations of fossils and artefacts, and are collectively referred to here as the Lower Fossil-Bearing Interval at Mata Menge (MM-LOW; Fig. 12D). It should be noted that the 'Unit B' described in earlier papers (Brumm et al., 2006; Brumm et al., 2010b; van den Bergh et al., 2009a) is a multilayered tuffaceous sandstone unit exposed in Excavations T1-T8 (Appendix A) adjacent to Verhoeven's original excavation site, and correlates laterally with the basal part of MM-LOW as defined here.

Within the MM-LOW, the majority of the fossil remains are concentrated in the lower 2 m (Fig. 12F). Most of the fossil specimens comprise indeterminable small bone fragments, many of which are rounded and worn by fluvial transport. There is additional evidence that fluvial currents and other taphonomic agents have acted on the bone assemblage prior to burial. *Stegodon* bones have been affected by fluvial sorting (van den Bergh et al., 2009a), and there is an absence of articulated skeletal elements. However, in the eastern part of Trench 25 there are also bone clusters comprising what appear to be single *Stegodon* carcasses, such as a concentration of ribs, vertebra, teeth and limb bones. These occur in the tuffaceous silty layer 8b (Fig. 12B, E, G).

Of further notice is a steep-walled, 2.5 m wide and 2.3 m deep channel-fill developed in the MM-LOW. This unit could be traced in the excavations over a horizontal distance of 35 m along the channel axis (Unit 2, see Fig. 12E, G). The palaeochannel has a high sinuosity and a predominantly N–S orientation in the excavation area. The channel-fill consists of massive clayey silt, suggesting that the channel was abandoned and subsequently filled with suspended sediments. Only a few reworked fossil fragments are present at the base of this channel fill. No palaeo-current measurements were able to be taken in the channel-fill unit, but the steep lateral sides of the erosive channel walls indicate that the underlying tuffaceous sediments were well consolidated during early diagenetic stages, and that reworking of fossil remains from older deposits likely occurred during periods of low sediment supply.

In 2013, excavations were initiated in a younger interval stratigraphically located 10 m above the top of the MM-LOW (Fig. 12D) and ~150 m further west. Excavations of this 90 cm thick interval, referred to here as the Mata Menge Upper Fossil-Bearing Interval (MM-UP) are ongoing. Within this interval (cut by step-Trench-12 and the various sectors of the larger Excavation 32) a well-developed palaeosol (Layer III) is unconformably overlain by a <30-cm thick bed of fluvial sands (Layer II), which in turn is overlain by a ~6.5-m thick sequence of multiple metre-thick clay-rich mudflow deposits (Layer I). The basal contact of Layer II is sharp but highly irregular and erosional, whereas the upper contact of Layer II with the base of mudflow Layer I is almost straight (Brumm et al., 2016). Towards the west Layer II pinches out against the irregular erosional surface of Layer III. Most of the fossil vertebrate specimens occur in the fluvial sandstone layer (Layer II), but fossils are also present within basal portions of the mudflow unit, and very few in the palaeosol underlying Layer II. In 2014, the excavation yielded the first hominin remains, belonging to at least three small-jawed and small-toothed individuals all recovered from the upper

centres that are encircled and on-lapped by lacustrine sediments, dm-thick mudflow deposits are recognised with numerous rip-up clasts of bedded lacustrine sediments (indicated by arrows). One clast (indicated) appears to have been actively disaggregating into the mudflow matrix as it was rotated in an anticlockwise direction during flowage; **D,** Compact, brownish-grey, shower-bedded fine-medium basaltic (phreatomagmatic) ash (~22 cm-thick) from the upper Mata Menge tephra sequence located above Trench 32 at Mata Menge (08° 41′ 29.7″ S; 121° 05′ 37.9″ E; see also Appendix A). This tephra bed has obvious open interstitial pore spaces indicative of syn-depositional rain flushing and is heavily penetrated by bioturbation traces; **E,** Highly irregular (erosional) basal contact of redeposited cross-bedded basaltic ash (hyperconcentrated-flood flow) exposed in step Trench 36 at Mata Menge (08° 41′ 32.3″ S; 121° 05′ 38.5″ E; for location **see** Appendix A). This mass-flow deposit is laterally equivalent to Upper Mata Menge tephra located in nearby exposures; **F,** A prominent (~1.4 m thick) mudflow deposit (Layer I) overlying fluvial pebbly sands (Layer II) exposed in Trench 32C at Mata Menge (08° 41′ 30.3″ S; 121° 05′ 38.7″ E). *Homo floresiensis*-like fossils originate from the top of sandy Layer II (van den Bergh et al., 2016). The upper contact of Layer I is indicated by a discontinuous and highly irregular fine-grained basaltic ash bed (red dashed line) that, while partially saturated, was plastically deformed during rapid deposition of an overlying mudflow deposit. **G, H,** Selected bulk solution nebulization ICP-MS (SN-ICP-MS) trace-element compositions (Th vs. Zr and Nd) from magmatic-phreatomagmatic tephra from Mata Menge and agglutinated scoria and diabase samples retrieved from a basaltic cinder cone complex (east, Wolo Muo) and lava dome (west, Wolo Mowa) within Welas Caldera (see Fig. 1 for location; Table B3). Analyses are indistinguishable and confirm an intra-Welas Caldera eruptive source. Note that phreatomagmatic tephra contain slightly higher values of Th and Nd (cf. magmatic tephra counterparts) and this elemental variation may reflect the incorporation of (and contamination by) lake sediment as the tephra was being violently erupted. Concentrations are expressed in ppm. (For interpretation of the references to color in this figure legend, the reader is referred to the Web version of this article.)

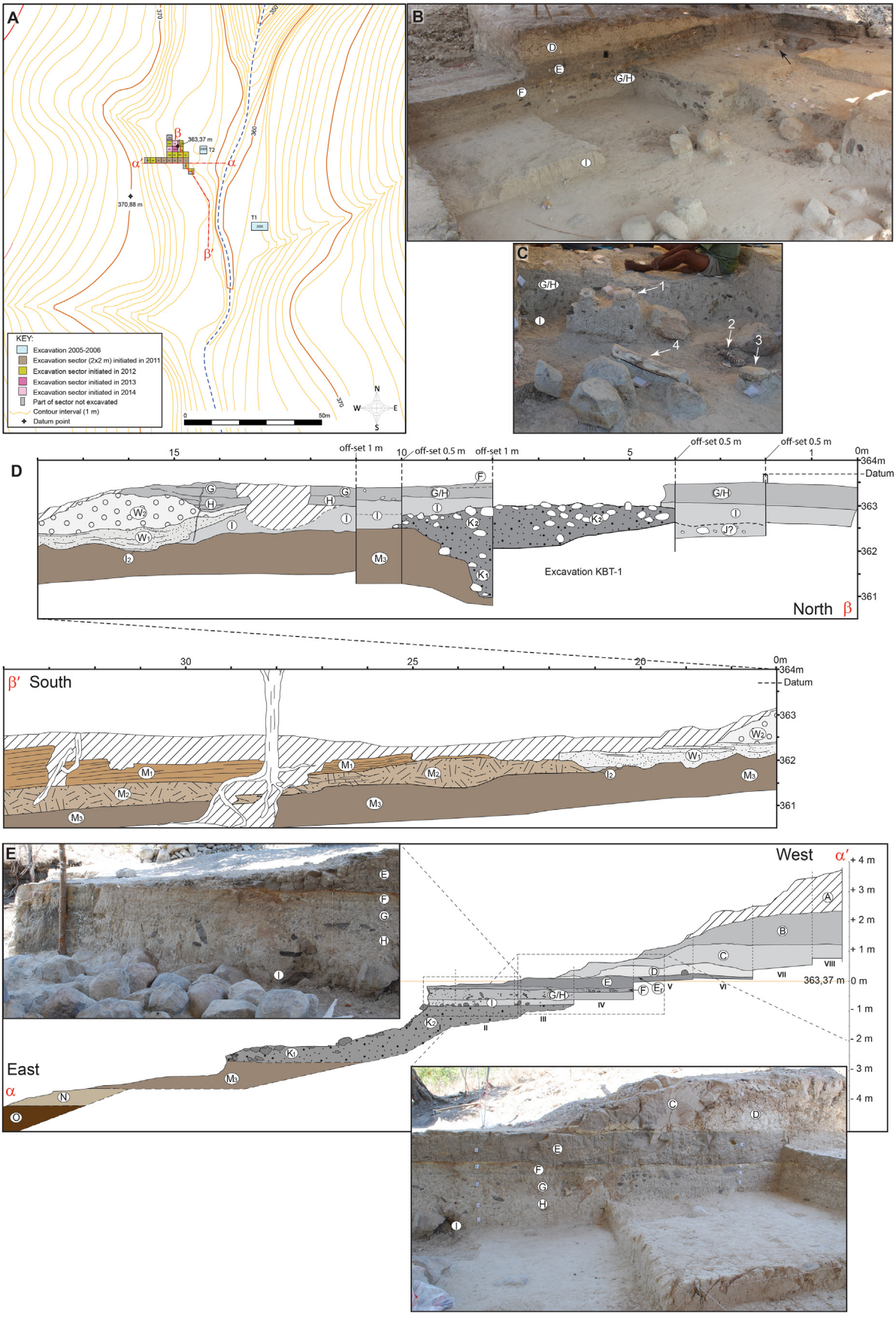
A
B
C
D
E
KEY:
Excavation 2005-2006
Excavation sector (2x2 m) initiated in 2011
Excavation sector initiated in 2012
Excavation sector initiated in 2013
Excavation sector initiated in 2014
Part of sector not excavated
Contour interval (1 m)
Datum point
363,37 m
370,88 m
T1
T2
α
α′
β
β′
N
S
E
W
0
50m
off-set 1 m
off-set 0.5 m
off-set 1 m
off-set 0.5 m
off-set 0.5 m
15
10
5
1
0m
364m
Datum
363
362
361
Excavation KBT-1
North β
β′ South
30
25
20
0m
West α′
East α
+ 4 m
+ 3 m
+ 2 m
+ 1 m
0 m
- 1 m
- 2 m
- 3 m
- 4 m
363,37 m
G/H
W1
W2
I2
M1
M2
M3
K1
K2
J?

part of Layer II (Brumm et al., 2016; van den Bergh et al., 2016). In September 2019, the excavations in the MM-UP had covered a horizontal area of ~204 m^2 (where the main fossil-bearing Layer II has been excavated to base; plus 34 m^2 in sectors where only Layer I and/or a part of Layer II has been excavated).

Palaeomagnetic samples initially taken from the MM-LOW sequence at Mata Menge suggested that the age of the tuffaceous layer with stone tools and fossils could be close to the Matuyama-Brunhes boundary (Sondaar et al., 1994). At that time this boundary was thought to be 0.73 Ma, but is now considered to be 0.773 Ma (Cohen and Gibbard, 2019; Mark et al., 2017). These palaeomagnetic results have been confirmed in a more recent study (Yurnaldi et al., 2018), indicating that the base of MM-LOW is younger than 0.773 Ma (Fig. 2). This age is within the error range of the previously obtained ZFT age of 0.80 ± 0.07 Ma for a sample taken from a normal polarized layer (Morwood et al., 1998: sample MM2 from Unit B1, described as a white tuff and laterally equivalent with the MM-LOW). However, another ZFT age of 0.88 ± 0.07 Ma, obtained 1.1 m lower in the stratigraphy (Morwood et al., 1998: sample MM1 from Unit C, described as a 'pink tuff') appears to be too old, since this same unit has normal magnetic polarity and should be included in the Brunhes Normal Epoch (Yurnaldi et al., 2018). It is likely that the zircon crystals used for fission track dating were reworked from older deposits, since the layer referred to as 'pink tuff' in the publication (Morwood et al., 1998) is now (this study), not considered as a tuff (or tephra) layer but rather represents a zone of intensely altered silty clay with prominent discoloration. This pedogenically-altered silty clay contains rare, poorly preserved bone fragments and stone artefacts (van den Bergh et al., 2009a, p. 66; note that here the fine-grained pink layer is referred to as 'Unit A'). Therefore, we favour the younger interpretation and conclude that the entire MM-LOW is included in the Brunhes Epoch, with an age younger than 0.773 Ma (Mark et al., 2017).

The WST is prominently represented ~ 4-m below MM-LOW in step Trench 9, with a white cm-thick silicic ash inter-bed (Wolowawu Tephra) occurring ~ 3.6 m below WST (Fig. 12D). At many sections within the So'a Basin, WST is frequently associated with the closely overlying Turakeo and Pu Maso Tephras. However, in step Trench E−9/10 these tephra units are conspicuously absent, but are instead recognised (along with the T3 tephra marker) 50-m further north in step Trench-34 (see Fig. 2 andAppendix A). The lateral discontinuity of these silicic tephra markers illustrates that the fluvial sequence corresponding with the MM-LOW interval clearly represents a younger in-fill sequence that has eroded into, and removed, the upper part of this tephra-bearing sequence. Within Trench-34, two successive radiometric dates of 0.90 ± 0.07 Ma (ITPFT), and 0.81 ± 0.04 Ma ($^{40}Ar/^{39}Ar$), were determined from T3 and Pu Maso tephras, respectively (Brumm et al., 2016).

The uppermost part of the Mata Menge section is dominated by lacustrine sediments of GLM as well as the presence of numerous mafic ash and lapilli inter-beds. A mafic coarse ash bed (PGt-02) situated just above the basal contact of GLM yielded a weighted mean $^{40}Ar/^{39}Ar$ age of 0.65 ± 0.02 Ma, providing a minimum age for the MM-UP (Brumm et al., 2016). This age is in accordance with an earlier published zircon FT age of 0.68 ± 0.07 Ma derived from a mafic tephra inter-bed similarly located near the base of the GLM but further east in the So'a Basin (sample 13 of O'Sullivan et al., 2001), which was obtained from the Ngamapa section NW of Lowo Mali: see inset map in Fig. 2). A rhyolitic tephra marker (T6) occurring ~ 6.2-m higher up in the Mata Menge section has a $^{40}Ar/^{39}Ar$ age of 0.51 ± 0.03 Ma (Brumm et al., 2016). Thus far, this is the youngest age obtained from the top of OBF. Notably, the stratigraphic level at which this sample was collected is only overlaid by ~2.5 m of sandy palaeosol (Trench 35; see Brumm et al., 2016), suggesting the age estimate of 0.51 ± 0.03 Ma is close to the *terminus ante quem* for the OBF depositional sequence.

6.2.2. Mata Menge fauna and archaeology

Both the MM-LOW and the MM-UP contain the same faunal assemblage. Only MM-UP has yielded direct evidence of the maker of the stone artefacts (van den Bergh et al., 2016), but hominin fossils are very rare (0.06% of the fossil specimens). As of December 2019, from the MM-LOW and MM-UP the total number of excavated fossils and fossil fragments amounts to 11,730 and 15,535 specimens, respectively. Of all the fossil specimens from these two intervals, those that are attributed to *Stegodon* amount to 49.4% for the MM-LOW and 33.9% for the MM-UP. These are followed by, in decreasing order of abundance, murine rodents (17.2% and 19.0%, respectively), crocodiles (5.8% and 2.0%), Aves (4.6% and 0.56%), *Varanus* (0.2% and 0.68%), Anura (frogs and toads; 0.8% and 0.28%), *H. floresiensis*-like Hominin (0% and 0.05%) and Ophidia (snakes; 0% and 0.01%). The remainder of the specimens (22% and 44%, respectively) represent unidentifiable bone fragments, many of the latter assumingly belonging to *Stegodon*—the only large-bodied animal—judging from the relatively thick cortical bone thickness (Powley et al., 2021). For both levels there are indications that the bone assemblages were subject to fracturing by trampling and fluvial transport, and weathering to various degrees (Powley et al., 2021; van den Bergh et al., 2009a). Hence articulated skeletal elements are very rare and limited to a few *Stegodon* vertebrae in the MM-UP (Brumm et al., 2016). However, concentrations of unarticulated ribs and vertebrae and molars of single *Stegodon* individuals found in close proximity do occur, suggesting that not all fossils have been thoroughly reworked by fluvial action.

The *Stegodon* fossils from both the MM-LOW and MM-UP can be ascribed to *Stegodon florensis*. The type specimen of *S. florensis*, a mandible, originates from the site Ola Bula (4 km east of Mata Menge) and was first described as *Stegodon trigonocephalus florensis* in by Hooijer (1957), who considered it to represent a subspecies of the Early and Middle Pleistocene *Stegodon trigonocephalus* known from Java. Following the collection of more complete material, all the *Stegodon* remains originating from layers stratigraphically occurring above the WST are considered to represent a single endemic species, *S. florensis* (Brumm et al., 2016; van den Bergh et al., 2001; van den Bergh, 1999; van den Bergh et al., 2008). The subspecies name *florensis* was added to distinguish the So'a Basin *Stegodon florensis* from its smaller-bodied Late Pleistocene descendant from Liang Bua, *S. florensis insularis*.

The vast majority of the murine rodent molars from both fossil-

Fig. 10. Site stratigraphy of the site Kobatuwa-I

A, Topographic map of KBT-I showing the sectors excavated since 2005. Profiles β-β′ and α-α′ are shown in Fig. 10D and E, respectively; **B**, View (July 2014) towards the northwest showing from left to right Sector IV, Sector XVI, Sector XIX and Sector XVII. Black arrow points to a *Stegodon* skull fragment. Letter codes refer to successive mass-flow deposits (see main text); **C**, View towards the north of Sector XV, showing various *Stegodon* molars (1−3) and a femur shaft (4) embedded in lahar deposit of Layer I; **D**, north-south profile (along transect β-β′ in Fig. 10A) at KBT-I. Fluvial boulder conglomerate unit K_1 contains large stone artefacts and also yielded two water worn *S. florensis* molar fragments. Basal units with M number codes dip slightly to the south and pertain to the OKF. Layers F, G, H, and I represent clay-rich mudflows that all contain stone artefacts and vertebrate fossils. Layer I is truncated to the south by a channel-fill unit (Layers W_1 and W_2), which consist of reworked pumice tuff that can be geochemically correlated to the Turakeo Tephra; **E,** east-west profile along the KBT-1 excavation trenches (along transect α-α′ in Fig. 10A) and detailed photos of areas framed by the two dashed rectangles. Layer A at the top of the profile can be correlated with the Pu Maso Tephra, providing a minimum age of 0.81 ± 0.04 Ma for the underlying sequence. As shown in Fig. 10D, the clay-rich mass-flow unit Layer I is truncated and overlain by reworked Turakeo Tephra, which dates between 0.9 and 1.0 Ma, providing a maximum age for the main fossil-bearing mudflow Layers G/H at Kobatuwa.

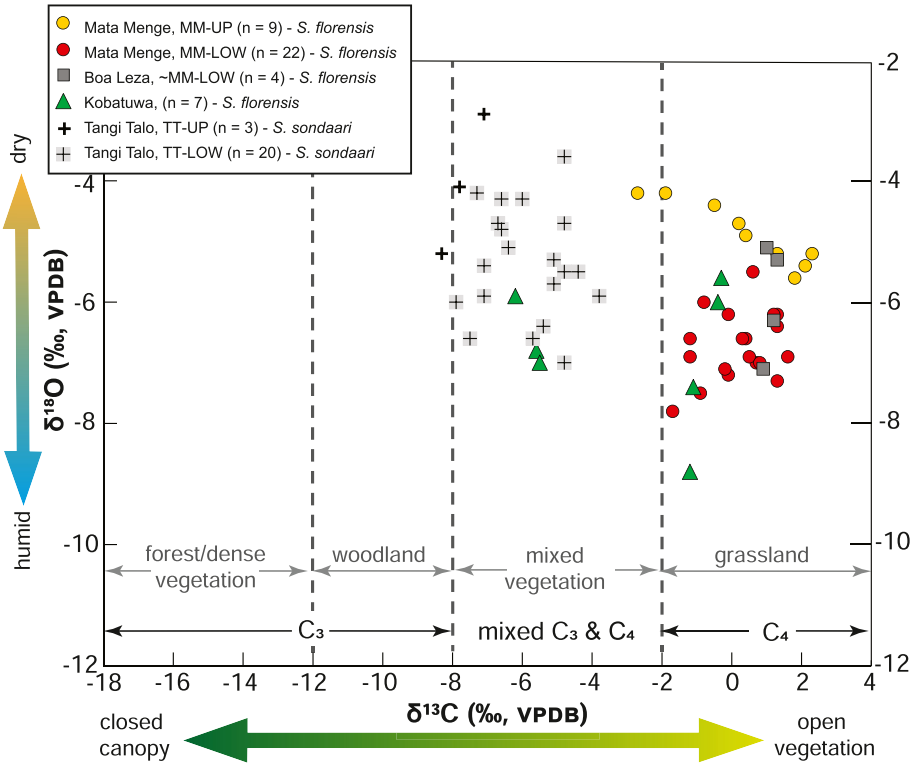

Fig. 11. Mean $\delta^{13}C$ and $\delta^{18}O$ values of *Stegodon* tooth enamel samples from fossil bearing intervals at the sites Mata Menge (MM-LOW and MM-UP), Boa Leza, Kobatuwa and Tangi Talo (TT-LOW and TT-UP) (Puspaningrum, 2016). Dashed lines represent boundaries between vegetation and diet types (Cerling and Harris, 1999; Cerling et al., 1997; MacFadden et al., 1999; Passey et al., 2002).

bearing levels can be attributed to the endemic extinct species *Hooijeromys nusatenggara*, a medium-sized rat that was excavated by Verhoeven at Ola Bula and first described by Musser (1981). Only a single molar of another large-bodied rat, provisionally attributed to *Spelaeomys florensis*, was identified in the MM-LOW (Excavation T-17). This species has not previously been documented from the OBF, but is well known, though relatively uncommon, from the Late Pleistocene and Holocene records of Liang Bua (Locatelli et al., 2012; Veatch et al., 2019). *Hooijeromys*, on the other hand, appears to be very rare in the Late Pleistocene Liang Bua sequence (Veatch et al., 2019), suggesting that these differences in rodent species abundances reflect contrasting environmental conditions rather than temporal differences.

The eight hominin fossils from the MM-UP comprise a small mandible fragment, six isolated teeth and a cranial fragment, and belonged to at least three small-jawed and small-toothed individuals, including one or two juveniles as represented by two deciduous canines (van den Bergh et al., 2016).

Various bird taxa have been identified among the fossil remains from Mata Menge (Meijer et al., 2015). From the MM-LOW seven taxa have been identified, including Anatidae (*Cygnus* sp., *Anas* cf. *gibberifrons* and cf. *Tadorna*), Rallidae (cf. *Gallinula/Fulica*), Accipitridae (cf. *Hieraaetus*), Charadriidae (*Vanellus* sp.), and Passeriformes indet. From the MM-UP a duck has been identified (cf. *Tadorna*) (Meijer et al., 2019), but many bird fossils excavated after 2014 await a detailed identification.

There are 23 varanid fossils from the MM-LOW that can all be attributed to *Varanus komodoensis*, based on the comparatively large size and/or morphology of skeletal elements, and isolated teeth. This material includes a right maxilla and mandible and an isolated parietal (Setiyabudi, 2017) found close together and presumably of a single individual, as well as vertebrae and a humerus. From the MM-UP in total 100 isolated *V. komodoensis* teeth (and tooth fragments) have been recovered, but only five identifiable skeletal fragments.

Crocodilian remains from both Mata Menge levels predominantly consist of isolated teeth, but a small number of skull and postcranial specimens have been recovered from MM-LOW. The anteroposterior diameter and height of the largest recovered tooth measures 13.44 mm and 29.0 mm, respectively, indicating that the Mata Menge crocodiles could reach a considerable size.

Fossils of Anura (frogs) were retrieved from both levels at Mata Menge and are quite rare, but this could be a taphonomic bias. The presence of permanent flowing water during deposition of the MM-LOW is indicated by poorly preserved (casts and moulds) fresh water gastropods, *Brotia testudinaria* and *Tarebia granifera*, indicative of running to episodically stagnant freshwater (van den Bergh et al., 2009a), whereas the MM-UP has yielded numerous moulds of *Cerithidea*, reflecting permanent freshwater conditions (Brumm et al., 2016).

Carbon and oxygen isotope analyses were conducted on tooth enamel samples collected from several *S. florensis* and murine rodent fossils from both fossil-bearing levels at Mata Menge (Brumm et al., 2016; Puspaningrum, 2016). The results indicate a diet dominated by C_4 grasses suggesting both species were grazers and imply that open grassland vegetation was predominant within the So'a Basin at that time. The Mata Menge values of $\delta^{13}C$ and $\delta^{18}O$ of *Stegodon* tooth enamel from both the MM-UP and MM-LOW are compared with the values of *Stegodon* samples from other So'a Basin localities (Fig. 11; Appendix G). Despite the larger number of samples analysed from both Mata Menge levels as compared to only seven samples from the older site Kobatuwa, the spread of $\delta^{13}C$ values in both Mata Menge levels is lower and except for one sample from the MM-UP generally above −2‰, indicating a grass-

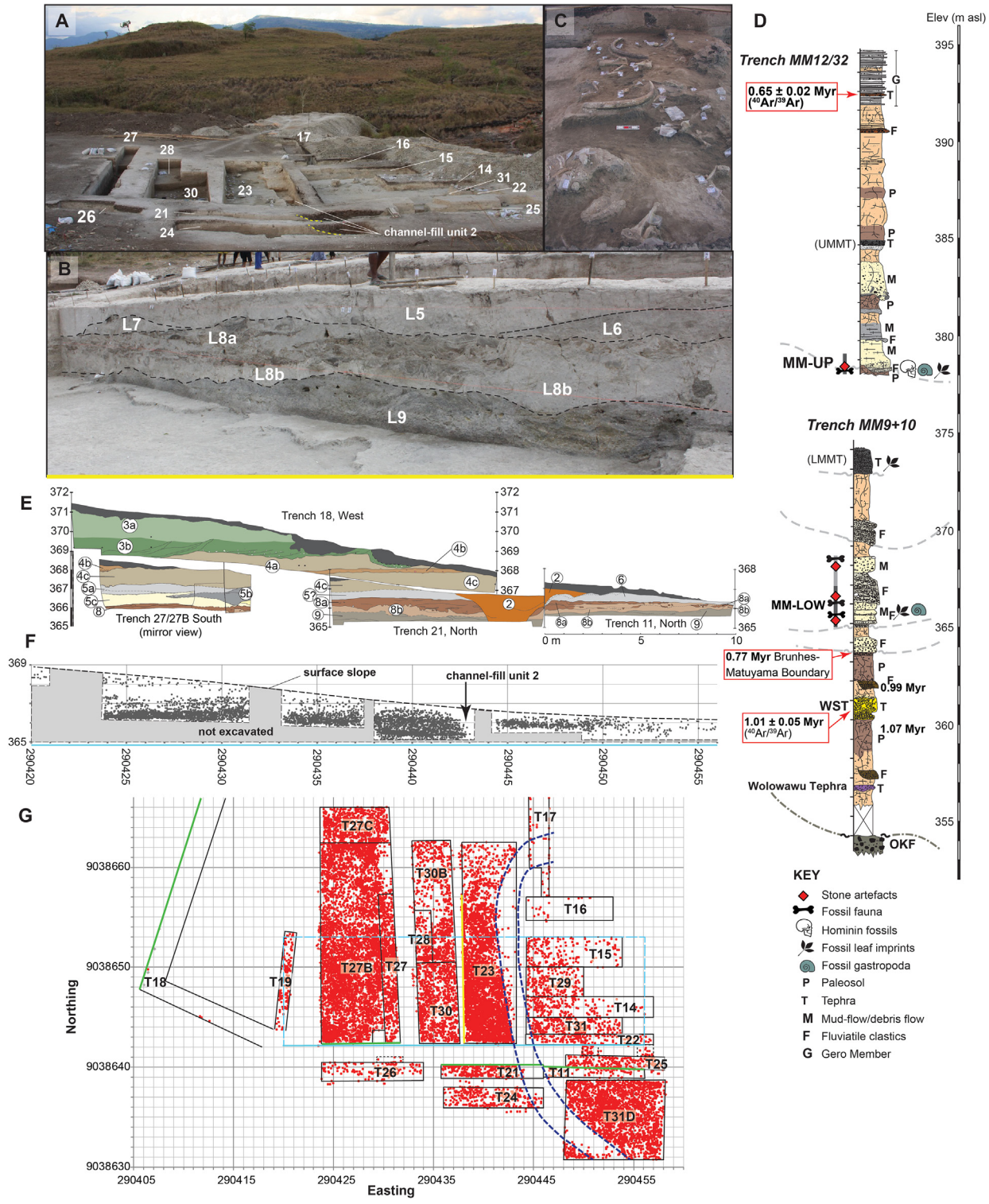

Fig. 12. Site stratigraphy and fossil and cultural finds at Mata Menge. **A,** view to the north of the excavations in the MM-LOW towards the end of the 2011 field season. Numbers refer to trenches. The dipslope visible on the horizon is the slope of the east rim of the Welas Caldera, which acted as source of the volcanogenic clay-rich mudflows deposited within the paleo-creek valley at Mata Menge; **B**, west profile of Trench 23 (MM-LOW) as exposed in 2012 (location indicated with yellow line in Fig. 12G) showing vertically-stacked, multiple horizons of hyperconcentrated stream flow, clay-rich lahar, and fluvially reworked volcaniclastic sand deposits. Numbers refer to layers. Note soft-sediment deformational structures in Layer 8a/b, suggesting very rapid deposition and loading. Layers 8 and 9 are both rich in fossil remains as well as stone artefacts. Poles at top profile are 1-m spaced; **C**, Concentration of *S. florensis* bones exposed in Trench 29, Layer 8b (tuffaceous silt); view is towards the west. Scale is 30 cm; **D**, Schematic stratigraphic section at Mata Menge as recorded in slot trenches MM9+10 and 12 (see **Appendix A**for locations), with the lower (MM-LOW) and upper (MM-UP) fossil-bearing intervals indicated. Sections are drawn to the same scale as the stratigraphic profiles covering the MM-LOW shown in Fig. 12E (for a more complete stratigraphy of the upper part of the sequence see Brumm et al. (2016); **E**, Profile drawings of selected excavation trenches shown in relative elevation. Orientation of the profiles is indicated by green lines in Fig. 12G. Numbers refer to layered units. Note the narrow channel fill (Unit 2) that cuts down into the rapidly deposited fluviovolcanic mass-flow sequence, which was deposited during and following a volcanic phase that generated abundant fine-grained volcaniclastic sediments. The rapid deposition and sediment coverage associated with this volcanic activity likely facilitated fossil preservation. Fluvial downcutting followed when sediment supply diminished (i.e., Unit 2, which hardly contains fossils as shown in Fig. 12F and G); **F**, East west cross-section through the MM-

dominated diet. While the $\delta^{13}C$ values of *Stegodon* tooth enamel samples from MM-LOW and MM-UP are both consistent with the range for grazers, there are significant differences in $\delta^{18}O$ between the two levels (Brumm et al., 2016). The positive shift in $\delta^{18}O$ values for the MM-UP could be the result of a distinct source of drinking water (i.e., run-off versus lacustrine) or warmer and drier conditions with increased evaporation for the MM-UP.

Pollen samples from both fossil-bearing intervals (Brumm et al., 2016), and phytoliths analysis of four samples from the MM-LOW (van den Bergh et al., 2009a), similarly indicate a grassland-dominated savannah-like landscape with nearby wetlands, as well as scattered patches of forest. The sandstone layers of both MM-LOW and MM-UP frequently contain abundant macro fragments of grassy leaves and strobili of *Equisetaceae* (horse-tail), the latter usually preferring wet sandy soils (van den Bergh et al., 2009a). The avian fauna from the MM-LOW also points to an open grassy environment, with nearby open water (Brumm et al., 2016; Meijer et al., 2015).

Stone artefacts occur in all excavated layers of the MM-LOW, but are more concentrated in sandy layers 8a and 8b and in pebbly sand layer 4b (Fig. 12E). A description of stone artefacts excavated from the MM-UP (T-32) until 2014 has been summarized previously (Brumm et al., 2016). Since then, a small number of additional stone artefacts have been excavated from MM-UP, resulting in a current total of 162 artefacts. The analysis presented in Appendix H does not include artefacts excavated between 2015 and 2019. Some of the artefacts are lightly to heavily abraded from water-transport, but a significantly high proportion (74.5%) are in fresh, as-struck condition, suggesting minimal dislocation from the nearby sites where they were originally flaked. To date, an analysis of a large assemblage ($n = 1680$) of *in situ* stone artefacts from the MM-LOW (Excavations T1 to T8 and T23 and T27) indicates 'least effort' reduction of locally available river pebbles and cobbles, resulting in single-platform, multiplatform, and bifacial centripetal cores. Flakes are abundant, some of which are retouched (Brumm et al., 2006, 2010b; Moore and Brumm, 2007).

6.3. Wolo Sege

6.3.1. Wolo Sege site stratigraphy

Wolo Sege is located half a kilometre east of Mata Menge (Appendix A) and occurs in the southwestern corner of a cattle enclosure at the head of a small gully, which is naturally bracketed on three sides by ~ 3-m-high vertical cliff embankments. These embankments substantively expose a ~4 m thick silicic pumiceous-ashy mass-flow deposit that upwardly transitions from pyroclastic flow (primary) deposit to overlying reworked (secondary) deposit (Fig. 7A and B). This deposit, with its unique depositional architecture, was named Wolo Sege Ignimbrite (here referred to as the WST - Wolo Sege Tephra) and yielded a crystal (hornblende) $^{40}Ar/^{39}Ar$ age at 1.02 ± 0.02 Ma (Brumm et al., 2010a). Directly beneath the WST is a ~0.4 m thick well-structured palaeosol developed into a ~0.7 m thick fluviatile sequence comprising multiply stacked gravelly-sand and sandy-gravel channel lenses overlying a ~ 1-m thick pedogenically-altered massive bedded silt layer, which in turn, is unconformably overlying indurated volcanic breccias of the OKF. Archaeological excavations were carried out in 2005 (Brumm et al., 2010a) and extended in 2010 to target the fluviatile layers underneath the WST (Fig. 13A–C). A step trench was excavated uphill, from the top of the WST, and covered 26 m of stratigraphy, which enabled a detailed comparison with the nearby Mata Menge sequence (Appendix A, Fig. 2**).**

Exposed in the step trench, and separated from WST below by a ~0.5 m thick strongly developed palaeosol, are two closely-spaced metre-thick silicic pumice-ash-dominated hyperconcentrated-flood flow deposits correlated with Turakeo and Pu Maso tephras, respectively. The T3-tephra marker is recognised as a discontinuous cm-thick fine ash inter-bed within a well-developed palaeosol intervening between these two tephra. The remainder of the section above Pu Maso Tephra (17m+) is predominantly massive pedogenically-altered silts and variably developed palaeosols with occasional outcropping cm-to dm-thick lenses and shallow scour-fills of fluvial-bedded cemented sands and gravels (Fig. 2). The coarse-grained cut and fill sequence observed in the MM-LOW at Mata Menge does not occur at Wolo Sege. Fine-grained mudflows sealing off fossil-rich layers as developed in the nearby Mata Menge and Boa Leza sequences (see sections 6.2.1 and 6.4.1) are not developed at Wolo Sege, and the site has not yielded any fossil vertebrates. However, apart from the lithic artefacts found in the archaeological excavations below the WST marker, sparse stone artefacts do also occur at two levels in palaeosols near the top of the Wolo Sege section.

6.3.2. Wolo Sege archaeology

As noted, the Wolo Sege excavations have yielded no faunal remains. However, 168 stone artefacts (including 48 artefacts reported in Brumm et al., 2010a) were recovered within the 2.5-m thick fluviatile sediment sequence intervening between the WST above and breccias of the OKF, below (Fig. 13B–C). Most of the Wolo Sege artefacts occur *in situ* within the fluvial conglomerate lenses, and consist of small and medium-sized flakes struck from water-rolled cobbles by direct hard-hammer percussion. Three large Acheulean pick-like implements were recovered at Wolo Sege, and are so far the only excavated examples from the So'a Basin sites (Brumm et al., 2006, 2010b, 2016). Three bifacially and centripetally worked cores, similar to those from Kobatuwa and Mata Menge, have also been identified (Moore and Brumm, 2007, 2009) (see Appendix H).

The Wolo Sege artefacts typically exhibit taphonomic alteration in accordance with the type of sedimentary material they are lodged within. By illustration, the majority of artefacts from the fluviatile conglomerates display heavy (~75%) to slight (~18%) surface abrasion and edge damage indicating fluvial transportation, whereas those from the palaeosol underlying WST and basal fluviatile silt layer overlying OKF are fresh and unabraded (Brumm et al., 2010a).

Toward the very top of the Wolo Sege step trench section, isolated *in situ* stone artefacts were retrieved from pedogenized silts ~15 and 16.8 m above the 0.81 Ma Pu Maso Tephra. These artefacts were deposited prior to the Gero lake formation at ~0.65 Ma and well after the deposition of Pu Maso tephra at ~0.81 Ma.

6.4. Boa Leza

6.4.1. Boa Leza site stratigraphy

Boa Leza, another of the sites originally excavated by Verhoeven,

LOW showing the vertical distribution of fossils excavated within the area indicated with the light blue dashed rectangle in the plan view of Fig. 12G. Each dot represents a fossil specimen with its vertical elevation projected onto the cross section; note that the scale of the projection is the same as in 11E, but smaller than in 11G; fossils occur in all layers but are concentrated in layers 8 and 9; **G**, Horizontal plan of the 2010–2014 Mata Menge excavations in the MM-LOW, showing the outlines of the trenches and the horizontal co-ordinates of fossil finds (red dots); green lines indicate profiles shown in Fig. 12 E; yellow line shows the orientation of the profile shown in Fig. 12B; dark blue dashed lines indicate the sinusoidal course of the channel-fill Unit 2; note that Trench 18 was dug by an excavator and therefore has very few fossil finds. (For interpretation of the references to color in this figure legend, the reader is referred to the Web version of this article.)

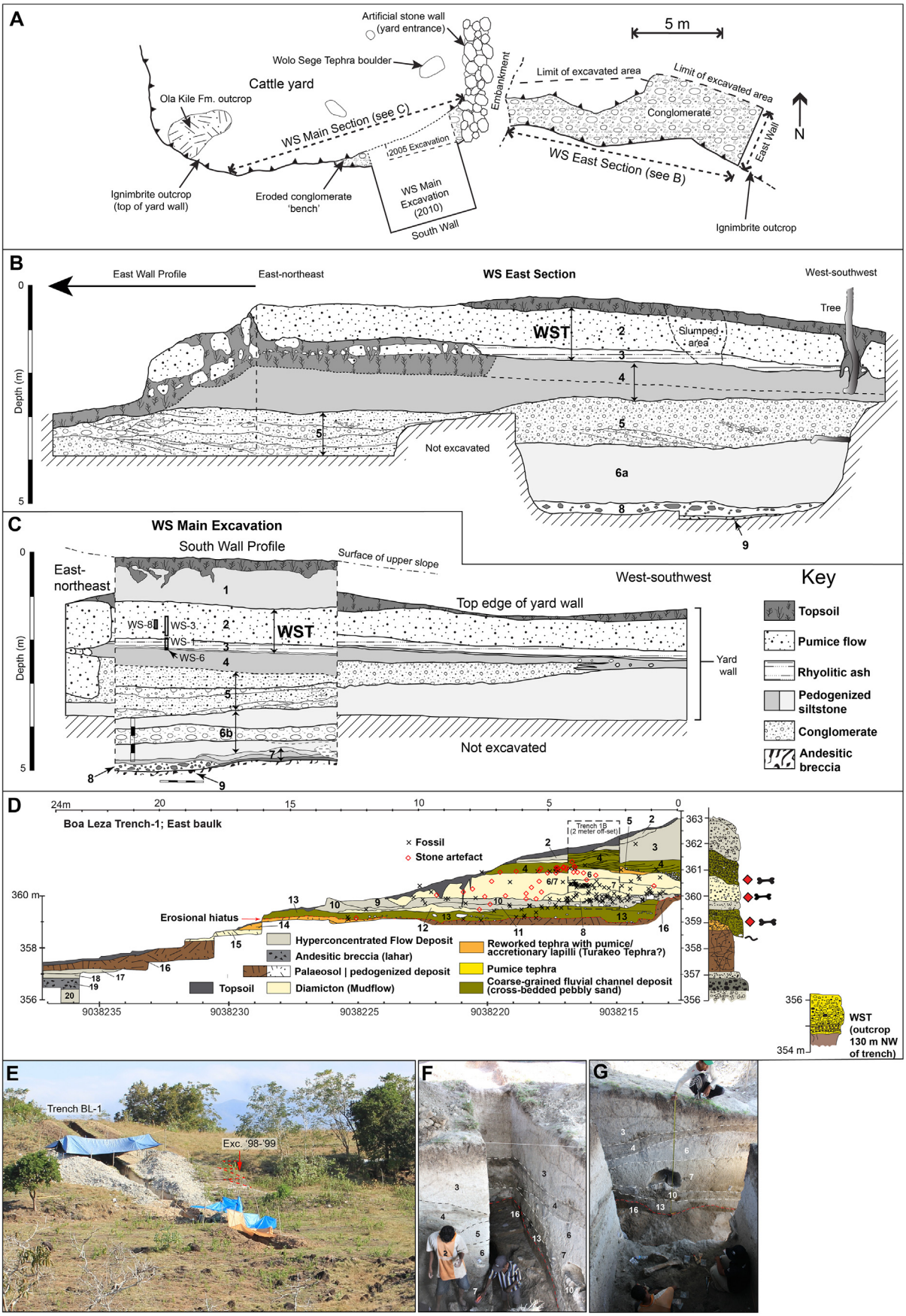
A
Artificial stone wall (yard entrance)
5 m
Wolo Sege Tephra boulder
Cattle yard
Ola Kile Fm. outcrop
Embankment
Limit of excavated area
Limit of excavated area
Conglomerate
East Wall
N
WS Main Section (see C)
2005 Excavation
WS East Section (see B)
Ignimbrite outcrop (top of yard wall)
Eroded conglomerate 'bench'
WS Main Excavation (2010)
South Wall
Ignimbrite outcrop
B
East Wall Profile
East-northeast
WS East Section
West-southwest
Tree
WST
Slumped area
Not excavated
Depth (m)
C
WS Main Excavation
South Wall Profile
Surface of upper slope
East-northeast
West-southwest
Top edge of yard wall
WS-8
WS-3
WS-1
WS-6
WST
Yard wall
Not excavated
Key
Topsoil
Pumice flow
Rhyolitic ash
Pedogenized siltstone
Conglomerate
Andesitic breccia
D
Boa Leza Trench-1; East baulk
Trench 1B (2 meter off-set)
Fossil
Stone artefact
Erosional hiatus
Hyperconcentrated Flow Deposit
Andesitic breccia (lahar)
Palaeosol | pedogenized deposit
Topsoil
Diamicton (Mudflow)
Reworked tephra with pumice/ accretionary lapilli (Turakeo Tephra?)
Pumice tephra
Coarse-grained fluvial channel deposit (cross-bedded pebbly sand)
WST (outcrop 130 m NW of trench)
E
Trench BL-1
Exc. '98-'99
F
G

is located 500 m south of Wolo Sege and 675 m southeast of Mata Menge (Appendix A). Verhoeven's site was re-excavated in 1998–99, revealing that *S. florensis* fossils and stone artefacts occurred here in a 2 m thick tuffaceous channel cut and fill sequence (Morwood et al., 2009). A ZFT age of 0.84 ± 0.07 Ma was obtained from a homogeneous white silt facies interbedded with fossiliferous coarse pebbly sandstone facies, suggesting broad contemporaneity with the MM-LOW (Morwood et al., 2009; O'Sullivan et al., 2001).

In 2012, we excavated a 1 m wide and 25 m long north-south oriented slot trench (BL1) 8 m east of the 1998 excavations, in order to place the Boa Leza fossil-bearing channel fill sequence in the general stratigraphic scheme. A 2 × 2 m extension (BL1b) was also excavated on the East side of the step trench. These excavations revealed a 7 m thick succession directly overlying the OKF, and in which twenty separate layers could be distinguished, exhibiting a complex cut and fill sequence of fine-grained diamictons or mudflows, pebbly sandstones and reworked tephra beds (Fig. 13D–G). Compared to the nearby sequences at Mata Menge and Wolo Sege, both the WST and Turakeo Tephra are missing in the Boa Leza trench, but the WST is exposed in several outcrops between 130 and 200 m northwest and west of the slot trench. Fluvial downcutting appears to have removed both of these marker tephras at the BL-1 trench site. The presence of a steep ENE dipping erosional surface that cuts down a well-developed palaeosol suggests that the channel axis was approximately oriented NNW-SSE, similar to the channel inferred from the adjacent excavations undertaken in 1998 (Morwood et al., 2009). A prominent boulder channel lag with large intraclasts of the underlying bedrock overlies the erosional surface, which is in turn covered by an interval of intercalating diamictons, cross-bedded pebbly sand lenses, and tuffaceous siltstone lenses (Fig. 13F and G), which is a facies association similar to the fossiliferous valley-fill sequence developed at Mata Menge.

6.4.2. Boa Leza fauna and archaeology

Stegodon fossils and stone artefacts are mostly associated with either massive-structured clay-rich mudflow or gravelly to silty sand bedded hyperconcentrated-to flood-flow deposits. In total, 478 fossil specimens were recovered from the Boa Leza trenches BL-1 and BL-1b, of which 119 were representing identifiable skeletal elements and molars of *S. florensis* (25%), along with one crocodile tooth, two *Hooijeromys nusatenggara* molars, and a tibiotarsus of a juvenile Eagle Owl, *Bubo* sp. (Meijer et al., 2015). The remainder are unidentified bone fragments. The more complete and larger *Stegodon* bones tend to be concentrated at the boundary surfaces of the diamicton layers. Although none of the *Stegodon* bones were articulated, the left and right humeri, left radius and left ulna of a single subadult individual, plus 23 costa and a number of vertebrae of likely the same individual, were found in close proximity (in a 4 m^2 area) at the boundary between diamicton layers 6 and 7. This indicates that these *Stegodon* bones were not transported far by the viscous mudflow that covered them. The minimum number of individuals based on identifiable molars is four individuals.

Four *S. florensis* molar fragments from the base of Layer 4 were used for $\delta^{13}C$ stable isotope analysis of the enamel. All four samples fall within a narrow range of $\delta^{13}C$ values between 0.9 and 1.3‰, reflecting a C_4-dominant (i.e., grass-dominated) diet (Fig. 11; Appendix G). This is within the range of −2.0 to 1.6‰ for samples reported from the MM-LOW (Brumm et al., 2016), but above the range for the Kobatuwa I samples.

The cross-bedded sandy Layer 4 (Fig. 13D) is largely devoid of fossils, but does contain stone artefacts near its base. A total of 39 *in situ* stone artefacts were excavated from the BL-1 trenches, which are in addition to the six artefacts excavated from the adjacent Boa Leza excavations in 1998 (Morwood et al., 2009). Detailed analysis of the Boa Leza artefact assemblage has yet to be undertaken.

6.5. Tangi Talo

6.5.1. Tangi Talo site stratigraphy

Tangi Talo (TT) is a significant fossil-bearing site located in the central part of the So'a Basin (Fig. 2) and close to its depocentre (Aziz et al., 2009a; O'Sullivan et al., 2001; van den Bergh, 1999). Here, an expanded sequence of lower OBF (Tuff Member) occurs in a ~31-m thick hillside exposure that rests unconformably upon lithified volcaniclastic deposits of OKF. Sections revealing such an expanded stratigraphy beneath WST are only developed in the

Fig. 13. Site stratigraphy of key sites in the So'a Basin: Wolo Sege and Boa Leza.
A-C, Site plan and stratigraphic profiles of excavations at the type locality of the Wolo Sege Tephra, Wolo Sege. The site is located at the head of a modern gully in which erosion of sediments within the basal part of the Ola Bula Formation has resulted in the formation of a steep-sided hollow, walled-off on one side and used as a cattle yard. The plan (**A**) shows the southern edge of the yard and adjacent area indicating the locations of the excavated trenches, Wolo Sege East Section and Wolo Sege Main, for which stratigraphic profiles are shown in **B** and **C**, respectively. Stratigraphic layers are: 1) co-ignimbritic ash with associated redeposited ash and lapilli; 2) pumice-rich ignimbrite; 3) basal stratified ash with accretionary lapilli; 4) silt-rich and pedogenically-altered overbank deposit; 5) fluvial conglomerate; 6a-b) pedogenically-altered silt-rich overbank deposits with interbedded gravels; 7) hydrothermally? altered crusts covering the unconformable contact with the underlying Ola Kile; 8) cemented crust with reworked breccia; 9) laharic breccia (OKF). $^{40}Ar/^{39}Ar$ dating of Layers 2 (WS-3) and 3 (WS-1/WS-6) yielded an isochron age of 1.01 ± 0.02 Ma (Brumm et al., 2010a) (±2σ; external uncertainty), and (U–Th-Sm)/He dating of Layer 2 (WS-8) has now yielded an age of 0.98 ± 0.05 Ma (±2σ). *In situ* artefacts were recovered from Layers 4–6. In 2005, a test-pit was excavated into a protruding conglomerate outcrop and associated overbank deposits exposed beneath the Wolo Sege Ignimbrite (Brumm et al., 2010a). No vertebrate fossils were found, but the excavations recovered a total of 65 *in situ* stone artefacts – a figure that now includes 20 previously unreported specimens. In 2010, an ~15 m^2 trench was excavated to the south of the previous test-pit and an outcropping exposure of the WST to the east of the excavation area was also cleared of overburden, revealing a 14.5 m long stratigraphic section. Excavations at these localities yielded 169 *in situ* flakes, cores and other implements from the conglomerate and overbank deposits, giving a total of 234 *in situ* stone artefacts from Wolo Sege. All of these artefacts were recovered from below the WSI and thus have a minimum age of ~1.0 Ma.
D-G, Site stratigraphy of Boa Leza: **D**, Stratigraphic profile of the eastern wall of Trench BL-1 (left) and the 7-m thick stratigraphic column recorded in the trench. Vertical scales indicate DGPS ellipsoid elevations in m, horizontal scale indicates the UTM northing coordinates. The 1-m wide Trench BL-1 is located adjacent to the 1998–99 excavation by Morwood (Morwood et al., 2009; O'Sullivan et al., 2001) (see **E**) and Verhoeven's 1963 excavation (see Maringer and Verhoeven, 1970a,b). Layering is horizontal and the trench cuts through the basal Tuff Member and the Sandstone Member, but the prominent marker tephras from the Tuff Member (WST, Turakeo Tephra and Pu Maso Tephra) are eroded and lacking. Similar to Mata Menge, at Boa Leza a complex cut-and-fill sequence of intercalating fossiliferous hyperconcentrated flow deposits, clay-rich mudflows, and coarse-grained cross-bedded fluvial channel deposits has filled in a deeply incised channel or valley eroded in an older prominently developed palaeosol with the same texture as the palaeosol underlying the WST in the Mata Menge section (Trench MM9/10: 357–359 m). Red crosses and green triangles indicate horizontal projections of vertebrate fossils and stone artefacts, respectively, which were excavated in the trench. Fossils tend to be primarily associated with the mass-flow deposits developed in the valley fill sequence, less so with the cross-bedded fluvial sands; **E**, View towards the southwest of the 24.5 m long Trench BL-1 in 2012. Red dashed line shows the outline of the 1998–99 excavation (Morwood et al., 2009); **F**, Southern end of Trench BL-1 and the 2 × 2 m eastward extension (Trench BL-1b) to the left. Red dashed line indicates the erosive surface that cuts down at least 2 m vertically into a well-developed palaeosol. This same erosive contact is also recorded in the 1998–99 excavations ((Morwood et al., 2009): boundary between Unit D and Unit C). The ZFT age of 0.84 ± 0.07 Ma reported in (O'Sullivan et al., 2001) was taken in a white tuffaceous siltstone layer ((Morwood et al., 2009): Layer B1, above Unit C), and thus corresponds with the valley fill sequence above the erosive contact. However, due to the short-distance lateral changes in lithology it is not possible to correlate Layer B1 exactly with the sequence exposed in Trench BL-1; **G**, Concentration of *Stegodon* bones in Trench BL-1B. The opposite wall is part of the west baulk of Trench BL-1, again showing the erosive contact indicated by the red dashed line. . (For interpretation of the references to color in this figure legend, the reader is referred to the Web version of this article.)

central and southern parts of the basin. The uppermost part of the TT sequence is dominated by two closely-spaced silicic mass-flow deposits correlated with Wolo Sege (lower) and Turakeo (upper) Tephra. Both tephras are characterized by an upward transition from pyroclastic flow (primary) deposits to overlying reworked (secondary) deposits. The Wolo Sege correlative at this section is here $^{40}Ar/^{39}Ar$-dated at 0.98 ± 0.02 Ma (SF-FLO12-TT1; **See** Appendix C, Fig. C2**)**, and is indistinguishable from the previously reported $^{40}Ar/^{39}Ar$ age obtained from WST at Wolo Sege (Brumm et al., 2010a). At Tangi Talo, below WST is a ~15-m thick sequence of dominantly fine-textured pedogenically-altered sands, silts and clays with intervening well-developed palaeosols. A conspicuous white cm-thick silicic ash inter-bed (Wolowawu Tephra) occurs at ~ 7 m depth below WST.

The lowermost part of the TT sequence (between 15 and 21 m below WST) contains three silicic air-fall ash beds (i.e., TTT-5 [Lowo Lele tephra], TTT-2 and TTT-1) as well as a complex cut-and-fill sequence of a series of clay-rich cohesive mass-flow (mudflow) deposits (Fig. 2). The lowest mudflow (TTT-3 in Fig. 3F) is white in color, with a matrix containing abundant dispersed pumiceous lapilli clasts, and can be traced laterally over several hundreds of metres. Locally, the upper surface of this mudflow is an erosive boundary and lenses of white parallel laminated tuffaceous silt have infilled depressions eroded in the top of this mudflow (see for example Fig. 14B). This pumice mudflow directly overlies a widespread bone bed (Fig. 3F), which represents the main fossiliferous layer at Tangi Talo. At the northern locations the fossil bones are concentrated near the base of the mudflow (Excavations TT-G and TT-L), whereas at the excavations further south (Excavation TT-H and TT-I) the bones are dispersed throughout the pumiceous mudflow, suggesting bones lying on the surface were incorporated into the mudflow downslope. Tephra TTT-5, with its base at 2 m above the main bone bed in Excavation TT-G (Fig. 3F), contains lapilli, whereas TTT-2 and TTT-1 below the bone bed are very fine-grained and incorporated in a 3.5 m thick sequence of pedogenically-altered silts and occasional lenses of fluvial-bedded conglomerates and sands.

The main bone bed and its associated pumice-rich mudflow were excavated at five sites spread out over a horizontal distance of 172 m **(**Fig. 14A–E). A total station was used to record 3D co-ordinates of fossils and layer boundaries. The bone layer is dipping between 0.8 and 2° towards the WSW, and the most likely source of the volcanic mudflow is to the east (see Fig. 14E).

Two $^{40}Ar/^{39}Ar$ ages were obtained from this lower interval. Hornblende crystals retrieved from pumice lapilli of Lowo Lele tephra (TTT-5) (Fig. 3F) yielded an age of 1.27 ± 0.03 Ma (SF-FLO12-TT7; see Appendix C). Plagioclase crystals, extracted 2 m lower in the sequence from pumice lapilli from the base of the white pumice-rich mudflow deposit that covers and incorporates the bones (TTT-3), yielded an older $^{40}Ar/^{39}Ar$ age of 1.418 ± 0.02 Ma (SF-10/TT/001; see Appendix C). As mudflow deposits frequently exhibit channel-margin and basal erosional contacts, it is possible that older material was entrained in this deposit. This is reflected in the Ar-isotope data, where individual crystals produced a range of apparent $^{40}Ar/^{39}Ar$ ages. However, stepped heating $^{40}Ar/^{39}Ar$ data from individual crystals with older apparent ages indicates thermal loss of radiogenic ^{40}Ar, implying that xenocrysts entrained during eruption were partially reset during emplacement. The 1.4 Ma age represents the youngest population of crystals analysed from the pumiceous mudflow unit and likely represents the emplacement age.

Six palaeomagnetic samples taken below the WST all returned reversed polarities while one sample at 80 cm above the top of the WST has a normal polarity (Fig. 2; see also Yurnaldi et al., 2018). The normal polarity is thought to correspond with the Jaramillo event (1.780–0.990 Ma: Cohen and Gibbard, 2019), while the reversed polarities below the WST correspond with the reversed period of the Matuyama Chron (1.780 Ma – 1.071 Ma). The Cobb Mountain Normal Event at 1.208 to 1.187 Ma is not recognised, which is not surprising considering the low sampling density in this interval. Two palaeomagnetic normal polarities previously reported from the 2 m interval directly underlying the Tangi Talo fossil-bearing horizon were initially interpreted as representing the Jaramillo (Sondaar et al., 1994). Combined with a ZFT age of 0.90 ± 0.07 Ma for the main fossil-bearing layer (Morwood et al., 1998), this interpretation appeared to confirm the age of ~0.90 Ma for the Tangi Talo fauna (Aziz et al., 2009a; Brumm et al., 2010a). However, this young age is incompatible with the revised stratigraphy and new age data reported here, including the recognition of the 1 Ma WST at 18 m above the bone bed, and the $^{40}Ar/^{39}Ar$ age of 1.27 ± 0.03 Ma for the Lowo Lele Tephra (TTT-5) at 2 m above the bone bed. A possible explanation for this anomalous ZFT date is that the sample was under-etched, and therefore not all spontaneous tracks were revealed for age counting, resulting in an erroneous minimum age determination. The two normal polarities directly below the bone bed reported by Sondaar et al. (1994) could not be replicated by Yurnaldi et al. (2018).

In 2012, a 15 m^2 excavation was carried out at a site ~ 300 m northwest of the main bone bed excavations (Excavation F; see Fig. 14A). This excavation revealed vertebrate fossils embedded in a silty fluvial channel-fill that cross-cuts underlying reworked Lowo Lele tephra (~TTT5, 1.27 ± 0.03 Ma) (Fig. 14F and G). The Excavation F fossil assemblage, here designated as TT-UP, is thus slightly younger than the main bone bed at Tangi Talo, hereafter indicated as TT-LOW.

6.5.2. *Tangi Talo fauna*

The main bone bed at Tangi Talo (TT-LOW) was previously excavated in 1991–92 and 1999 (excavation sectors A-D) (Aziz et al., 2009a; van den Bergh, 1999) and the excavations were extended in 2012 (sectors E, G) and 2013–14 (sectors H, I, K, L).

Fossils are concentrated at the base of an up to 50 cm thick pumice mudflow layer that, as mentioned above, can be traced for at least 172 m from NNE to SSW, and slopes between 0.8 and 2° in WSW direction (Fig. 14A, E). By 2014, a total of 216 m^2 of the bone bed had been excavated, yielding a total of 1877 fossil specimens, primarily representing the giant tortoise (*Megalochelys* sp. (~74% of finds, consisting mostly of broken plastron and carapace fragments); and small pygmy elephant *Stegodon sondaari* (~16% of finds; see Fig. 3F) (Aziz et al., 2009a; Setiyabudi, 2017; van den Bergh, 1999). Rarer are fossils of Komodo dragon (*Varanus komodoensis*), including isolated teeth and postcranial elements. Undiagnostic remains of a murine rodent of similar body size as *Hooijeromys nusatenggara* (which is common in the younger Mata Menge sites), isolated crocodile teeth, and a small freshwater turtle (cf. *Cuora amboinensis*) (Setiyabudi, 2017; Takahashi et al., 2015) have also been identified. The presence of an unidentified giant rat within the TT-LOW fauna, based on incisors, two femur fragments and a tibia fragment, extends the known range of murine rodents on the island by half a million years.

S. sondaari and *V. komodoensis* fossils are both present in the slightly younger stratigraphic level of Excavation F (number of fossil specimens from TT-UP is 304 specimens) (see Fig. 14D), but *Megalochelys* fossils are completely absent from TT-UP. Based on the dental remains from this layer, the *S. sondaari* assemblage of Excavation F comprises an MNI of 35, of which 86% represent

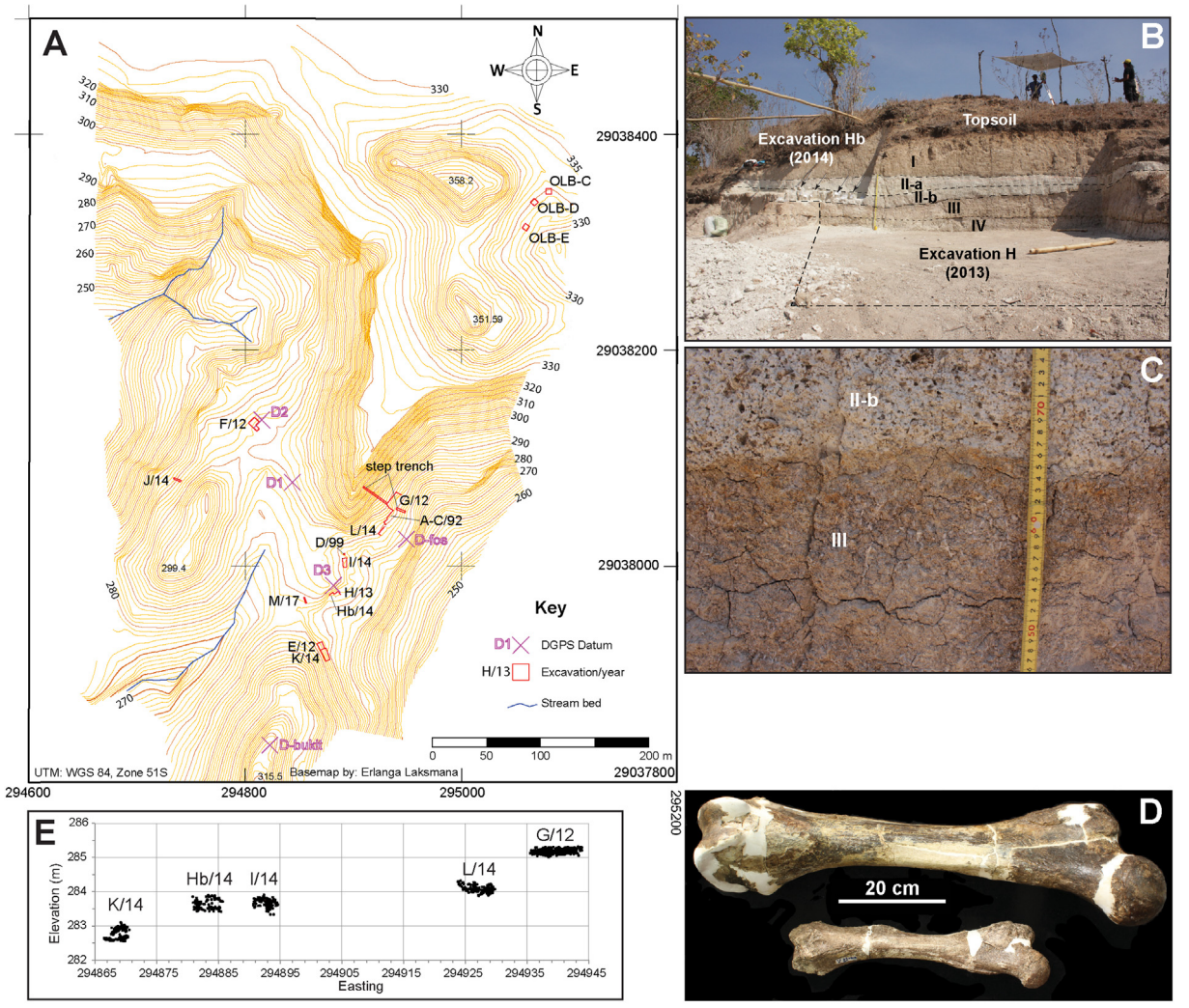
A
N
W
E
S
OLB-C
OLB-D
OLB-E
F/12
D2
J/14
D1
step trench
G/12
A-C/92
L/14
D-fos
D/99
I/14
D3
M/17
H/13
Hb/14
E/12
K/14
D-build
Key
D1 DGPS Datum
H/13 Excavation/year
Stream bed
0 50 100 200 m
UTM: WGS 84, Zone 51S
Basemap by: Erlanga Laksmana
29038400
29038200
29038000
29037800
294600
294800
295000
B
Topsoil
Excavation Hb (2014)
I
II-a
II-b
III
IV
Excavation H (2013)
C
II-b
III
D
20 cm
E
Elevation (m)
Easting
K/14
Hb/14
I/14
L/14
G/12
F
315∞ northwest
135∞ southeast
Tangi Talo
Excavation F
0 m (=288.25 m)
0
1
2a
2b
3a
3b
4a
4b
5
G
H

juveniles. This is in sharp contrast with the *S. sondaari* assemblage from TT-LOW (MNI = 52), which has only 35% of the MNI based on fossil teeth representing juveniles. The combined evidence from both levels suggests that *S. sondaari* and *V. komodoensis* persisted in the area following a mass-death event that may be associated with the emplacement of the white pumice-rich mass-flow layer. However, the *Megalochelys* population may have been critically affected by this event, as this species does not re-appear in the slightly younger TT-UP deposits, nor in any of the younger fossil sites in the So'a Basin. However, the absence of *Megalochelys* from the TT-UP could also be due to the much smaller sample size, in addition to the distinct taphonomy of this abandoned channel fill compared to the widespread laharic mass-flow layer for the TT-LOW.

In total, 23 enamel samples of adult *S. sondaari* individuals were analysed for $\delta^{13}C$ and $\delta^{18}O$ contents (see Appendix G). As adult molar fragments from Excavation F were very rare, only three enamel samples could be obtained from the TT-UP, while the remainder of the samples are from the main Tangi Talo bone-bed (TT-LOW). The $\delta^{13}C$ values of *S. sondaari* individuals plot in a narrow range (−8.3‰ to −3.8‰) that is consistent with mixed C_3–C_4 feeders (see Fig. 11), except for a single individual from the TT-UP that just falls within the range of a C_3-dominant diet ($\delta^{13}C = -8.3$). The three samples from TT-UP show comparatively low $\delta^{13}C$ values close the lower boundary of the observed range; similarly, these samples also exhibit $\delta^{18}O$ values at the higher end of the range. This difference may reflect different climate-vegetation conditions, as both levels are separated by ~100,000 years.

The overall low $\delta^{13}C$ values for the *S. sondaari* individuals from both TT-LOW and TT-UP are in sharp contrast to $\delta^{13}C$ values of *S. florensis* from the Sandstone Member, which, except for one specimen from the MM-UP, cluster above −2.0‰, and are indicative of a predominantly C_4 diet. This difference is statistically significant as there is no overlap in values between the two groups (Two-tailed Mann-Whitney *U* test = 0, $p < 0.0001$). The *S. florensis* individuals from Kobatuwa from the top of the Tuff Member have overlapping values between those of Tangi Talo and of Mata Menge/Boa Leza (Fig. 11), suggesting a transition in climate-vegetation conditions.

6.5.3. Tangi Talo archaeology

No stone artefacts have been recovered at Tangi Talo, despite the large excavations undertaken at this site (~216 m^2 in TT-LOW, and ~ 15 m^2 in the at least ~ 100,000 years stratigraphically younger TT-UP). Furthermore, neither the 1-m-wide stepped trench excavated in 2010 that exposed the full stratigraphic sequence up to the WST, nor the fluvial conglomerate that overlies the fossil-bearing channel fill at Excavation F, has yielded a single stone artefact or other proxy evidence for the presence of hominins either at the site (e.g., cut marks on fossil bone) or in the wider landscape. Excavations at other sites in the upper part of the OKF (Excavations T3 at Kobatuwa-I, T1 at Kobatuwa-II) likewise did not yield any artefacts or other signs of hominin occupation. In sharp contrast, excavations and fossil sites in fluvial deposits above and directly below the WST, including fluvial conglomerates and pedogenized floodplain sediments, have invariably yielded stone artefacts. For instance, excavations T2 at Kobatuwa-I, T1 at Kobatuwa-IV, Wolo Sege Main, Wolo Sege East and Wolo Sege slot trench T1, all excavations in MM-LOW and MM-UP and slot trench T10 at Mata Menge, trench BL-T1 at Boa Leza, and Excavation T1 at Kobatuwa-I, plus additional sites not dealt with in detail here (Dozu Dhalu, Wolo Milo, Lembah Menge, Wolo Keo, Pauphadhi, Kopowatu and Ngamapa; see Aziz et al., 2009b; Morwood et al., 1999), have all yielded *in situ* stone artefacts. This pattern suggests that hominins were not yet established in the So'a Basin at the time when the lower part of the Tuff member was deposited, although absence of direct fossil evidence or proxy evidence in the form of stone artefacts, does not preclude a hominin presence before 1.27 Ma.

To further increase our efforts to test for the presence of *in situ* stone artefacts in strata with an age of ~1.27 Ma, we performed additional excavations in fluvial sandy and/or pebbly layers that occur stratigraphically directly above the 1.27 Ma old Lowo Lele Tephra (TTT-5). In 2014, a 1 × 6 m step trench was excavated 200 m west of Tangi Talo in an attempt to trace back the main fossil bearing layer further west (Excavation J; Fig. 14A). This was a 1 × 5 m large test excavation in a 0.5 m thick fluvial pebbly sandstone layer, which yielded a single *Stegodon sondaari* molar fragment, but no stone artefacts. Although the exact stratigraphic correlation of this trench with the dated Tangi Talo sequence could not be reconstructed, its location is at the same altitude as the main bone bed, combined with the fact that the main bone bed slopes weakly down towards the WSW, indicates that this fluvial layer is probably younger than the main bone bed. Another 1 × 5 m trench was excavated in 2017, in a fluvial channel deposit 2-m above the top of the main fossil layer at Tangi Talo (Excavation M; Fig. 14A, H). This excavation was within fluvial cross-bedded pebbly sands and likewise yielded a single rolled *Stegodon sondaari* molar fragment, but again, no stone artefacts, despite the availability of pebbles and cobbles of rock suitable for knapping, such as aphanitic basalt and chalcedony. Based on the combined lack of evidence for stone artefacts in the lowermost part of the OBF at Tangi Talo and other sequences in the lower part of the Tuff Member, we hypothesise that hominins were not yet present in the So'a Basin prior to

Fig. 14. Site stratigraphy of key sites in the So'a Basin: Tangi Talo

A, Topographic map of the Tangi Talo area, showing the location of all the excavations. Excavations TT-A-C, D, E, TT-G (see also Fig. 3F), TT-H, TT-I, TT-K and TT-L are all in the main bone bed (~TT-LOW), which is a gently ESE dipping, pumice-rich lahar covering and partly embedding the bones. $^{40}Ar/^{39}Ar$ isochron dating of single plagioclase crystals from pumices from this layer yielded an age of 1.4 Ma. Tangi Talo excavation F is younger (TT-UP), representing a channel fill that cut down in reworked Lowo Lele tephra (TTT-5), which is dated at 1.27 Ma; **B**, stratigraphic profile of west baulk of Excavation Tangi Talo H/Hb. Stratigraphic layers are from top to bottom: I) mudflow deposit, > 1 m thick, matrix supported, with pumice clasts and angular granules and rip-clasts, few angular pebbles concentrated near erosive basal contact, pedogenically-altered; II) pumice-rich mudflow deposit (= main bone bed); in Sector H/Hb the main bone bed can be subdivided in an upper (II-a) and lower (II-b) sub-layer, with the main bone concentration occurring in sub-layer II-b (see fossils on pedestals in sector Hb to the left indicated by arrows); sub-layer II-a is a white siliceous tuff with few pumice fragments, fining upward from low-angle cross-laminated sand near the base and massive to faintly laminated silt with sparse pumice fragments at the top, whereas sub-layer II-b is massive, white siliceous tuff with abundant pumice fragments and silty matrix, the base is erosive filling in a channel (Sub-layer II-b wedges out toward the northeast); Layers III and IV are massive mudflow deposits, pedogenically-altered; **C**, detail of the boundary between layers II-b and III in Sector H; note fossil rhyzomes in the Layer III palaeosol; **D**, adult *Stegodon* femurs from Tangi Talo (bottom; originating from Area F, TT-UP; GM Coll. Nr. TT12-TF-F3) and from Mata Menge (top; MM-LOW; GM Coll. Nr MM11-T23B–F176), showing size differences between the pygmy *S. sondaari* and the medium-sized *S. florensis*, respectively; **E**, Elevations of individual fossil specimens excavated at the five excavations in the main bone bed (TT-LOW; see Fig. 14A for locations), projected along an east-west transect; note that the main bone bed decreases in elevation from east to west; **F**, Profile drawing of the northeast baulk of Tangi Talo Excavation F (TT-UP). Stratigraphic layers are: 0) topsoil; 1) weathered sandstone; 2a) mudflow with rounded matrix-supported boulders; 2b) pebbly sand channel-fill; 3) clayey silt; this layer yielded 230 fossil fragments directly to the northwest of the profile in a channel-fill; 4) Pale green colored pumiceous lapilli-bearing tephric sands with planar and low-angle cross-bedded laminations (reworked); upper part (4a) is overprinted by a palaeosol containing distinct rhyzomorphs; Layer 4 represents reworked Lowo Lele Tephra (TTT-5), which in the Tangi Talo area G section (see Fig. 3F) was $^{40}Ar/^{39}Ar$ dated to 1.27 ± 0.038 Ma; 5) pedogenised light brownish yellow clay-rich mudflow; **G**, Fossil concentration in abandoned channel-fill of Tangi Talo Excavation F (Layer 3b in Fig. 14F); **H**, View towards the west and north baulks of Excavation M at Tangi Talo; a cross-bedded gravel bar deposit (lower left corner) occurs stratigraphically at ~ 2 m above the main bone bed (TT-UP as exposed in Tangi Talo Excavation H), and is overlaid by cross-bedded sandstones and siltstone layers. (For interpretation of the references to color in this figure legend, the reader is referred to the Web version of this article.)

~1.27 Ma. If this hypothesis holds, the first hominin arrival in the basin, and possibly the colonization of Flores itself, would most likely have taken place between ~1.27 Ma and the emplacement of the WST around 1 Ma. Further research into deposits predating 1.3 Ma are necessary to confirm this assessment.

6.6. Mata Go

6.6.1. Mata Go site stratigraphy and archaeology

Mata Go is a roadside quarry in the central part of So'a Basin ~2.3 km south of Tangi Talo (Fig. 2). At this locality, an isolated section of WST is exposed in a small quarry. Here the lowermost ~3.2 m of WST is exposed and reveals basal surge-fall-flow beds overlying a ~0.30 m thick well-structured palaeosol developed into underlying very coarse-grained (bouldery) channel lag deposits (see Fig. 7D). Along the section, basal surge beds of WST perceptibly 'pinch-and-swell' over bouldery obstacles protruding from the surface of the palaeosol (the then ground surface at the time of WST emplacement). During a field survey in 2012, one stone core was noted *in situ* at the very top of a silty palaeosol, with the basal WST pyroclastic surge sub-unit draped over the protruding core (see Fig. 7E and F). The minimum age of this artefact corresponds with the age of the WST emplacement at ~1 Ma.

6.7. Ulu Mala Kata

6.7.1. Ulu Mala Kata site stratigraphy and palaeontology

Ulu Mala Kata, discovered in 2015, is located along the east bank of the Ae Sesa River, near the confluence with the Lowo Lele River (Fig. 1). Both rivers have incised the OKF basement rocks in this location. A badly damaged *Stegodon* mandible and an upper molar were found eroding out of riverbank within a weakly consolidated lahar deposit (Fig. 15A–C). This coarse-grained lahar is massive, at least 7 m-thick, and forms a remnant fill terrace along the east side of the Ae Sesa river valley. The lahar deposit commonly contains metre-sized blocks of older Ola Kile breccia that were incorporated during flowage along the Ae Sesa valley. Pumice and charcoal fragments were also entrained within the flow. The source of this lahar deposit is presently unknown. It could have originated from the Ebu Lobo Volcano, which is the main source of the Ae Sesa River, but it is equally possible that this lahar deposit could be derived from a tributary extending eastwards originating in the BCCC. Ula Mala Kata is of great importance because it represents the youngest *Stegodon* occurrence in the So'a Basin, and extends the local record of *Stegodon* by 600 ka. The fossils represent a smaller-bodied *Stegodon* than known from the OBF, and is similar in size and shape to the Late Pleistocene *Stegodon florensis insularis* that is well-known from Liang Bua (van den Bergh et al., 2008) (see Fig. 15D–G). The Ulu Mala Kata fossils are here attributed to *S. florensis insularis* (see Appendix I).

In order to obtain a minimum age for these fossils, we undertook laser ablation multi-collector ICP-MS Uranium-series dating on two enamel/dentine fragments that could not be refitted to the main fossil. One sample consisted of an enamel fragment (UMK15-1a), while the other was an isolated molar ridge fragment (UMK15-1b) that included the worn occlusal surface of one of the worn lower molars that were originally embedded at the front of the mandible distally of the unworn last molars.

The two subsamples yielded overlapping minimum ages of 34.2 + 0.3/-0.5 ka (UMK15-1a) and 31.0 + 0.5/-0.7 ka (UMK15-1b), respectively (see Appendix E). Two charcoal samples from the lahar provided further support for a Late Pleistocene age, and yielded slightly older but overlapping conventional AMS ^{14}C ages of 47,699 ± 1342 BP (Wk-48668) and 45,807 ± 1042 BP (Wk-48669), respectively, confirming the relatively young age of the terrace fill. These conventional ages would translate to calibrated (OxCal v4.3.2) ages in excess of 49,900 cal BP and 47,250 cal BP, respectively (these are the lower ages at 2σ; the upper boundaries for both samples fall outside the calibration curve). These *Stegodon* fossils are equivalent in age with the most recent *S. florensis insularis* record from Liang Bua, estimated at 50 ka (Sutikna et al., 2016, 2018), but could even be several thousand year younger.

7. Discussion

7.1. Silicic tephra source(s)

The occurrence of silicic tephra marker beds within OBF sedimentary sequences raises obvious questions regarding their eruptive origins. Indications of potential source locations can be broadly resolved by combining field observations (i.e., thickness, texture, bedding variations) with comparative glass shard geochemistry. While sporadic tephra beds with uniform field attributes over their lateral extent may be suspected of having a distal (inter-regional) source, the majority of silicic tephra represented within So'a Basin are more likely sourced from adjacent eruptive centres.

7.1.1. Silicic tephra within lower OBF

Sedimentary sequences of lower OBF (Tuff Member) are dominated by metre-to decimetre-thick silicic pyroclastic mass-flow deposits of Wolo Sege, Turakeo and Pu Maso tephras (Figs. 2 and 6). The westward thinning of these deposits across the So'a Basin, coupled with overall textural fining, suggests an eastward source. In addition, the pumice-rich mudflow that covers the main bone bed at Tangi Talo, with its shallow dip towards the WSW, probably has its volcanic source in the east as well. Based on glass shard major element geochemistry determined from electron microprobe (EMP) analysis (Fig. 4, Table 1), these silicic mass-flow deposits typically form a tightly clustered compositional grouping and are indistinguishable (±1 SD). However, individual analyses from each unit typically occupy subtly different domains within that clustered grouping which, in addition to stratigraphic association and sedimentary architecture, permit these mass-flow deposits to be distinguished. Nevertheless, the tight geochemical association suggest that Wolo Sege, Turakeo and Pu Maso Tephra are closely related and likely derived from the same eruptive source. Older (air-fall) tephra (TTT-1, TTT-2, TTT-5 (Lowo Lele) and Wolowawu Tephra) also have strong geochemical affinity with the Wolo Sege-Turakeo-Pu Maso compositional grouping, and are therefore also likely sourced from the same eruptive centre.

Evidence associating this compositional grouping to a potential eruptive source is exposed in a roadside quarry (08° 34′ 27.4″ S; 121°18′ 05.1″ E) in the vicinity of Mbai on the northern Flores coastal plain, 26 km north-east of Mata Menge (see Fig. 1 and 16). Here, two prominent silicic deposits are observed separated by a prominent well-structured ~0.4 m thick palaeosol containing conspicuous rhyzomorph casts and root moulds. This succession forms the upper portion of an inclined volcaniclastic surface that extends upward from the coastal plain to an eroded rim remnant of an ancestral caldera complex on which the present-day Keli Lambo Volcano is constructed (see Figs. 1 and 16F). The upper silicic deposit at Mbai comprises the following sequence: i) an upper 1.4 m + thick poorly-sorted, matrix-supported, pumiceous diamict (pyroclastic flow deposit) with the upper part truncated at the present-day ground surface; ii) a middle ~ 1.3 m thick faintly stratified vitric ash and lapilli layer containing centimetre (cm)-sized accretionary lapilli (fall deposit); and iii) a basal ~ 0.26-m-thick, cross-bedded, well-sorted cm-to mm-bedded vitric sands (surge deposit). The lower silicic unit on which the overlying palaeosol is formed into comprises a ~4.5-m sequence of well-

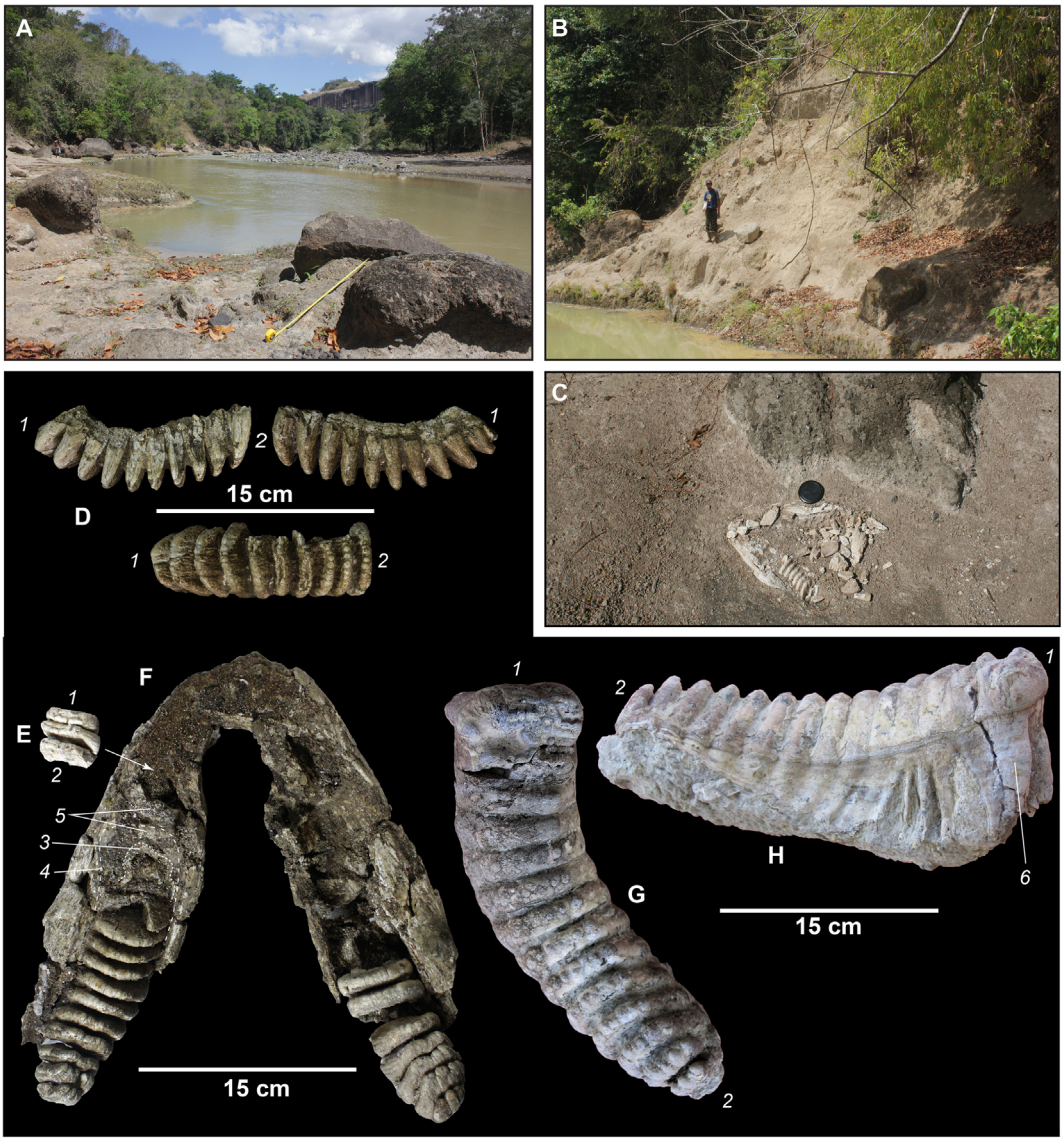

Fig. 15A. ~ Site stratigraphy of key sites in the So'a Basin: Ulu Mala Kata
A, Massive coarse-grained laharic terrace fill exposed downstream of the confluence of the Ae Sesa and the Lowo Lele rivers at Ulu Mala Kata; note large blocks embedded in the lahar (scale is 1 m); **B**, erosional profile in the same terrace fill; outcrop is ~7 m high; **C**, *in situ* mandible of *S. florensis insularis* (see Fig. 15E and F) embedded in the Ulu Mala Kata laharic terrace fill; **D-F**, *S. florensis insularis* fossils from the Ulu Mala Kata lahar deposit: **D**) upper left M3 fragment (Coll. MG UMK15-1); the most anteriorly preserved ridge is slightly worn on the buccal side, indicating that the molar had just erupted and is in the same dental wear stage as the mandible figured in F; **E**) lower m2 fragment from mandible (Coll. MG UMK15-2b; due to damage no fit with mandible); **F**) mandible with fragmentary left and right m3s with unworn ridges (Coll. MG UMK15-2a); note that the most complete left m3 is missing a few anterior ridges, but based on the root outline it is estimated that three ridges are missing mesally in front of the fourth ridge, which is partly preserved); **G**,**H**, *S. florensis* lower right m3 from the MM-LOW at Mata Menge (Coll. MG MM05-27); **G)** occlusal view; **H)** buccal view; note the size difference with the m3s in the mandible from Ulu Mala Kata. *1* = mesial; *2* = distal; *3* = broken mesial root of m3 (anterior hook) in cross-section; *4* = estimated original outline of m3 crown; *5* = cancellous bone in between root masses of m3 and m2; 6 = mesobuccal root (anterior hook).

sorted cm-thick planar-bedded vitric coarse sandy ash. Low-angle cross-beds, pinch-and-swell, scour and rip-up structures together with evidence for constituent density segregation and fines depletion (ash elutriation), collectively indicate successive pyroclastic surge deposition (Fig. 16B–E).

The upper and lower Mbai units are correlated, on the basis of glass shard major-element chemistry (Fig. 17), with Pu Maso and Turakeo deposits from the Soa Basin, respectively. Older pyroclastic deposits at Mbai were not exposed (i.e., Wolo Sege correlative). Nevertheless, the proximal-medial silicic architecture of these two correlatives, along with their corresponding stratigraphic association and occurrence forming part of an inclined depositional surface flanking remnants of an ancestral caldera complex, provides compelling evidence that the majority of lower OBF silicic tephra are sourced from this ancestral Keli Lambo eruptive centre.

7.1.2. Silicic tephra within upper OBF

Four silicic tephra have so far been identified within GLM lacustrine sediments, and are interbedded with numerous tephra and scoria-bearing debris flow deposits of basaltic composition. The silicic deposits interbedded within GLM are usually cm-to dcm-(deci-centimetre) thick and have bedding features consistent with either airfall (primary) or debris-to hyperconcentrated-flow deposition (i.e., Fig. 3C and D). Major-element glass data (Fig. 4, Table 1) for these silicic tephra (i.e., Wulubara, Nata Radang, Poma and Kolopanu) form compositional groupings distinct from those of

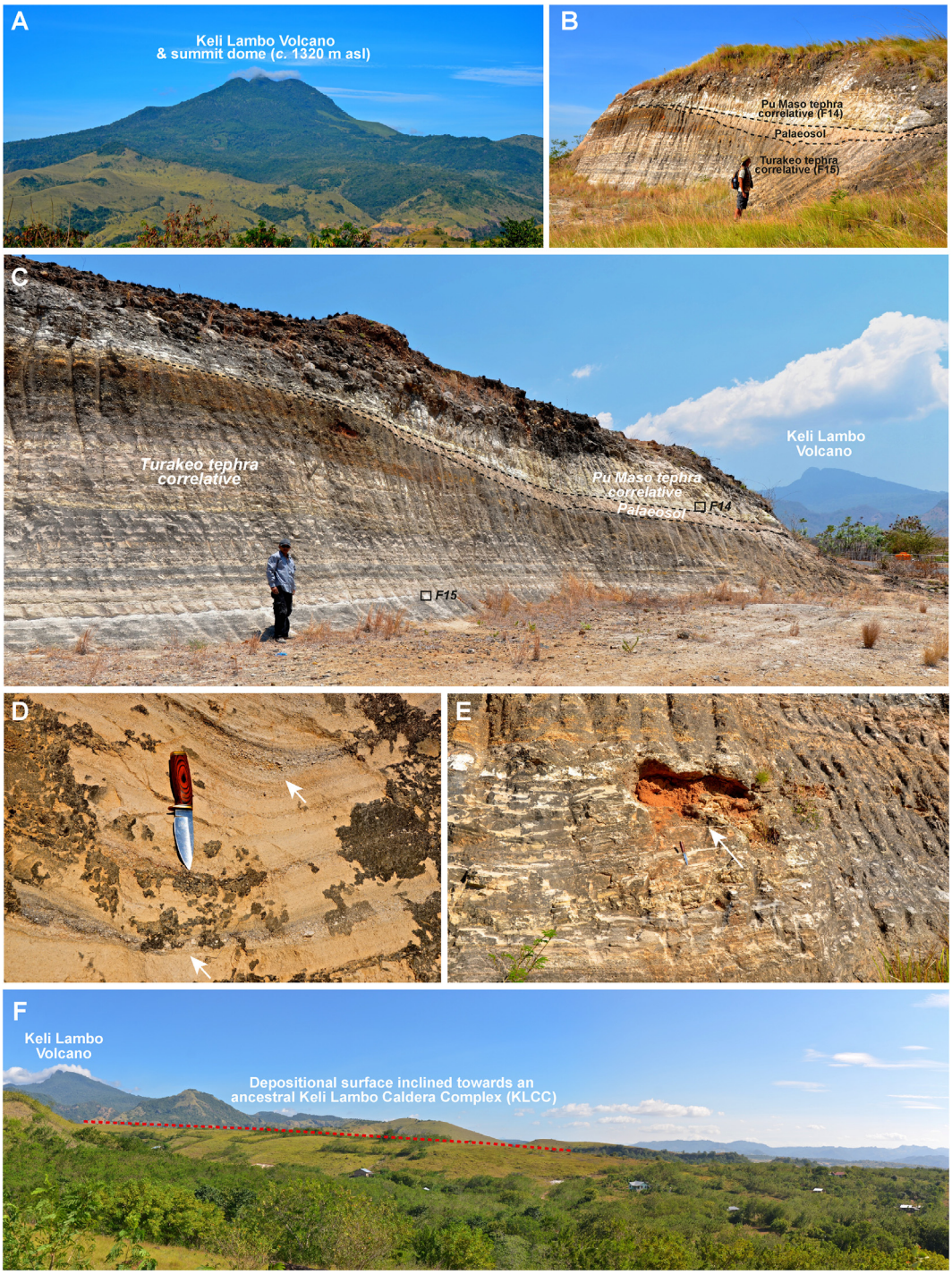

Fig. 16. A. Keli Lambo (with a conspicuous summit lava dome ~ 1320-m above-sea-level) is a forested Late Quaternary composite stratovolcano located east of So'a Basin, and constructed upon the eroded remnants of a much older caldera complex; **B, C,** In a roadside quarry (08° 34′ 27.4″ S; 121° 18′ 05.1″ E; see Fig. 1B: 'quarry') in the vicinity of Mbai adjacent the northern Flores coastal plain, two prominent silicic deposits are observed separated by a prominent well-structured palaeosol; **D, E,** The lower deposit comprises a ~4.5 m thick sequence of well-sorted, cm-thick, planar to low-angle cross-bedded coarse vitric sandy ash that exhibit pinch-and-swell structures and incorporate large 'rip-up' soil clasts (indicated by arrows). The characteristics of this deposit are indicative of successive (turbulent) pyroclastic surge bed emplacement; **F.** The inclined depositional surface on which these two silicic deposits were emplaced, extends upward from the coastal plain to an eroded rim remnant of an ancestral Keli Lambo caldera complex.

Wolo Sege-Turakeo-Pu Maso, suggesting different eruptive sources from those older tephra represented within lower sequences of OBF. One of the four identified silicic deposits of the GLM can be attributed to an intra-Welas caldera source with any certainty. In the vicinity of Nata Radang, in the northwest inner sector of Welas caldera, a 40-m + thick sequence of coarse-grained pyroclastic surge beds can be recognised (Fig. 3A and B). This sequence is associated with a succession of systematically oriented fluvially dissected ridges that are inclined in elevation towards the north-west, and laterally transition to a lava flow deposit (though the contact between the two deposits on the same surface was not observed) originating from a subtly-expressed remnant crater

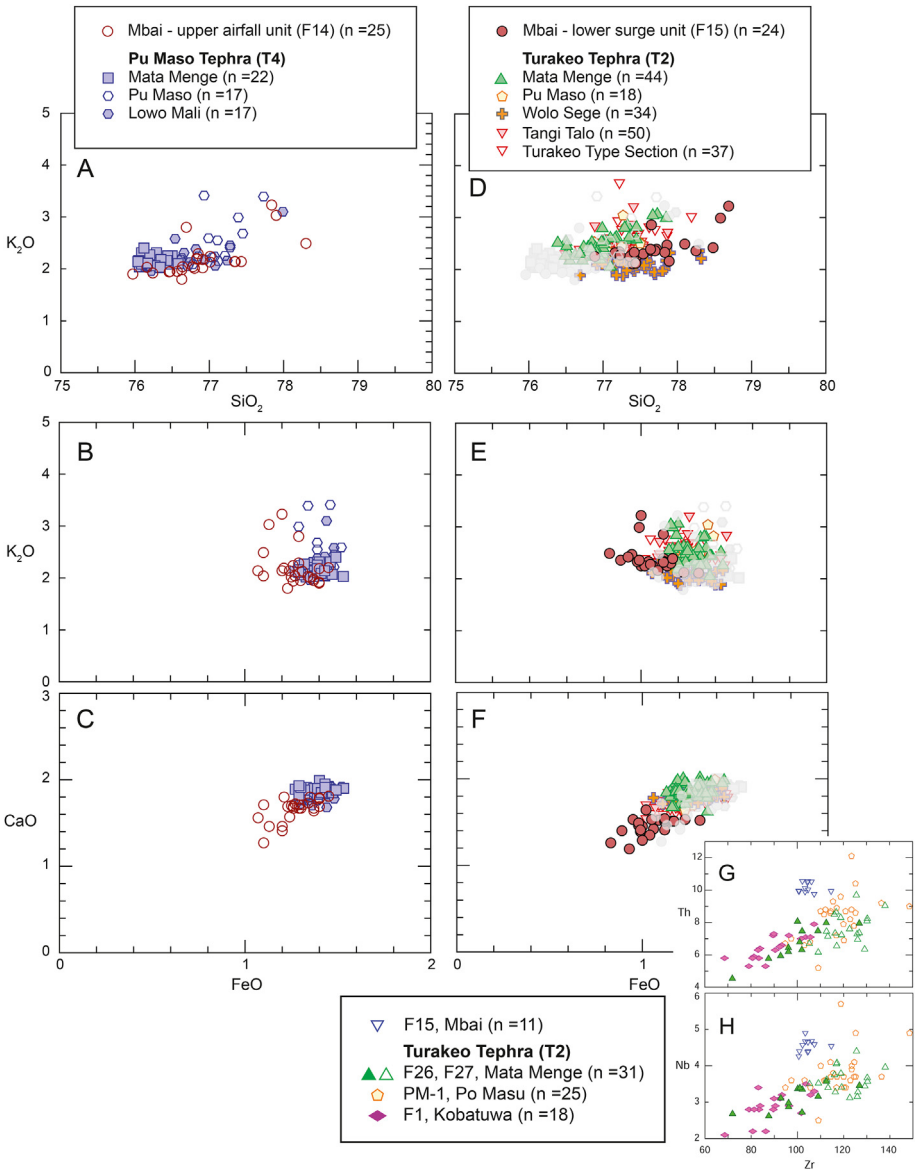

Fig. 17. Selected major element compositions (weight percent SiO_2 vs. K_2O and FeO vs. CaO and K_2O) of glass shards from the upper (airfall) unit at Mbai (F14) compared with equivalent elemental data from Pu Maso Tephra (Mata Menge, Pu Maso, Lowo Mali; **A-C**) and lower (surge) unit at Mbai (F15) compared with equivalent elemental data from Turakeo Tephra (Mata Menge, Pu Maso, Wolo Sege, Tangi Talo and Turakeo reference section; **D-F**). Pu Maso tephra analyses (transparent grey symbols) are superimposed upon Turakeo tephra analyses (D–F) and further affirm correlation – though Turakeo tephra has a broader major element compositional spread; **G, H,** Selected trace element compositions Zr vs. Th and Nb of glass shards from the lower surge unit at Mbai (F15) compared with equivalent elemental data from Turakeo Tephra (Mata Menge, Pu Maso and Kobatuwa).

(~0.8-km diameter) breached to the south-east, and located close to the inner Welas caldera wall.

The glass chemistry of the source-proximal Nata Radang pyroclastic surge beds is very similar to that of Poma tephra, and this similarity may also reflect a localized (i.e., intra-Welas Caldera) source, though this is yet to be unequivocally established.

The numerous basaltic tephra layers in the GLM likely relate to the emergence of intra-caldera scoria cones within the ancestral Welas Caldera lake system.

7.1.3. *Inter-regional silicic tephra*

Glass shard major-element data from T6 tephra at Mata Menge as well as T3 tephra from Mata Menge, Lowo Mali and Kopowatu sections confirm their glass compositions are different to all other silicic tephra represented within the So'a Basin, and suggest inter-regional (distal) eruptive sources (Figs. 4 and 5). The distinct elemental clustering of these tephra is further supported by trace-element data. Selected T3 and T6 elemental data (i.e., Sr vs' Th and Zr, and Y vs' Nb, Ce and Th bivariate plots) were compared against potential ultra-distal tephra correlatives (i.e., Youngest Toba Tuff (YTT), Middle Toba Tuff (MTT), Oldest Toba Tuff (OTT) and Unit E from ODP-758) (Fig. 18; SI Table B3). These are the most widespread tephra markers so far known from the Indonesian archipelago. T6 tephra does not correlate with any of the well-known Toba-sourced tephra (YTT, MTT, OTT), though it is geochemically similar to (but distinguishable from) Unit E. The glass shard composition of T3 tephra is distinctive with a consistently wide elemental spread and has no resemblance to far-field (i.e., Toba) or regionally- (Keli

Lambo) and/or locally- (intra-Welas) derived silicic tephra found within the So'a Basin. On this basis, the distal eruptive origins of both T6 and T3 ash beds currently remain unknown, but this result does not diminish their stratigraphic utility within the overall So'a Basin sedimentary succession.

7.2. Synthesis of faunal changes and palaeoenvironment

This current synthesis of the stratigraphic and dating evidence from the So'a Basin enables a revision of the chronostratigraphic framework, with important implications for the faunal and archaeological sequence and timing of new arrivals and extinctions, as summarized in Fig. 19.

7.2.1. Revised biostratigraphy of Tangi Talo, Kobatuwa and Mata Menge

The earliest evidence of vertebrate fauna on Flores, characterized by the presence of *S. sondaari*, is the widespread bone bed at Tangi Talo (TT-LOW). The pumice-rich lahar that covers this bone bed and embeds the fossils, was previously thought to be 0.9 Ma old based on palaeomagnetic (Sondaar et al., 1994) and zircon fission-track data (Brumm et al., 2010a; Morwood et al., 1998), but is now firmly dated at 1.4 Ma. In addition, we have now documented a new fossil assemblage (TT-UP) from a slightly younger site at Tangi Talo, Excavation TT-F, with a maximum age of 1.27 Ma.

Previous age estimates for the fossil and artefact assemblages from Kobatuwa-I ranged between 0.80 ± 0.09 Ma and 0.70 ± 0.07 Ma, based on two of zircon fission-track dates of tuffaceous siltstone layers bracketing the fossil-bearing layers. Considering the relatively large error ranges in these fission-track ages, this would correspond with a broad range of between 0.89 and 0.63 Ma for the Kobatuwa assemblage. Based on the new tephrostratigraphic correlations, this age range is probably an underestimate, and the Kobatuwa-I fossil and artefact-bearing strata are likely older than the Pu Maso Tephra, which is $^{40}Ar/^{39}Ar$ dated at 0.81 ± 0.04 Ma in the Mata Menge section. These strata are also older than the dated T3 interregional tephra at 0.90 ± 0.07 Ma, suggesting a minimum age of 0.83 Ma for the Kobatuwa assemblage. This minimum age is still in accordance with the ZFT data, but locates the minimum age of Kobatuwa further back in time, indicating that the fossil assemblage and artefacts are certainly older than the ones from the lower fossil-bearing interval at Mata Menge (MM-LOW, see below). At Kobatuwa-I the basal conglomerate (Unit K1, see Figs. 2 and 10; referred to as 'Unit F' in Jatmiko

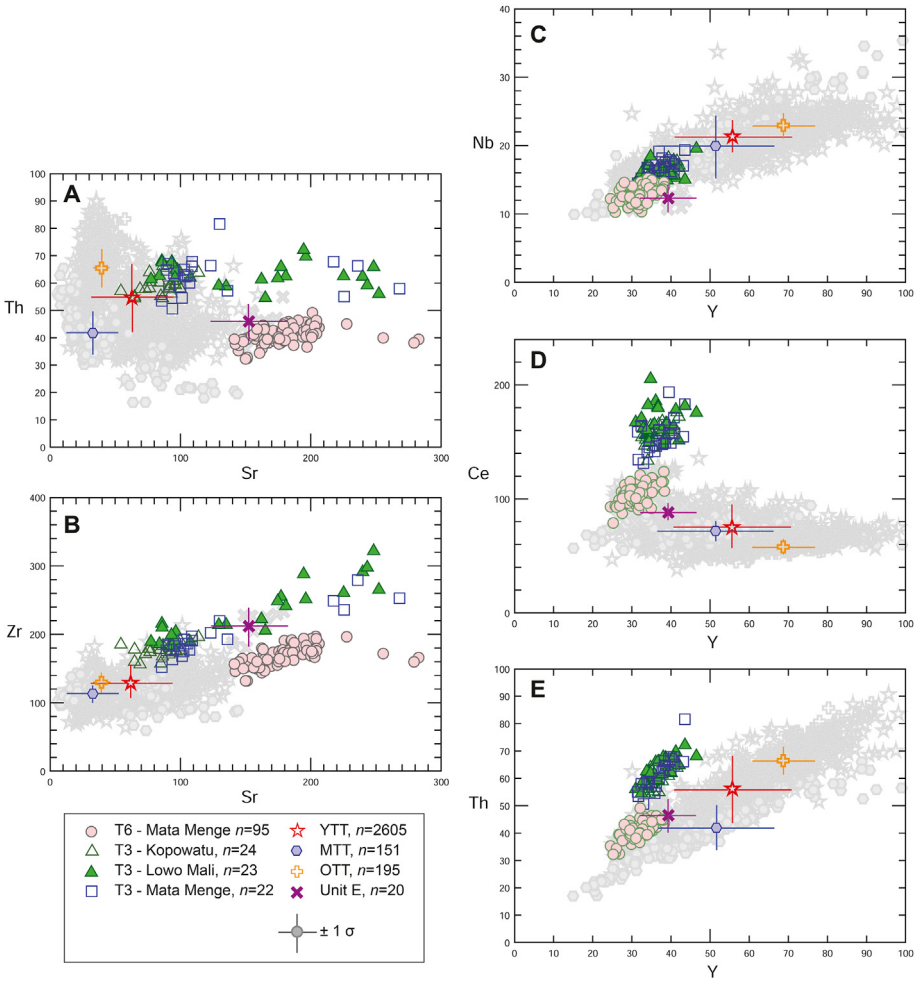

Fig. 18. Selected trace element compositions Sr vs. Th and Zr **(A, B)**, and Y vs. Nb, Ce and Th, (**C-E**)) of glass shards from T3 correlatives from Mata Menge, Lowo Mali and Kopowatu, as well as T6 (uppermost inter-regional marker) from Mata Menge. All trace element concentrations in ppm unless otherwise stated (see **Table B.3**). This data is plotted against equivalent elemental mean and standard deviation (represented as ± 1σ error bars) reference data from potential distal tephra correlatives (i.e., Youngest Toba Tuff (YTT), Middle Toba Tuff (MTT), Oldest Toba Tuff (OTT) and Unit E from ODP-758) acquired on the same instrument using the same standards and under the same analytical conditions (see Pearce et al., 2014); N.J. Pearce, *unpublished data*). Trace element data indicate that the upper (T6) and lower (T3) inter-regional marker beds occurring at Mata Menge cannot be geochemically related to any known Toba-sourced tephra.

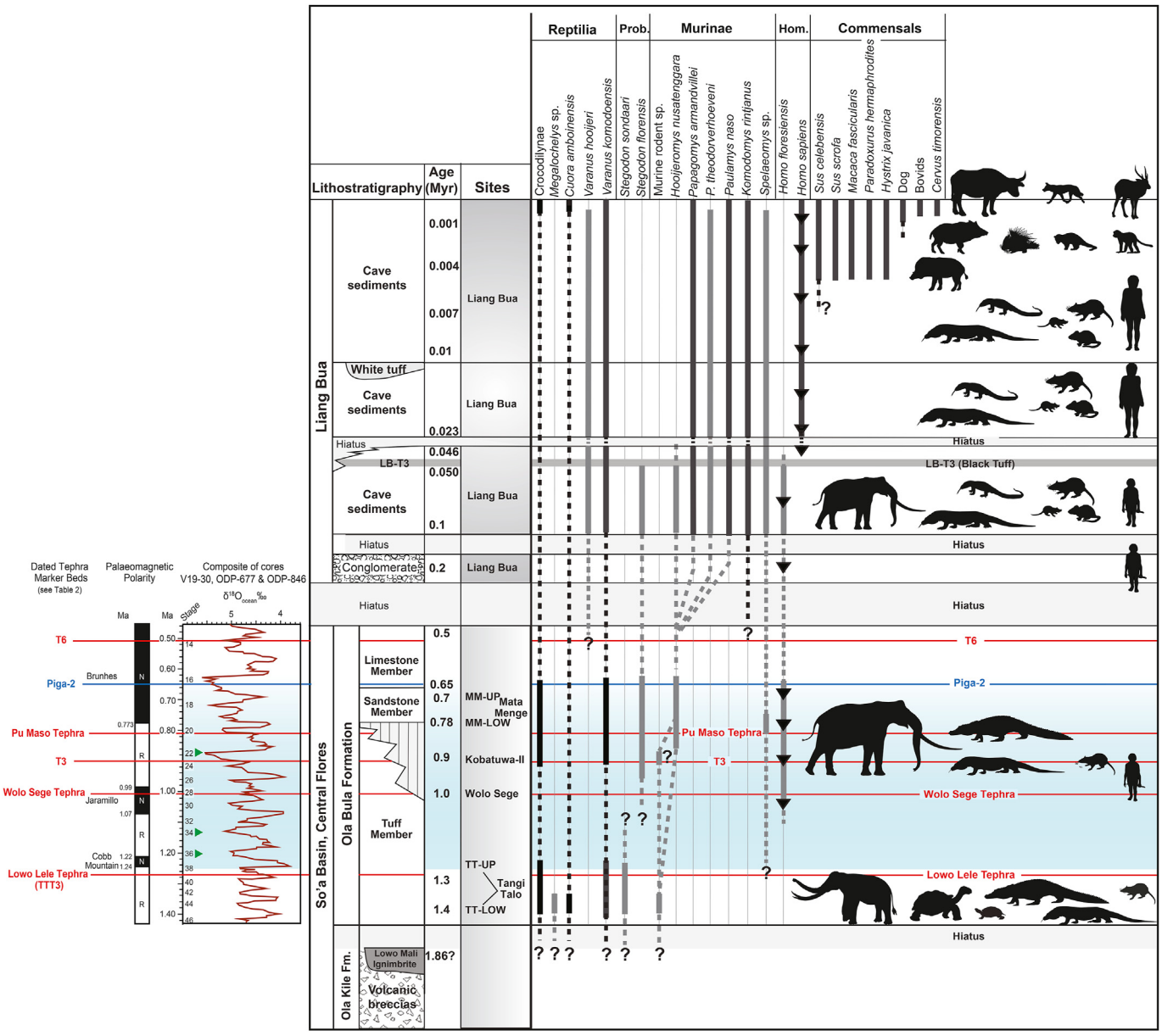

Fig. 19. Fauna sequence of Flores, based on a combination of tephrostratigraphic correlations, chronometric age estimates, and paleontological and archaeological data. On the lower left is the Palaeomagnetic and Marine Isotope Record (modified from Head and Gibbard, 2005) spanning the So'a Basin record. The position of dated tephra marker beds from the So'a Basin are included (see Table 2) and the Middle Pleistocene Transition (MPT; ~1.25–0.7 Ma; i.e., Clark et al., 2006) is indicated in light blue shading. Green triangles indicate major glaciations within the MPT including the first major worldwide event (MIS 22; ~870–880 ka) with substantial ice volumes that typify later Pleistocene glaciations (Ehlers and Gibbard, 2007). Note there is a ~300,000 year hiatus between the end of the So'a Basin record and the beginning of the Liang Bua record. Black triangles indicate occurrences of stone artefacts as proxy evidence for hominins. A major fauna turnover occurs between 1.3 and 0.9 Ma, and hominins are thought to have arrived between 1.3 and 1.0 Ma ago. *S. florensis*, the largest animal on Flores, must also have arrived during that same time interval. After that there appears to be a long period of relative faunal stability, characterized only by the gradual dwarfing of the *S. florensis* lineage and possibly a radiation of murine rodents, although it is conceivable that the differences between the Liang Bua and So'a Basin rats are primarily the results of environmental differences. Note that the youngest occurrence of *S. florensis insularis* at the site Ulu Mala Kata in the So'a Basin (not depicted in this figure) is slightly younger than the youngest record in Liang Bua. Known bird taxa have been omitted, as well as several commensal rodents that arrived to Flores during Neolithic times (10–4.5 ka). Liang Bua data based on Sutikna et al. (2016, 2018). For explanation of the Pleistocene fossil animal icons see Fig. 2. (For interpretation of the references to color in this figure legend, the reader is referred to the Web version of this article.)

et al., 2009) contains the oldest record of *S. florensis* in the So'a Basin. Although no direct dates are available for this conglomerate, the new tephrostratigraphic correlations indicate that this basal conglomerate was deposited before the emplacement of the Turakeo tephra. The emplacement of the Turakeo Tephra, in turn, occurred before the deposition of the overlying T3 interregional tephra, which is dated at 0.9 ± 0.07 Ma in the Mata Menge sequence. Thus, this basal conglomerate at Kobatuwa-I could be as old as the basal conglomerate lenses underlying the 1 Ma WST at Wolo Sege and Kobatuwa-IV, which also contain stone artefacts but have not yielded any fossils.

At Mata Menge the combined palaeomagnetic evidence and tephro-chronological framework allows us to confidently date the MM-LOW at ~0.77 Ma. *S. florensis* is widely represented in the MM-LOW and MM-UP levels, and in a number of other Sandstone Member localities, mostly restricted to the northern part of the So'a

Basin (e.g. Boa Leza, Ruda Olo, Ola Bula, Mala Huma, Ngamapa, Pauphadhi, Kopo Watu, Dozu Dhalu and Wolo Keo (Suminto et al., 2009) (see Fig. 2). The latest occurrence of *S. florensis* in the OBF is in the MM-UP, estimated to be ~0.7 Ma. MM-UP is certainly older than 0.65 ± 0.02 Ma, which is the age of the $^{40}Ar/^{39}Ar$ dated air-fall tephra T-Piga-02 at 15 m above the MM-UP interval in the basal part of the Limestone Member (Brumm et al., 2016). The newly documented fossil-bearing lahar terrace at Ulu Mala Kata, with a calibrated age in excess of 47,250 extends the record of *Stegodon* in the So'a Basin by ~650,000 years, and may represent the last occurrence of *Stegodon* on Flores.

7.2.2. Fauna sequence

The most common megafauna in the oldest recorded vertebrate assemblage on Flores (from the main bone bed at Tangi Talo (TT-LOW), now dated at ~1.4 Ma), are *Stegodon sondaari* (~16% of fossil specimens) and *Megalochelys* sp. (~74% of all fossil specimens). Other vertebrates present in this large assemblage are Komodo dragon (*Varanus komodoensis*), unidentified crocodiles, and a pelvis and marginal carapace fragment of a box turtle (cf. *Cuora amboinensis*) (Setiyabudi, 2017; Takahashi et al., 2015; van den Bergh, 1999). An unidentified large-bodied murine rodent can now be added to this faunal assemblage, and which extends the earliest record of murine rodents on Flores with more than 500,000 years.

The slightly younger fossil Tangi Talo assemblage from Excavation F (TT-UP) estimated to be ~1.27 Ma, still contains *S. sondaari* (35% of the total number of fossil specimens), *V. komodoensis* (22% of specimens) and crocodiles (3.3% of specimens). The remainder (39.5%) are unidentified bone fragments, but the site clearly lacks evidence for the presence of *Megalochelys*, of which small carapace and plastron fragments would have been easily recognizable if they were present. Of the *S. sondaari* fossils, several long bones, two tusks, a mandible, vertebrae, ribs and 12 articulated caudal vertebrae can be ascribed to a single adult individual, but a large portion of the *S. sondaari* fossils from TT-UP represents juvenile individuals, such as isolated milk molars and milk tusks. The MNI of *S. sondaari*, based on dental elements, amounts to 35. Two *V. komodoensis* thoracic vertebrae were found articulated, and most if not all vertebrae and costa fragments may represent a single individual, hence the relatively large proportion of *V. komodoensis* fossils in the assemblage, but a MNI of one.

Above TT-UP there is a gap in the fossil record of several hundred thousand years, with the next oldest fossil-bearing layer being represented by the basal conglomerate at Kobatuwa-I, which has an estimated age of between 1 and 0.9 Ma (**see 7.2.1**). This fluvial conglomerate yielded only two rolled molar fragments of a medium to large-sized *Stegodon* cf. *florensis* (Jatmiko et al., 2009), representing the earliest appearance of this taxon on Flores. The same basal conglomerate at Kobatuwa-I contains stone artefacts, proxy evidence for a hominin presence at this site. These conglomerates may be of similar age as the basal conglomerates from three other sites in the So'a Basin where stone artefacts occur just below the 1 Ma dated WST (Wolo Sege, Kobatuwa-IV, and Mata Go), providing a minimum age for the earliest appearance of hominins.

The fossil assemblage from layers directly on top of the basal conglomerate at Kobatuwa-I (layers I, J, H), is slightly older than the emplacement of the Pu Maso Tephra (Fig. 10), which is dated at 0.81 ± 0.04 Ma. The Kobatuwa-I layers I to H contain abundant *S. florensis* remains, together with crocodiles (possibly *Crocodylus siamensis* (Setiyabudi, 2017);), *V. komodoensis*, and lithic artefacts indicating a continuing hominin presence. Two unidentified rodent fossils were also recovered.

The largest fauna assemblage documented from the So'a Basin is from the lower fossil-bearing interval at Mata Menge (MM-LOW), with an age of between 0.77 Ma (the base of the Brunhes Chron) and 0.73 Ma, with this younger age limit representing the upper error range of the ZFT age from the MM-LOW interval as reported by (Morwood et al., 1998). MM-LOW has the same taxa as recorded at Kobatuwa, and likewise contains stone artefacts (Brumm et al., 2010b). Because of the large fossil sample from the MM-LOW interval (11,730 fossil specimens), there are a number of other vertebrates represented that are usually less commonly found in the fossil record, such as several bird species and frogs (Meijer et al., 2015). The birds include various wetlands taxa (a swan *Cygnus* sp.; a duck *Anas* cf *gibberifrons*; a large rail cf. *Gallinula*/*Fulica*; and a lapwing *Vanellus* sp.) and a medium-sized bird of prey (*Hieraaetus* sp.) (Meijer et al., 2015).

Most of the numerous diagnostic murine rodent fossils (molars, mandibles and maxillae) from the MM-LOW interval belong to *Hooijeromys nusatenggara*, which could be a descendant of the unidentified giant rat from TT-LOW. *H. nusatenggara*, first described by Musser (1981) and based on fossil tooth rows from the sites Ola Bula and Boa Leza, is by far the most abundant rodent species documented for the late Early Pleistocene of the So'a Basin, with the exception of a single *Spelaeomys florensis* molar from the MM-LOW interval.

Broadly contemporaneous with the MM-LOW is the site of Boa Leza, which, based on its proximity to Mata Menge, its similar sedimentary facies association, and a ZFT date of 0.84 ± 0.07, is not distinguishable from the MM-LOW in either age or depositional environment. Both *S. florensis* and *H. nusatenggara* have been found at Boa Leza, but not Komodo dragon, which could be due to the much smaller sample size obtained from Boa Leza (478 versus 11,730 fossil specimens, respectively). The Boa Leza assemblage, however, includes an Eagle Owl (*Bubo* sp.) (Meijer et al., 2015).

The common fauna elements from MM-LOW and Boa Leza continue to be present in the Mata Menge sequence in the MM-UP level, which, with an estimated age ~0.7 Ma, represents the youngest record of megafauna in the OBF, followed by a gap in the fossil vertebrate record of ~650,000 years. The MM-UP assemblage includes a small number of *H. floresiensis*-like fossils (van den Bergh et al., 2016), and a coracoid of a shelduck (cf. *Tadorna*) (Meijer et al., 2019), but a large portion of the fossil assemblage from the MM-UP has not yet been analysed in detail.

No vertebrate fossils were recovered from the lacustrine interval at the top of the OBF. However, the terrace remnant along the Ae Sesa at the site Ula Mala Kata now provides the youngest, Late Pleistocene megafauna record from the So'a Basin. The *Stegodon* from this site is smaller than its putative ancestor from the OBF, with a size and morphology conform the smaller subspecies *S. florensis insularis*, known from the Late Pleistocene cave deposits in Liang Bua.

The MNI for *S. sondaari* based on dental elements from the TT-LOW amounts to 52 individuals who died at varying life stages. By assigning each of these 52 individuals to one of five age groups spanning the entire life history of these animals (see van den Bergh, 1999 for the methods used) an age profile of the TT-LOW assemblage was constructed (van der Geer et al., 2017). The resultant profile resembles the Type A age profile of Haynes (Haynes, 1991), which is characterized by a predominance of juvenile individuals and progressively decreasing proportions of successively older age classes. In the TT-LOW, 35% of the individuals represent juveniles with milk teeth (either dP2, dP3 and dP4) in various degrees of occlusal wear. Subsequently older age groups comprise 29% (young adults), 21% (prime adults), 6% (old adults) and 10% (senescent). This age structure of the death assemblage resembles that of a

stable living population, and is indicative of non-selective mortality, e.g. caused by a catastrophic event affecting the mortality of all age groups equally (Haynes, 1991). The main bone bed at Tangi Talo (TT-LOW) is associated with a large volcanic eruption as represented by the pumice-rich lahar covering the bones. This eruption could therefore account for a local population of *S. sondaari* being affected by the non-selective mortality of all age groups (Aziz et al., 2009a; van den Bergh, 1999; van der Geer et al., 2017). A partially preserved *Megalochelys* carapace–plastron with pelvic girdle and left femur and tibia unearthed in 1992 from the main bone bed contained four isolated teeth of *V. komodoensis* inside, suggesting that Komodo dragons fed on this tortoise carcass. It is also possible that after emplacement of the pumice lahar Komodo dragons dug through this deposit to scavenge the buried animal carcasses. Such scavenging behavior has been observed elsewhere following a major volcanic eruption (Lyman, 1989). The fragmentary and scattered nature of the TT-LOW bone assemblage and the lack of articulated skeletal elements suggests a time gap between death and final burial, as was initially proposed by van den Bergh (1999).

The age structure of the *S. sondaari* death assemblage from the fluvial channel infill of Excavation F (TT-UP) is quite distinct from that of the TT-LOW. The MNI of TT-UP amounts to at least 35 individuals, 86% of which represent juveniles. This proportion could even be an underestimate, considering that bones of young individuals are less likely to be preserved (Damuth, 1982). The TT-UP age profile corresponds with the Type B of Haynes (1991), in which juveniles greatly outnumber mature individuals. A Type B profile is established when juveniles are disproportionally affected by mortality, but does not suggest a sudden catastrophic event as the main cause of death. Instead, Type B could be the result of predation, possibly by Komodo dragons or crocodiles, or other factors causing selective juvenile mortality, such as food shortages or a period of extreme draught (cf. Haynes, 1991; van der Geer et al., 2014)). A direct association with volcanic activity is not evident for the TT-UP, nor are there stone artefacts associated with the TT-UP sequence, which, had they been present, might indicate hominin predation.

It is important to note here that *S. sondaari* and *V. komodoensis* both occur in the fluvial channel fill of Excavation F in the TT-UP, and therefore the volcanic event that supposedly generated the earlier mass death (as exemplified by the main bone bed, TT-LOW) apparently had not impacted the entire population of these animals on Flores. However, the volcanic event associated with the lahar that covered the main bone bed of TT-LOW may have wiped out the *Megalochelys* population, since this taxon has not been recorded from any younger strata throughout the So'a Basin. What eventually caused the extinction of *S. sondaari* between 1.27 Ma and 0.9 Ma remains speculative, due to the gap in the fossil record. This species' disappearance from the fossil record could be associated with the later arrival of hominins (predation) and/or interspecific competition following the arrival of the larger *S. florensis* sometime before 0.9 Ma, and/or other indirect ecological impacts caused by this newly-arrived larger proboscidean taxon. An increase in aridity around the Middle Pleistocene transition could also have played a role (see section 7.2.4).

The youngest *Stegodon* fossils in the So'a Basin are now represented by the *S. florensis insularis* fossils from Ulu Mala Kata. Over a period of more than half a million years, the So'a Basin *Stegodon* decreased ~30% in linear body size dimensions to reach the size of its Late Pleistocene descendants (van den Bergh et al., 2008). Based on body weight estimates derived from limb bone dimensions, the anatomical changes between the So'a Basin and Liang Bua *S. florensis* would have amounted to a 67% decrease in body weight (van der Geer et al., 2016). This is why the So'a Basin and Liang Bua *S. florensis* have been given distinct chrono-subspecies names: *S. florensis* from the OBF, and *S. florensis insularis* from Liang Bua (van den Bergh et al., 2008; van den Bergh et al., 2009b) and Ulu Mala Kata.

7.2.3. Hominin arrival

The new stratigraphic and dating evidence strongly indicates that the Tangi Talo main bone bed (TT-LOW) is half a million years older than previously thought (Brumm et al., 2010a; Morwood et al., 1998; O'Sullivan et al., 2001; Sondaar et al., 1994), and that the youngest occurrence of *S. sondaari* (TT-UP) predates the oldest occurrence of stone artefacts by an estimated 250,000 years. When the age of the Tangi Talo fauna was still thought to be ~0.9 Ma (e.g., Aziz et al., 2009a; Brumm et al., 2010a; Morwood et al., 1998), it was assumed that *S. sondaari* had been present on Flores at least 100,000 years *after* the arrival of hominins, and therefore that the extinction of *S. sondaari* and giant tortoise – and the arrival of a new larger-bodied *S. florensis* – occurred during the ensuing 100,000 years. This suggested that the arrival of hominins on Flores did not have any immediate impact on the *Stegodon* and *Megalochelys* populations (Brumm et al., 2010a). Our revision of the dating of the Tangi Talo fauna now demonstrates there is no evidence of an overlap of 100,000 years. Instead, there is a time gap in the So'a Basin between the latest occurrence of *S. sondaari* at 1.27 Ma and the earliest record of stone artefacts at slightly older than 1 Ma. At present it cannot be conclusively demonstrated that the Tangi Talo fauna did *not* overlap in time with the arrival of hominins on Flores. This is because the stratigraphically oldest stone artefacts from directly beneath the WST have a minimum age of 1 Ma, and none of the three sites where this association has been observed (Wolo Sege, Kobatuwa-IV, and Mata Go) have produced fossil evidence. The oldest occurrence of *S. florensis* in the basal conglomerate at Kobatuwa-I could be as old as the artefact-bearing conglomerates at these three sites, though no conclusive evidence provides a minimum age in excess of 1 Ma at Kobatuwa-I, and based on the current data it could be 0.9 Ma. However, given stone artefacts are absent from all excavated sites equivalent in age, or older than, 1.27 Ma ($n = 7$), it is unlikely that hominins were present before 1.27 Ma. Therefore, it remains an open question whether hominins were involved in the demise of the Early Pleistocene megafauna on Flores.

What about the arrival of modern humans during the Late Pleistocene? In Liang Bua the youngest *S. florensis insularis* fossils are directly overlaid by, and partly embedded in, ash layer LB-T3, which is estimated to be 50 ka (Sutikna et al., 2016). The *S. florensis insularis* occurrence from Ulu Mala Kata may be equivalent in age or slightly younger, with a minimum calibrated age of ~47.250 cal BP (upper calibrated age boundary is > 50,000 cal BP), and may represent the youngest recorded occurrence of *Stegodon* on Flores. This last recorded presence of *Stegodon* is just a few thousand years older than the earliest evidence for the arrival of modern humans on Flores at ~46 ka cal BP (Sutikna et al., 2018) and on Sulawesi north of Flores, where the earliest known cave art is dated to at least 45.5 ka (Brumm et al., 2021).

It is therefore tempting to speculate that modern humans were the main factor in the demise of *S. florensis,* an animal that had shared the island of Flores for almost a million years with *H. floresiensis* despite fluctuating climatic conditions and major volcanic eruptions. *Homo sapiens* must have crossed Wallacea on the way to Australia even before 46 ka, as there is now widespread evidence that modern humans were well established on that

continent from around 50 ka (Hamm et al., 2016; Veth et al., 2017), and may have even reached there as early as 65 ka (Clarkson et al., 2017). If this early age for the occupation of Australia can be maintained, it could be possible that *H. sapiens* initially by-passed Flores taking the northern route via Sulawesi, Seram and Halmahera (Kealy et al., 2017), but archaeological evidence for an occupation as early as 65 ka on these islands, or any Wallacean island for that matter, is so far lacking.

7.2.4. Palaeoenvironmental changes

It is possible that cataclysmic volcanic activity, such as the caldera forming eruption that deposited the WST at 1 Ma ago, may have caused or contributed to the eventual disappearance of *S. sondaari*. However, hominins were already present on Flores when the WST was emplaced, and they continued to be present following this event, with the earliest post-WST record of hominins represented by the lithics in layers I-G at Wolo Sege, and possibly the basal conglomerate (layer K), at Kobatuwa-I. The eruption may therefore have only affected biota surrounding the Kelilambo volcano – including in the So'a Basin – but did not lead to extinction in other parts of Flores. This would allow repopulation of the So'a basin following this volcanic event, at least as far as hominins are concerned.

S. sondaari may have already been extinct when hominins first set foot on the island. Another explanation for the demise of *S. sondaari* could be a drying climate resulting in an increase of C_4 plants in open grassland at the expense of C_3 plants in forested areas. C3 vegetation constituted an important part of the diet of *S. sondaari*, which was a mixed feeder of leafy C_3 plants besides C_4 grasses (Puspaningrum, 2016). In contrast, *S. florensis* seems to have thrived in a drier, grass-dominated landscape, at least after 0.9 Ma, as demonstrated by the significantly higher $\delta^{13}C$ contents of the tooth enamel of *S. florensis* from the Middle Pleistocene Sandstone Member of the OBF (see Fig. 11). The prevalence of an open grassland environment during the Early Middle Pleistocene is supported by other observations, such as the fossil avifauna and a limited set of palynological data (Brumm et al., 2016; Meijer et al., 2015). However, no indicators are currently available for the Early Pleistocene palaeoenvironmental conditions, other than the stable isotope analyses of *S. sondaari* tooth enamel. The observed difference in diet between *S. sondaari* and *S. florensis* suggests an increase in relative availability of C_4 resources and could signify a significant reduction in rainfall or increased seasonality. Because some of the Kobatuwa individuals before 0.9 Ma were also mixed feeders, *S. florensis* may have been more flexible in its diet, but under drying conditions was eventually forced to primarily feed on grasses. This trend continued into the Late Pleistocene, evidenced by the Liang Bua *S. florensis insularis*, which had reached a similar small body-size as the much older *S. sondaari* lineage, but had a diet dominated by C_4 grasses (Puspaningrum, 2016). On the island of Sumba directly south of Flores a single *Stegodon sumbaensis* molar from the site Lewa Paku, with an estimated age of ~1 Ma, also had a mixed diet as indicated by a $\delta^{13}C$ value of −4.8‰, and similar to *S. sondaari*. Although only one early Pleistocene *Stegodon* individual is known from Sumba, more data is available from the adjacent island of Timor. All *Stegodon timorensis* molars on Timor are dated as younger than 0.81 Ma ($n = 6$), and thus of Middle or Late Pleistocene age, had a $\delta^{13}C$ above −2‰ and were grazers (Puspaningrum, 2016). This could indicate that a similar trend of increased aridity could have affected not just Flores, but the wider region of East Nusatenggara. A trend of forested areas being replaced by savannah environments around the Mid-Pleistocene Transition (MPT) has also been demonstrated for both Java and the wider SE Asian region (Louys and Roberts, 2020; Puspaningrum et al., 2020).

A reduction in rainfall is in accordance with Quaternary global climate models, which indicate that between 1.25 and 0.7 Ma ago there was a gradual transition from low amplitude and high-frequency climatic oscillations (~ 41,000-year cycles) to high amplitude and low frequency oscillations (100,000-year cycles). This resulted in lower overall sea surface temperatures together with increasing aridity and monsoonal intensity in Asia (Clark et al., 2006). In the So'a Basin, Kobatuwa, the oldest site with *S. florensis*, is estimated to be between 1.0 and 0.83 Ma old. This site records a transition and has yielded both mixed C_3/C_4 individuals and individuals with a higher C_4 component in their diet, whereas all of the younger sites are characterized by grazers (*S. florensis* and *H. nusatenggara*) that primarily fed on C_4 resources (Brumm et al., 2016).

High tempo explosive silicic volcanism in the So'a Basin, shifts in faunal composition and diet, and the arrival of humans on Flores (Fig. 19) are all broadly coincident with the onset of the MPT at ~1.25 Ma (Marine Isotope Stages (MIS) 38 (Clark et al., 2006). In terrestrial realms of the western Pacific and south-east Asia little is known about MPT orbitally-forced biotic effects, though increases in African and Asian aridity and monsoonal intensity have been postulated (Clemens et al., 1996; Head and Gibbard, 2005; Sun et al., 2019; Tiedemann et al., 1994; Williams et al., 1997). Changes in astronomically-forced climate response at the onset of the MPT, leading to overall increase in aridity and/or seasonality between 1.4 and 0.8, as evidenced by the observed shift in herbivore feeding habits, could be a causative factor that impacted browsing insular fauna on Flores such as *S. sondaari*. However, the arrival of other large mammals (hominins and *S. florensis*), during broadly the same time interval, combined with a significant gap of 400,000 years in the fossil record, complicates determining what factor(s) ultimately led to the extinction of *S. sondaari*.

7.3. Archaeological observations

The stone artefact assemblages recovered from the So'a Basin sites reflect a similar approach to hard-hammer direct percussion of cobbles and pebbles available in local gravel deposits (Fig. 20). Cores were reduced bifacially, producing centripetal 'radial' cores, but were sometimes rotated out of the radial plane, resulting in multiplatform cores. Core reduction was usually non-intensive, and flakes struck from these cores were sometimes retouched. Raw material procurement appears to reflect careful selection for the more siliceous varieties of stones from local gravel deposits; chalcedony and silicified tuff (including opalescent variants) are relatively rare in these gravels, yet compose ~10–30% of the flaked-stone assemblages (SI Table H.1). The conjoined flake (Fig. 20-J) and core (Fig. 20-I) from Kobatuwa—and the presence of minimally-reduced 'assayed cobbles' at all sites—may indicate that cobbles were partly or entirely reduced at the stone source areas, with tools carried away for use elsewhere.

A comparison of assemblage counts shows similar proportions of artefact types spanning some 300,000 years across a variety of sites and contexts (Fig. 20; Table H.1). This technological stability attests to the importance of the stone technology to hominin adaptation to this insular environment. Although the stone technology was not lost entirely, despite the putative changes to brain structure that may have occurred through the process of island endemism (Falk et al., 2005, 2009), neither are there clear signs of technological innovation in the face of the stresses imposed by the

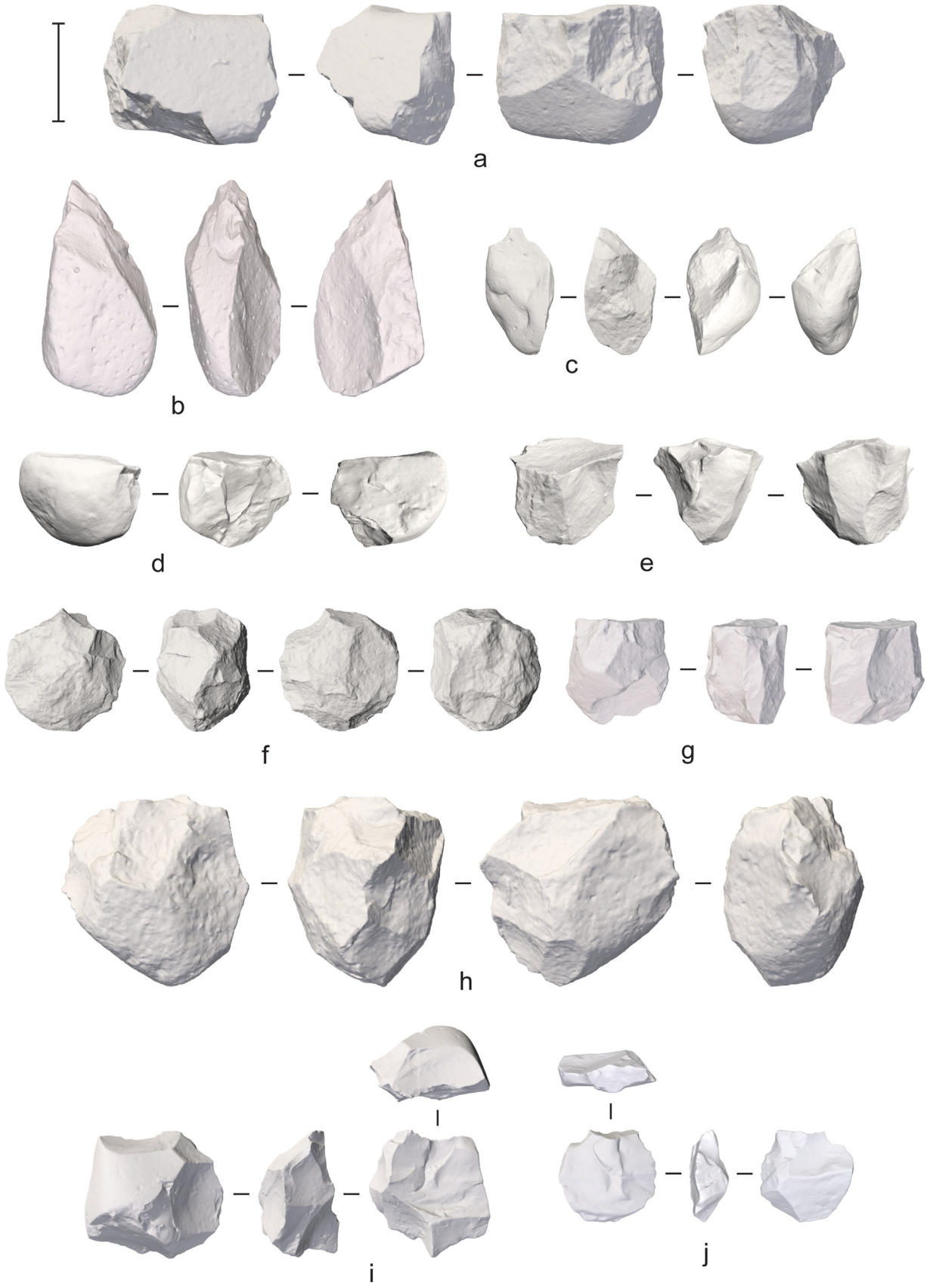

Fig. 20. 2D representations of 3D scans of various stone artefacts excavated *in situ* at So'a Basin sites. **A,** Multiplatform core from Wolo Sege, Upper Trench, No. A4; **B,** Pick-like multiplatform core from Wolo Sege, Main Trench Conglomerate, No. WS/10/71; **C,** Perforator-like retouched cobble fragment from Kobatuwa, Sector 18, Layer H, No. 72; **D,** Bifacial core from Kobatuwa, sector 16, No. 9; **E,** Multiplatform core from Mata Menge Trench 25 (MM-LOW), No. A107; **F,** Multiplatform core from Mata Menge, Trench 27B (MM-LOW), No. A-1636; **G,** Multiplatform core from Wolo Sege, Main Trench Conglomerate, No. WS/10/116; **H,** Multiplatform core from Mata Menge, Trench 27B (MM-LOW), No. S914; **I,** Bifacial

dynamic environment, (i.e., volcanism and variable Pleistocene climate). This has larger implications for interpreting hominin stone tool-kits, as it implies that a simple 'Oldowan-like' technology is sufficient for a technological adaptation to a dramatically variable environment. One possible exception is the apparent diminution of 'picks' at Wolo Sege to small 'perforators' at Kobatuwa and Mata Menge (Brumm et al., 2006), and, much later, at Liang Bua (Moore and Brumm, 2009; Moore et al., 2009). However, during surveys large picks made on cobbles have been recovered from the surfaces of eroding contexts of a variety of ages at Mata Menge/Boa Leza, Tangi Talo (at Tangi Talo these surface tools likely originated from the younger part of the sequence exposed in the steep hill slope, equivalent in age with the WST or younger), and elsewhere in the So'a Basin. Given how rare picks are relative to other artefact classes, their absence from excavated assemblages from later deposits may be a sample size effect. Alternatively, the variation may be related to differences in the types of activities that occurred across the excavated sites, although the functions of picks and perforators is presently unknown.

Theoretical and experimental research into early stone tools emphasises that the skills necessary to strike well-controlled flakes – like the tools made by So'a Basin hominins – suggest relatively advanced cognitive abilities, beyond the capabilities of living primates, and unique to the hominin lineage (Moore, 2019). However, the preponderance of bifacial reduction and multiplatform cores at the So'a Basin sites is consistent with simple reduction to produce sharp edges rather than to produce formal tool forms that reflect a hominin 'mental template' (Moore and Perston, 2016). The So'a Basin tools are similar in technology and form to the earliest stone tool assemblages from Africa (Moore and Brumm, 2009), and they can be produced without higher-order intentions (Moore, 2011, 2020; Moore and Perston, 2016). Picks and perforators are the possible exception to this, with hints of 'Acheulean-like' technology, and documenting the chronology and natures of these tool forms – and the cognitive capacities they might imply – is a priority for further So'a Basin research.

8. Conclusions

Our identification of the Wolo Sege Tephra at Tangi Talo, combined with our new radiometric age results, has led to fresh insights into the insular faunal composition existing during the time the lower Ola Bula sediments were being deposited. This revision of the faunal succession now rejects the earlier interpretation that a fauna turnover occurred at least ~100,000 years *after* the first arrival of hominins to the island – and which occurred before 1 Ma (Brumm et al., 2010a). Instead, the new chronostratigraphy, which is based on tephrostratigraphic correlations combined with new radiometric ages, indicates that an early Pleistocene insular fauna (comprising the small-bodied proboscidean *Stegodon sondaari*, the giant tortoise *Megalochelys* sp., Komodo dragon *Varanus komodoensis*, a box turtle *Cuora* cf. *amboinensis*, crocodiles, and unidentified murine rodents) were present on Flores ~1.4 Ma ago, which is half a million years earlier than had previously been assumed.

The subsequent disappearance of the small-bodied *S. sondaari* and giant tortoise from the sedimentary record likely occurred before, and/or is coeval with, the earliest occurrence of hominin stone artefacts: the artefacts recovered from beneath the Wolo Sege Tephra, dated at slightly more than 1 Ma, at three different sites in the So'a Basin (Kobatuwa IV, Wolo Sege and Mata Go).

The interval broadly encapsulating the WST is characterized by a closely-spaced succession of explosive eruptions where the So'a Basin was repeatedly inundated by voluminous pyroclastic flow events originating from a now extinct volcanic complex on the east side of the basin, which is most likely the Keli Lambo Volcano. In the aftermath of these successive events, the extensive secondary reworking of these mass-flow deposits indicates sustained landscape instability and readjustment, which in turn would have had important, and recurrent, effects on the So'a Basin vegetation and resident insular fauna. In addition to these volcanic events, climatic changes coinciding with the Early to Middle Pleistocene transition could have contributed to the extinction of *S. sondaari* and giant tortoise, but further evidence is required to clarify this, as well as the possibility that the arrival of hominins and/or another larger *Stegodon* species, could also have facilitated these extinctions.

Following the emplacement of the Pu Maso Tephra around 0.8 Ma, the influx of volcaniclastic materials into the So'a Basin from the east either decreased, or stopped altogether. In the western portion of the basin, at Mata Menge and Boa Leza, this reduced sediment supply seems to have resulted in downcutting of the sequence, removing the upper marker tephra layers (Pu Maso and Turakeo tephras), by a fluvial system likely originating from the Welas Caldera. At what age the Welas Caldera started to fill in with a lake and produce the lacustrine sediments at Poma remains unknown, but lake expansion appears coincident with an emergent intra-caldera cone formation (see Fig. 9 a-c). Phreatomagmatic activity associated with initial cone emergence and growth likely displaced the lake waters, causing them to spill into adjacent tributaries and form mudflows of admixed lake and ash sediments. Within the Sandstone Member at Mata Menge and Boa Leza, the cut-and-fill sequence contains multiple metre-thick mudflow units that are interbedded with fluvial sands and gravel layers that contain prolific stone artefacts and fossil bones. This suggests that by 0.77 Ma, which is the age of the lower fossil-bearing interval at Mata Menge, a lake was already present within the Welas Caldera, and perhaps even earlier at the time that the Kobatuwa-I fossil-bearing mudflows and lahars were emplaced. The presence of a permanent water body in the Welas Caldera lake could have attracted hominins, which would explain the abundance of stone tools in the cut-and-fill sequences exposed near Kobatuwa, Mata Menge and Boa Leza.

By 0.65 Ma the lake had expanded to the extent that the remaining subaerial portions of the So'a Basin had become submerged (see Fig. 2A). The ancestral basin outlet (paleo Ae Sesa valley) was likely blocked by rapidly aggrading fluvio-volcanic debris fans extending down the flanks of the Raja Caldera (Fig. 1). However, the exact reasons for this blockage require further investigation. This palaeolake existed for at least 150,000 years, before it drained in response to head-wall erosion with the ancestral Ae Sesa river and its tributaries incising further back within the confines of the basin, while volcaniclastic influxes from the active volcanoes south of the So'a Basin continued to build peripheral aprons of coalescing fluvio-volcanic debris fans. Of special notice is a remnant of a massive coarse-grained lahar exposed in the terrace remnant along the Ae Sesa river at Ulu Mala Kata (Fig. 2), originating from the south and containing fossils attributed to *S. florensis insularis*. These Late Pleistocene *Stegodon* fossils may represent the last dated occurrence of this taxon on Flores and predate the known first appearance date of modern humans in Liang Bua by just a few thousand years. It is now evident that both *Stegodon* and a lineage of diminutive hominins persisted on the island for almost one million years prior to the arrival of

core from Kobatuwa, Sector 14, Layer G/H, No. 82; **J,** Flake from Kobatuwa, Sector 14, Layer G/H. Flake (J) conjoins onto the large scar on core (I). Scale bar 50 mm. Photogrammetric 3D models of these tools can be viewed at https://archaeology.une.pedestal3d.com/grid.

H. sapiens. Considering the long co-occurrence of these two iconic Flores endemics, it appears increasingly probable that modern humans played a key role in the extinction of both.

Author contributions

Gerrit van den Bergh: Conceptualization, Methodology, Project administration, Investigation, Formal analysis, Writing - original draft, Writing - Review and editing, Supervision, Funding acquisition. **Brent Alloway**: Conceptualization, Methodology, Investigation, Formal analysis (tephrostratigraphy), Resources, Supervision, Writing - original draft, Writing - Review and editing. **Michael Storey**: Formal analysis, Resources, Investigation, Writing - review and editing. **Ruly Setiawan**: Formal analysis, Investigation, Resources, Project administration. **Dida Yurnaldi**: Formal analysis, Investigation. **Iwan Kurniawan**: Formal analysis, Investigation, Supervision, Resources. **Mark Moore**, Methodology, Formal analysis, Investigation, Writing – Review and editing. **Jatmiko**: Investigation, Supervision. **Adam Brumm**: Conceptualization, Methodology, Investigation, Writing - original draft, Supervision, Writing – Review and editing. **Stephanie Flude**: Formal analysis ($^{40}Ar/^{39}Ar$ dating), Investigation, Writing – review and editing. **Thomas Sutikna**: Investigation, Supervision. **Unggul Prasetyo**: Investigation, Data curation. **Erick Setiabudi**: Formal analysis, Investigation. **Mika Puspaningrum**: Formal analysis, Investigation. **Ifan Yoga**: Investigation, data curation. **Halmi Insani**: Investigation. **Hanneke Meijer**: Formal analysis, Investigation, Writing – Review & editing. **Barry Kohn:** Formal analysis, Investigation, Writing - review and editing. **Brad Pillans:** Investigation, Supervision. **Indra Sutisna:** Formal analysis, Investigation, Data curation. **Anthony Dosseto**: Formal analysis. **Susan Hayes:** Investigation, Writing - original draft, Writing - Review and editing. **John Westgate**: Formal analysis. **Nick Pearce:** Formal analysis. **Fachroel Aziz:** Conceptualization, Investigation, Supervision, Resources. **Rokus Awe Due**: Investigation, Formal analysis. **Michael Morwood:** Conceptualization, Methodology, Project administration, Investigation, Supervision, Funding acquisition.

Declaration of competing interest

The authors declare that they have no known competing financial interests or personal relationships that could have appeared to influence the work reported in this paper.

Data availability

All data are presented in the appendices

Acknowledgements

This article is dedicated to the memory of Professor Mike Morwood (*b.* Auckland, New Zealand, 27-10-1950; *d.* Darwin, Northern Territory, Australia, 23-07-2013).

This research was financially supported by the Australian Research Council (grant numbers DP1093342, FT100100384, DP1096558 and DP190100164); The Geological Survey Institute (GSI), Bandung, Indonesia; the Villum Foundation, Denmark; the Faculty of Science, Medicine and Health (SMAH) of the University of Wollongong (grant 2018/SPGc-S/01); Museum Geologi Bandung; and Pusat Penelitian Arkeologi Nasional, Jakarta. Permission to undertake this research was granted by the Indonesian State Ministry of Research and Technology (RISTEK permits 0107/SIP/FRP/SM/VI/2010, 300/SIP/FRP/SM/VIII/2013, 276/E5/E5.4/SIP/2019). Local research permissions were issued by the provincial government of East Nusa Tenggara at Kupang, and the Ngada and Nage Keo District administrations. We also thank the Provincial and Ngada Tourism, Culture and Education Departments for their ongoing support. Scientific and technical personnel involved at some stage during the successive fieldwork campaigns included: T. Suryana, S. Sonjaya, H. Oktariana, A. Rahman, S. Bronto, E. Sukandar, A. Gunawan, Widji, A. T. Hascaryo, S. Wasisto, Y. Perston, K. Grant, M. Marsh, D. McGahan, A. M. Saiful, B. Burhan, L. Siagian, D. Susanti, P. D. Moi, A. R. Chivas, A. Cahyana, M. Powley, M. Wahyudiono, Budiyanto, A. Rozak, B. Jones, S. Sudjarwadi, L.D. Santi, J. Stocker and J. Tode Solo. Geodetic surveys and measurements were conducted by Y. Sopyan, E. E. Laksmana, A. Rahmadi, and G. Hazell. Our team was supported each year by up to 140 local people from the villages Mengeruda, Piga-I, Piga-II, Wolowawu and Nagerawe.

Mr Andy Brown (IGES, Aberystwyth University, UK) is thanked for conducting solution-ICP-MS acid digestions. Ms. Jane Chewings and Dr Ian Schipper (SGEES, Victoria University of Wellington, New Zealand) kindly assisted BVA with laser diffraction particle size analysis and acquisition of EMP data, respectively. Prof. Stephen Eggins and Dr James Tolley (Research School of Earth Sciences, Australian National University, Canberra, Australia) are thanked for assisting BVA with instrument access as well as, setting up and acquisition of LA-ICP-MS data. The LA-ICP-MS laboratory at RSES is supported by the Australian Federal Government's National Institute's Grant to the Australian National University, and the LA-ICP-MS analyses were funded by a post-cruise analytical grant from the Australian IODP Office. The University of Melbourne (U–Th)/He thermochronology laboratory receives support under the AuScope program of the Australian Government National Collaborative Research Infrastructure Strategy (NCRIS).

Appendix A. Supplementary data

Supplementary data to this article can be found online at https://doi.org/10.1016/j.quascirev.2022.107721.

References

Alloway, B., Westgate, J., Pillans, B., Pearce, N., Newnham, R., Byrami, M., Aarburg, S., 2004. Stratigraphy, age and correlation of middle Pleistocene silicic tephras in the Auckland region, New Zealand: a prolific distal record of Taupo Volcanic Zone volcanism. N. Z. J. Geol. Geophys. 47, 447–479.

Argue, D., Groves, C.P., Lee, M.S., Jungers, W.L., 2017. The affinities of Homo floresiensis based on phylogenetic analyses of cranial, dental, and postcranial characters. J. Hum. Evol. 107, 107–133.

Argue, D., Morwood, M.J., Sutikna, T., Jatmiko, Saptomo, E.W., 2009. *Homo floresiensis*: a cladistic analysis. J. Hum. Evol. 57, 623–639.

Aziz, F., Bergh, G.D.v.d., Morwood, M.J., Hobbs, D.R., Collins, J., Jatmiko, Kurniawan I., 2009a. Excavations at Tangi Talo, central Flores, Indonesia. In: Aziz, F., Morwood, M.J., Bergh, G.D.v. (Eds.), Pleistocene Geology, Palaeontology and Archaeology of the Soa Basin, Central Flores, Indonesia. Centre for Geological Survey, Bandung Indonesia, Bandung, pp. 41–58. Special Publication of the Centre for Geological Survey, vol. 36.

Aziz, F., Morwood, M.J., van den Bergh, G.D., 2009b. Pleistocene Geology, Palaeontology and Archaeology of the Soa Basin, Central Flores, Indonesia. Centre for Geological Survey, Bandung Indonesia, Bandung, p. 146. Special Publication of the Centre for Geological Survey, vol. 36.

Baab, K., Brown, P., Falk, D., Richtsmeier, J., Hildebolt, C., Smith, K., al, e., 2016. A critical evaluation of the down syndrome diagnosis for LB1, type specimen of Homo floresiensis. PLoS One 11, e0155731.

Brown, P., Maeda, T., 2009. Liang Bua *Homo floresiensis* mandibles and mandibular teeth: a contribution to the comparative morphology of a new hominin species. J. Hum. Evol. 57, 571.

Brown, P., Sutikna, T., Morwood, M.J., Soejono, R.P., Jatmiko, Saptomo, E.W., Due, R.A., 2004. A new small-bodied hominin from the Late Pleistocene of Flores, Indonesia. Nature 431, 1055–1061.

Brumm, A., Aziz, F., Van den Bergh, G.D., Morwood, M.J., Moore, M.W., Kurniawan, I., Hobbs, D.R., Fullagar, R., 2006. Early stone technology on Flores and its implications for *Homo floresiensis*. Nature 441, 624–628.

Brumm, A., Jensen, G., Bergh, G.D.v.d., Morwood, M.J., Kurniawan, I., Aziz, F., Storey, M., 2010a. Hominins on Flores, Indonesia, by one million years ago. Nature 464, 748–752.

Brumm, A., Moore, M.W., van den Bergh, G.D., Kurniawan, I., Morwood, M.J., Aziz, F., 2010b. Stone technology at the middle Pleistocene site of Mata Menge, Flores,

Indonesia. J. Archaeol. Sci. 37, 451–473.
Brumm, A., Oktaviana, A.A., Burhan, B., Hakim, B., Lebe, R., Zhao, J.-x., Sulistyarto, P.H., Ririmasse, M., Adhityatama, S., Sumantri, I., 2021. Oldest cave art found in Sulawesi. Sci. Adv. 7, eabd4648.
Brumm, A., van den Bergh, G., Storey, M., Kurniawan, I., Alloway, B.V., Setiawan, R., Setiyabudi, E., Grün, R., Moore, M.W., Yurnaldi, D., Puspaningrum, M.R., Wibowo, U.P., Insani, H., Sutisna, I., Westgate, J.A., Pearce, N.J., Duval, M., Meijer, H.J., Aziz, F., Sutikna, T., van der Kaars, S., Morwood, M.J., 2016. Stratigraphic context and age of hominin fossils from Middle Pleistocene Flores. Nature 534, 249–253.
Cerling, T.E., Andanje, S.A., Blumenthal, S.A., Brown, F.H., Chritz, K.L., Harris, J.M., Hart, J.A., Kirera, F.M., Kaleme, P., Leakey, L.N., 2015. Dietary changes of large herbivores in the turkana basin, Kenya from 4 to 1 Ma. Proc. Natl. Acad. Sci. USA 112, 11467–11472.
Cerling, T.E., Harris, J.M., 1999. Carbon isotope fractionation between diet and bioapatite in ungulate mammals and implications for ecological and paleoecological studies. Oecologia 120, 347–363.
Cerling, T.E., Harris, J.M., Ambrose, S.H., Leakey, M.G., Solounias, N., 1997. Dietary and environmental reconstruction with stable isotope analyses of herbivore tooth enamel from the Miocene locality of Fort Ternan, Kenya. J. Hum. Evol. 33, 635–650.
Cerling, T.E., Harris, J.M., Leakey, M.G., 1999. Browsing and grazing in elephants: the isotope record of modern and fossil proboscideans. Oecologia 120, 364–374.
Clark, P.U., Archer, D., Pollard, D., Blum, J.D., Rial, J.A., Brovkin, V., Mix, A.C., Pisias, N.G., Roy, M., 2006. The middle Pleistocene transition: characteristics, mechanisms, and implications for long-term changes in atmospheric pCO2. Quat. Sci. Rev. 25, 3150–3184.
Clarkson, C., Jacobs, Z., Marwick, B., Fullagar, R., Wallis, L., Smith, M., Roberts, R.G., Hayes, E., Lowe, K., Carah, X., Florin, S.A., McNeil, J., Cox, D., Arnold, L.J., Hua, Q., Huntley, J., Brand, H.E.A., Manne, T., Fairbairn, A., Shulmeister, J., Lyle, L., Salinas, M., Page, M., Connell, K., Park, G., Norman, K., Murphy, T., Pardoe, C., 2017. Human occupation of northern Australia by 65,000 years ago. Nature 547, 306–310.
Clemens, S.C., Murray, D.W., Prell, W.L., 1996. Nonstationary phase of the plio-pleistocene asian monsoon. Science 274, 943–948.
Cohen, K., Gibbard, P., 2019. Global chronostratigraphical correlation table for the last 2.7 million years, version 2019 QI-500. Quat. Int.
Damuth, J., 1982. Analysis of the preservation of community structure in assemblages of fossil mammals. Paleobiology 8, 434–446.
DeNiro, M.J., Epstein, S., 1978. Influence of diet on the distribution of carbon isotopes in animals. Geochem. Cosmochim. Acta 42, 495–506.
Ehlers, J, Gibbard, P.L., 2007. The extent and chronology of Cenozoic global glaciation. Quat. Int. 164, 6–20. https://doi.org/10.1016/j.quaint.2006.10.008.
Falk, D., Hildebolt, C., Smith, K., Morwood, M.J., Sutikna, T., Brown, P., Saptomo, E.W., Brunsden, B., Prior, F., 2005. The brain of LB1, Homo floresiensis. Science 308, 242–245.
Falk, D., Hildebolt, C., Smith, K., Morwood, M.J., Sutikna, T., Wayhu Saptomo, E., Prior, F., 2009. LB1's virtual endocast, microcephaly, and hominin brain evolution. J. Hum. Evol. 57, 597–607.
Hamm, G., Mitchell, P., Arnold, L.J., Prideaux, G.J., Questiaux, D., Spooner, N.A., Levchenko, V.A., Foley, E.C., Worthy, T.H., Stephenson, B., Coulthard, V., Coulthard, C., Wilton, S., Johnston, D., 2016. Cultural innovation and megafauna interaction in the early settlement of arid Australia. Nature 539, 280–283.
Hartono, H.M.S., 1961. Geological Investigations at OLabula, Flores. Djawatau Geologi Bandung.
Haynes, G., 1991. Mammoths, Mastodonts, and Elephants: Biology, Behavior and the Fossil Record. Cambridge University Press.
Head, M., Gibbard, P., 2005. Early Middle Pleistocene Transitions: an overview and recommendation for the defining boundary. Early Middle Pleistocene Transitions: the Land-Ocean Evidence. In: Head, M, Gibbard, P. (Eds.), In: Geological Society of London, Special Publication, 247. Geological Society of London, Special Publication, Bath, UK, pp. 1–18.
Hooijer, D., 1957. A *Stegodon* from Flores. Treubia 24, 119–129.
Jatmiko, van den Bergh, G.D., Morwood, M.J., Kurniawan, I., 2009. Excavations at Kobatuwa, central Flores, Indonesia. In: Aziz, F., Morwood, M.J., van den Bergh, G.D. (Eds.), Geology, Palaeontology and Archaeology of the Pleistocene Soa Basin, Central Flores, Indonesia. Geological Survey Institute Bandung, Bandung, pp. 105–117.
Jungers, W.L., Harcourt-Smith, W.E.H., Wunderlich, R.E., Tocheri, M.W., Larson, S.G., Sutikna, T., Due, R.A., Morwood, M.J., 2009. The foot of *Homo floresiensis*. Nature 459, 81–84.
Kaifu, Y., Baba, H., Sutikna, T., Morwood, M.J., Kubo, D., Saptomo, E.W., Awe, R.D., Djubiantono, T., 2011. Craniofacial morphology of *Homo floresiensis*: description, taxonomic affinities, and evolutionary implication. J. Hum. Evol. 61, 644–682.
Kealy, S., Louys, J., O'Connor, S., 2017. Reconstructing palaeogeography and inter-island visibility in the Wallacean Archipelago during the likely period of Sahul colonization, 65–45 000 years ago. Archaeol. Prospect. 24, 259–272.
Lister, A.M., 2013. The role of behaviour in adaptive morphological evolution of African proboscideans. Nature 500, 331–334.
Locatelli, E., Due, R.A., van den Bergh, G.D., Van Den Hoek Ostende, L.W., 2012. Pleistocene survivors and Holocene extinctions: the giant rats from Liang Bua (Flores, Indonesia). Quat. Int. 281, 47–57.
Louys, J., Roberts, P., 2020. Environmental drivers of megafauna and hominin extinction in Southeast Asia. Nature 586, 402–406.
Lyman, R., 1989. Taphonomy of cervids killed by the May 18, 1980, volcanic eruption of Mount St. Helens, Washington. In: Bonnichsen, R., Sorg, M. (Eds.), Bone Modification. Orono: Center for the Study of the First Americans. University of Maine, pp. 149–167.
Lyras, G., Dermitzakis, M., Van der Geer, A., Van der Geer, S., De Vos, J., 2009. The origin of Homo floresiensis and its relation to evolutionary processes under isolation. Anthropol. Sci. 117, 33–43.
MacFadden, B.J., Solounias, N., Cerling, T.E., 1999. Ancient diets, ecology, and extinction of 5-million-year-old horses from Florida. Science 283, 824–827.
Maringer, J., Verhoeven, T., 1970a. Die steinartefakte aus der Stegodon-fossilschicht von Mengeruda auf Flores. Indonesien. Anthropos 65, 229–247.
Maringer, J., Verhoeven, T., 1970b. Note on some stone artifacts in the national archaeological Institute of Indonesia at Djakarta, collected from the stegodon-fossil bed at Boaleza in Flores. Anthropos 65, 638–639.
Mark, D.F., Renne, P.R., Dymock, R.C., Smith, V.C., Simon, J.I., Morgan, L.E., Staff, R.A., Ellis, B.S., Pearce, N.J., 2017. High-precision 40Ar/39Ar dating of Pleistocene tuffs and temporal anchoring of the Matuyama-Brunhes boundary. J Quaternary Geochronology 39, 1–23.
Meijer, H.J., d'Errico, F., Queffelec, A., Kurniawan, I., Setiabudi, E., Sutisna, I., Brumm, A., van den Bergh, G.D., 2019. Characterization of bone surface modifications on an Early to Middle Pleistocene bird assemblage from Mata Menge (Flores, Indonesia) using multifocus and confocal microscopy. Palaeogeogr. Palaeoclimatol. Palaeoecol. 529, 1–11.
Meijer, H.J., Kurniawan, I., Setiabudi, E., Brumm, A., Sutikna, T., Setiawan, R., van den Bergh, G.D., 2015. Avian remains from the early/middle Pleistocene of the so'a basin, central Flores, Indonesia, and their palaeoenvironmental significance. Palaeogeogr. Palaeoclimatol. Palaeoecol. 440, 161–171.
Moore, M.W., 2011. The design space of stone flaking: implications for cognitive evolution. World Archaeol. 43, 702–715.
Moore, M.W., 2019. Flake-making and the 'cognitive Rubicon': insights from stone-knapping experiments. In: KA, O., FL, C. (Eds.), Squeezing Minds from Stones: Cognitive Archaeology and the Evolution of the Human Mind. Oxford University Press, Oxford, pp. 179–199.
Moore, M.W., 2020. Hominin stone flaking and the emergence of 'top-down'Design in human evolution. Camb. Archaeol. J. 30, 647–664.
Moore, M.W., Brumm, A., 2007. Stone artifacts and hominins in island Southeast Asia: new insights from Flores, eastern Indonesia. J. Hum. Evol. 52, 85–102.
Moore, M.W., Brumm, A., 2009. Homo floresiensis and the african oldowan. In: Hovers, E., Braun, D.R. (Eds.), Interdisciplinary Approaches to the Oldowan. Springer, New York, pp. 61–69.
Moore, M.W., Perston, Y., 2016. Experimental insights into the cognitive significance of early stone tools. PLoS One 11, e0158803.
Moore, M.W., Sutikna, T., Morwood, M., Brumm, A., 2009. Continuities in stone flaking technology at Liang Bua, Flores, Indonesia. J. Hum. Evol. 57, 503–526.
Morwood, M., Aziz, F., O'Sullivan, P., Hobbs, D., Raza, A., 1999. Archaeological and palaeontological research in central Flores, east Indonesia: results of fieldwork 1997–98. Antiquity 73, 273–286.
Morwood, M.J., Aziz, F., Nasruddin, Hobbs, D.R., van den Bergh, G.D., Kurniawan, I., 2009. Archaeological and palaeontological excavations at Boa Lesa, central Flores, Indonesia. In: Aziz, F., Morwood, M.J., van den Bergh, G.D. (Eds.), Pleistocene Geology, Palaeontology and Archaeology of the Soa Basin, Central Flores, Indonesia. Pusat Survei Geologi, Bandung, Indonesia, pp. 95–104.
Morwood, M., Aziz, F., Van den Bergh, G., Sondaar, P., De Vos, J., 1997. Stone artefacts from the 1994 excavation at Mata Menge, west central Flores, Indonesia. Aust. Archaeol. 44, 26–34.
Morwood, M.J., Brown, P., Jatmiko, Sutikna, T., Saptomo, E.W., Westaway, K.E., Due, R.A., Roberts, R.G., Maeda, T., Wasisto, S., Djubiantono, T., 2005. Further evidence for small-bodied hominins from the late Pleistocene of Flores, Indonesia. Nature 437, 1012–1017.
Morwood, M.J., O'Sullivan, P.B., Aziz, F., Raza, A., 1998. Fission-track ages of stone tools and fossils on the east Indonesian island of Flores. Nature 392, 173–176.
Muraoka, H., Nasution, A., Urai, M., Takahashi, M., Takashima, I., Simanjuntak, J., Sundhoro, H., Aswin, D., Nanlohy, F., Sitorus, K., Takahashi, H., Koseki, T., 2002. Tectonic. volcanic and stratigraphic geology of the Bajawa geothermal field, central Flores, Indonesia. Bull. Geol. Surv. Jpn. 53, 109–138.
Musser, G.G., 1981. The giant rat of Flores and its relatives east of Borneo and Bali. Bull. Am. Mus. Nat. Hist. 169, 67–176.
O'Sullivan, P.B., Morwood, M., Hobbs, D., Suminto, F.A., Situmorang, M., Raza, A., Maas, R., 2001. Archaeological implications of the geology and chronology of the Soa basin, Flores, Indonesia. Geology 29, 607–610.
Passey, B.H., Cerling, T.E., Perkins, M.E., Voorhies, M.R., Harris, J.M., Tucker, S.T., 2002. Environmental change in the Great Plains: an isotopic record from fossil horses. J. Geol. 110, 123–140.
Pearce, N.J., Westgate, J.A., Gatti, E., Pattan, J.N., Parthiban, G., Achyuthan, H., 2014. Individual glass shard trace element analyses confirm that all known Toba tephra reported from India is from the c. 75-ka Youngest Toba eruption. J. Quat. Sci. 29, 729–734.
Pillans, B., Alloway, B., Naish, T., Westgate, J., Abbott, S., Palmer, A., 2005. Silicic tephras in Pleistocene shallow-marine sediments of Wanganui Basin, New Zealand. J. Roy. Soc. N. Z. 35, 43–90.
Powley, M.J., Sutisna, I., Mikac, K.M., Wibowo, U.P., van den Bergh, G.D., 2021. The *Stegodon* bonebed of the middle Pleistocene archaeological site Mata Menge (Flores, Indonesia): taphonomic agents in site formation. Quaternary 4, 31.
Puspaningrum, M.R., 2016. Proboscidea as Palaeoenvironmental Indicators in Southeast Asia. University of Wollongong, Australia, p. 318.
Puspaningrum, M.R., van den Bergh, G.D., Chivas, A.R., Setiabudi, E., Kurniawan, I.,

2020. Isotopic reconstruction of proboscidean habitats and diets on Java since the early Pleistocene: implications for adaptation and extinction. Quat. Sci. Rev. 228, 106007.
Setiawan, R., 2018. Geoarchaeology of the Soa Basin, Flores, Indonesia: New Considerations on Stratigraphy, Chronology and Palaeoenvironment. University of Wollongong, Australia.
Setiyabudi, E., 2017. Pleistocene reptiles of the Soa Basin (Flores, Indonesia): adaptation and implication for environment. Jurnal Geologi dan Sumberdaya Mineral 17, 107–124.
Smith, G.A., Lowe, D.R., 1991. Lahars: volcano hydrologic-events and deposition in the debris flow—hyperconcentrated flow continuum. In: Fisher, R., Smith, G. (Eds.), Sedimentation in Volcanic Settings. SEPM Special Publication, pp. 59–70.
Sondaar, P.Y., van den Bergh, G.D., Mubroto, B., Fachroel, A., de Vos, J., Batu, U.L., 1994. Middle Pleistocene faunal turnover and colonization of Flores (Indonesia) by *Homo erectus*. Comptes rendus de l'Académie des sciences. Série 2. Sciences de la terre et des planètes 319, 1255–1262.
Sucipta, E., Takashima, I., Muraoka, H., 2006. Morphometric age and petrological characteristics of volcanic rocks from the Bajawa cinder cone complex, Flores, Indonesia. J. Mineral. Petrol. Sci. 101, 48–68.
Suminto, Morwood, M.J., Kurniawan, I., Aziz, F., Bergh, G.D.v.d., Hobbs, D.R., 2009. Geology and fossil sites of the Soa Basin, Flores, Indonesia. In: Aziz, F., Morwood, M.J., Bergh, G.D. vd (Eds.), Palaeontology and Archaeology of the Soa Basin, Central Flores, Indonesia. Indonesian Geological Survey Institute, Bandung, pp. 19–40.
Sun, Y., Yin, Q., Crucifix, M., Clemens, S.C., Araya-Melo, P., Liu, W., Qiang, X., Liu, Q., Zhao, H., Liang, L., Chen, H., 2019. Diverse manifestations of the mid-Pleistocene climate transition. Nat. Commun. 10, 1–11.
Sutikna, T., Tocheri, M.W., Faith, J.T., Awe, R.D., Meijer, H.J., Saptomo, E.W., Roberts, R.G., 2018. The spatio-temporal distribution of archaeological and faunal finds at Liang Bua (Flores, Indonesia) in light of the revised chronology for *Homo floresiensis*. J. Hum. Evol. 124, 52–74.
Sutikna, T., Tocheri, M.W., Morwood, M.J., Saptomo, E.W., Jatmiko, Awe R.D., Wasisto, S., Westaway, K.E., Aubert, M., Li, B., Zhao, J.-x., Storey, M., Alloway, B.V., Morley, M.W., Meijer, H.J.M., van den Bergh, G.D., Grün, R., Dosseto, A., Brumm, A., Jungers, W.L., Roberts, R.G., 2016. Revised stratigraphy and chronology for *Homo floresiensis* at Liang Bua in Indonesia. Nature 532, 366–369.
Takahashi, A., Setiyabudi, E., Van den Bergh, G.D., 2015. *Cuora amboinensis* (Testudines: Geomydidae) from the Lower Pleistocene of Flores Island, Indonesia. 2015 Annual Meeting of the Herpetological Society of Japan. Herpetological Society of Japan, Chiba, Japan, p. 68.
Tiedemann, R., Sarnthein, M., Shackleton, N.J.J.P., 1994. Astronomic timescale for the pliocene atlantic δ18O and dust flux records of ocean drilling program site 659. Paleoceanography 9, 619–638.
Tocheri, M.W., Orr, C.M., Larson, S.G., Sutikna, T., Saptomo, E.W., Due, R.A., Djubiantono, T., Morwood, M.J., Jungers, W.L., 2007. The primitive wrist of Homo floresiensis and its implications for hominin evolution. Science 317, 1743–1745.
van den Bergh, G.D., De Vos, J., Aziz, F., Morwood, M., 2001. Elephantoidea in the Indonesian Region: New *Stegodon* Findings from Flores, the World of Elephants. Proceedings of the 1st International Congress, Rome, pp. 16–20.
van den Bergh, G.D., 1999. The Late Neogene elephantoid-bearing faunas of Indonesia and their palaeozoogeographic implications: a study of the terrestrial faunal succession of Sulawesi, Flores and Java, including evidence for early hominid dispersal east of Wallace's Line. Scripta Geol. 117, 1–419.
van den Bergh, G.D., Awe, R.D., Morwood, M.J., Sutikna, T., Jatmiko, Wahyu Saptomo, E., 2008. The youngest *Stegodon* remains in Southeast Asia from the late Pleistocene archaeological site Liang Bua, Flores, Indonesia. Quat. Int. 182, 16–48.
van den Bergh, G.D., Kaifu, Y., Kurniawan, I., Brumm, A., Kono, R.T., Setiabudi, E., Aziz, F., Morwood, M.J., 2016. *Homo floresiensis*-Like fossils from the early middle Pleistocene of Flores. Nature 534, 245–248.
van den Bergh, G.D., Kurniawan, I., Morwood, M.J., Lentfer, C.J., Suyono, Setiawan, R., Aziz, F., Suyono, 2009a. Environmental reconstruction of the middle Pleistocene archaeological/palaeontological site Mata Menge, Flores, Indonesia. In: Aziz, F., Morwood, M.J., van den Bergh, G.D. (Eds.), Palaeontology and Archaeology of the Soa Basin, Central Flores, Indonesia. Geological Survey Institute, Bandung.
van den Bergh, G.D., Meijer, H.J.M., Due Awe, R., Morwood, M.J., Szabo, K., van den Hoek Ostende, L.W., Sutikna, T., Saptomo, E.W., Piper, P.J., Dobney, K.M., 2009b. The Liang Bua faunal remains: a 95 k.yr. sequence from Flores, East Indonesia. J. Hum. Evol. 57, 527–537.
van der Geer, A.A.E., van den Bergh, G.D., Lyras, G.A., Prasetyo, U.W., Awe, R.D., Setiyabudi, E., Hara, D., 2016. The effect of area and isolation on insular dwarf proboscideans. J. Biogeogr. 43, 1656–1666.
van der Geer, A.A.E., Lyras, G.A., MacPhee, R.D.E., Lomolino, M., Drinia, H., 2014. 2014. Mortality in a predator-free insular environment: the dwarf deer of Crete. Am. Mus. Novit. 1–26.
van der Geer, A.A.E., van den Bergh, G.D., Prasetyo, U.W., 2017. Beyond the Horizon: the Predictive Power of Palaeoecology and Dispersal of Insular Dwarf Proboscideans in Models on the Dispersal of Hominins into Wallacea. SAGE 2017 3rd Southeast Asian Gateway Evolution Meeting. August 28-31, Bogor, Indonesia. Conference Program and Abstracts. Research Center for Biology, Indonesian Institute of Sciences, Bogor Indonesia, p. 217.
Veatch, E.G., Tocheri, M.W., Sutikna, T., McGrath, K., Saptomo, E.W., Helgen, K.M., 2019. Temporal shifts in the distribution of murine rodent body size classes at Liang Bua (Flores, Indonesia) reveal new insights into the paleoecology of *Homo floresiensis* and associated fauna. J. Hum. Evol. 130, 45–60.
Verhoeven, T., 1958. Pleistozäne Funde in Flores. Anthropos 53, 264–265.
Veth, P., Ward, I., Manne, T., Ulm, S., Ditchfield, K., Dortch, J., Hook, F., Petchey, F., Hogg, A., Questiaux, D., 2017. Early human occupation of a maritime desert, Barrow Island, North-West Australia. Quat. Sci. Rev. 168, 19–29.
Williams, D., Peck, J., Karabanov, E., Prokopenko, A., Kravchinsky, V., King, J., Kuzmin, M., 1997. Lake Baikal record of continental climate response to orbital insolation during the past 5 million years. Science 278, 1114–1117.
Young, C.B., 2020. Static allometry of a small-bodied omnivore: body size and limb scaling of an island fox and inferences for Homo floresiensis. J. Hum. Evol. 149, 102899.
Yurnaldi, D., Setiawan, R., Patriani, E.Y., 2018. The magnetostratigraphy and the age of so'a basin fossil-bearing sequence, Flores, Indonesia. Indonesian Journal on Geoscience 5, 221–234.
Zanolli, C., Kaifu, Y., Pan, L., Xing, S., Mijares, A.S., Kullmer, O., Schrenk, F., Corny, J., Dizon, E., Robles, E., 2022. Further analyses of the structural organization of *Homo luzonensis* teeth: evolutionary implications. J. Hum. Evol. 163, 103124.